Recent Progress in Molecular Electronics

Hirokazu TADA@Osaka-U

Molecular (-based) Electronics
Organic Electronics
Plastic Electronics

Molecular (-scale) Electronics
Molectronics

molectronics.com
molectron.com
...... com

1 μ m　100 nm　10 nm　1 nm

molectronics.jp

有機エレクトロニクス
有機薄膜デバイス
（有機ＥＬ、有機ＦＥＴ）

分子エレクトロニクス
単一分子デバイス

OLED display

flexible display

Carbon nanotube transistor

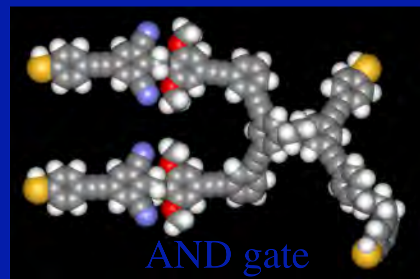

molecular transistor

Current Stage of Molecular Electronic Devices

①Organic LED
（実用化）
駆動は
無機トランジスター

SONY PEGVZ90
Sep.2004

大日本印刷

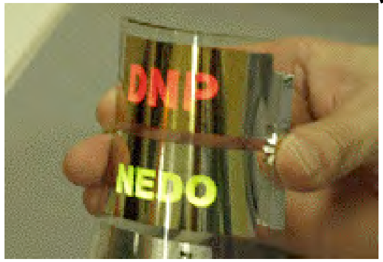

Flexible Display

②Organic FET （開発競争が活発化）

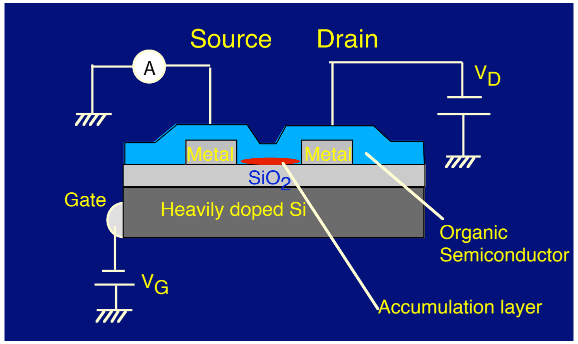

③Organic Solar Cell
（開発競争が活発化）

④ CNT-FET (高密度・高速化へ期待)

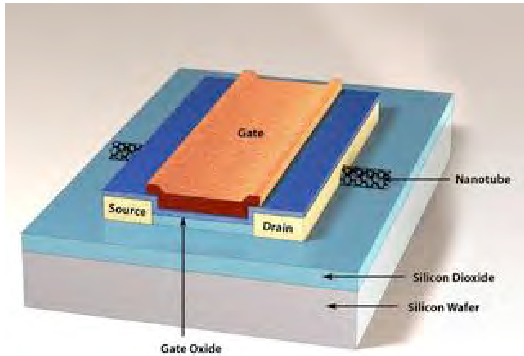

IBM
(2002)

⑤Single Molecule FET

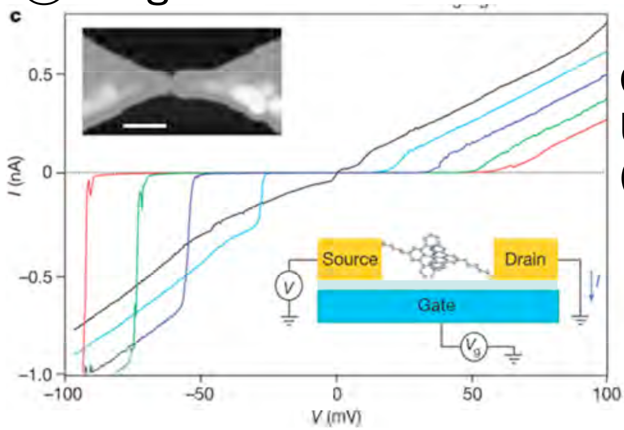

Cornell
UC Berkeley
(2002)

History

1824 尿素の合成（F. Wöhler）：有機合成化学の幕開け
1865 ベンゼン構造の決定（F. A. Kekulé）
1938 ナイロンの合成
1947 Development of Inorganic Transistor
1950 Organic Semiconductor (Akamatsu, Inokuchi): 有機半導体（ビオラントロン）の発見
1954 Organic Conductor; 有機伝導体（ペリレン-臭素）の発見（赤松、井口、松永）
1964 分子による高温超伝導体の提案（W. A. Little）
1973 Organic Metals: 有機金属（TTF-TCNQ）の発見（J. P. Ferraris ら）
1974 Polyacetylene (Shirakawa); ポリアセチレン膜の作製法の発見
1977 Conductive Polymer (Shirakawa) :導電性ポリマーの発見
1980 Organic Superconductor (Jerome) :有機超伝導体の発見
1981 Molecular Electronic Devices に関するワークショップ（米国）
福井謙一ら　ノーベル化学賞（量子化学の発展）
1982 走査トンネル顕微鏡の発明
1985 サッカーボール型分子フラーレンの発見（R. Smalley ら）
1986 有機薄膜電界効果トランジスターの発明（肥塚ら）：ＯＦＥＴ
1987 積層型有機薄膜電界発光素子の発明（C. W. Tang ら）：ＯＬＥＤ
1991 Carbon Nanotube (Iijima) の発見
1998 Molectronics と題したワークショップ（米国）
1999 ＯＬＥＤ　実用化（パイオニア）
ＯＦＥＴ　キャリア移動度　数 cm2V-1s-1 へ（PennState）
2000 ~~ＯＦＥＴ　超伝導の発見（Bell Lab. Lucent）~~
白川英樹ら　ノーベル化学賞（導電性ポリマーの発見）
2001 野依良治ら　ノーベル化学賞（不斉合成反応の開発）
井口洋夫　文化勲章（分子素子）

http://www.nanoelectronics.jp/

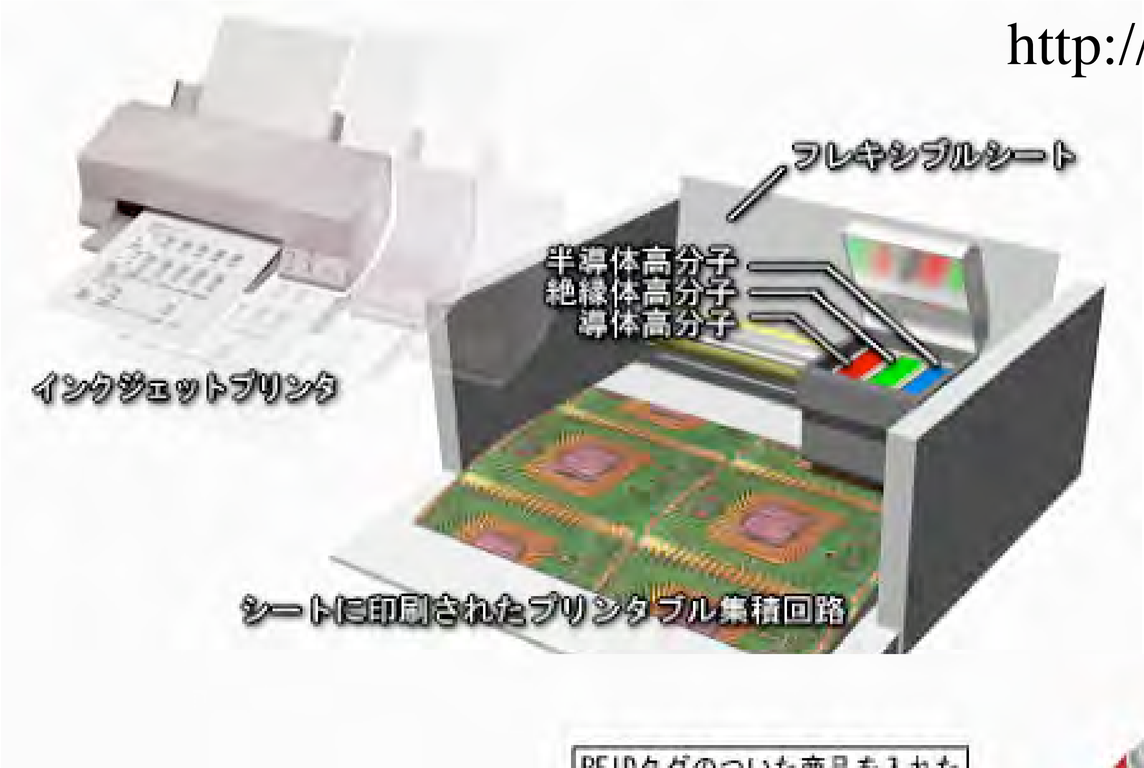

High-Resolution Inkjet Printing of All-Polymer Transistor Circuits
H. Sirringhaus, T. Kawase, R. H. Friend, T. Shimoda et al.,
@ Cavendish & Epson, Science 290, 2123 (2000).

μ(p)=0.02 cm^2/Vs
On/off ratio =10^5

Stable in Air

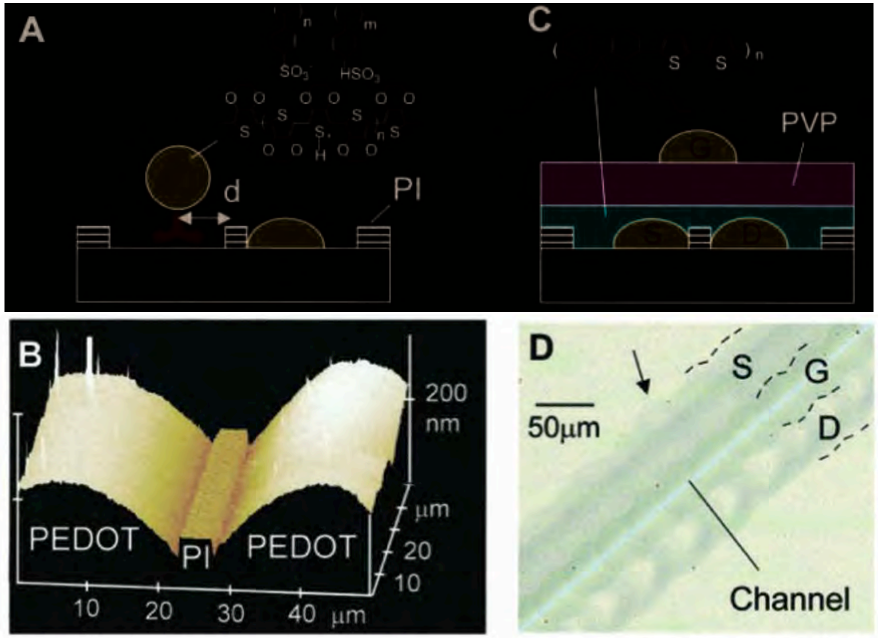

Fig. 1. (A) Schematic diagram of high-resolution IJP onto a prepatterned substrate. **(B)** AFM showing accurate alignment of inkjet-printed PEDOT/PSS source and drain electrodes separated by a repelling polyimide (PI) line with $L = 5$ µm. **(C)** Schematic diagram of the top-gate IJP TFT configuration with an F8T2 semiconducting layer (S, source; D, drain; and G, gate). **(D)** Optical micrograph of an IJP TFT ($L = 5$ µm). The image was taken under crossed polarizers so that the TFT channel appears bright blue because of the uniaxial monodomain alignment of the F8T2 polymer on top of rubbed polyimide. Unpolarized background illumination is used to make the contrast in the remaining areas visible, where the F8T2 film is in an isotropic multidomain configuration. The arrow indicates pronounced roughness of the unconfined PEDOT boundary.

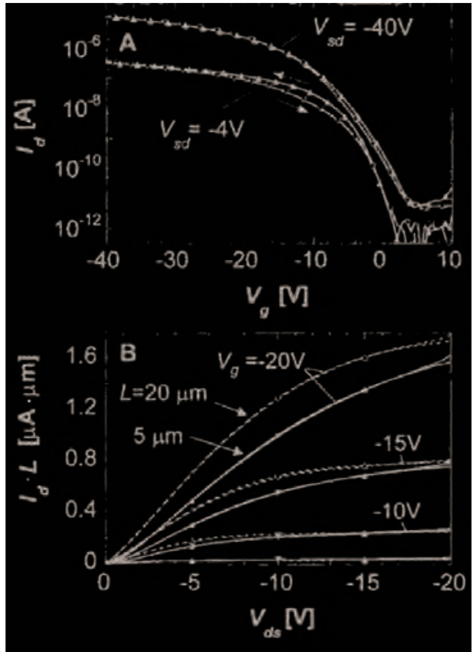

Fig. 2. (A) Transfer characteristics of an IJP TFT with F8T2 aligned uniaxially parallel to the current flow ($L = 5$ µm, $W = 3000$ µm) measured under an N_2 atmosphere. Subsequent measurements with increasing (solid symbols) and decreasing (open symbols) gate voltage are shown. **(B)** Scaling of the output characteristics of IJP F8T2 TFTs normalized by multiplying the drain current by the channel length (dashed lines with open symbols, $L = 20$ µm; solid lines with solid symbols, $L = 5$ µm). Subsequent measurements with increasing (upward triangles) and decreasing (downward triangles) gate voltage are shown.

Outline

- Electrical Properties of Organic Semiconductors
  - Gas Adsorption and Chemical Carrier Doping
- Organic Field Effect Transistors (OFETs)
  - FET Based on Organic Thin Films
  - FET Based on Organic Single Crystals
- Molecular-scale Devices
  - Preparation of Nano-gap Electrodes
  - Preparation of Molecule/Electrode Interfaces
- Electronic Structure of Molecule/Electrode Interfaces

Change of Electrical Characteristics of TiOPc films in Chemical Environments

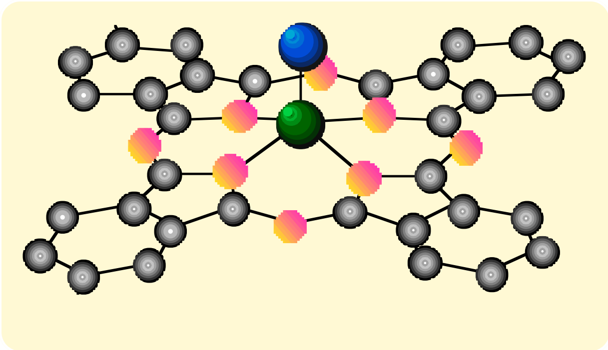

TiOPc

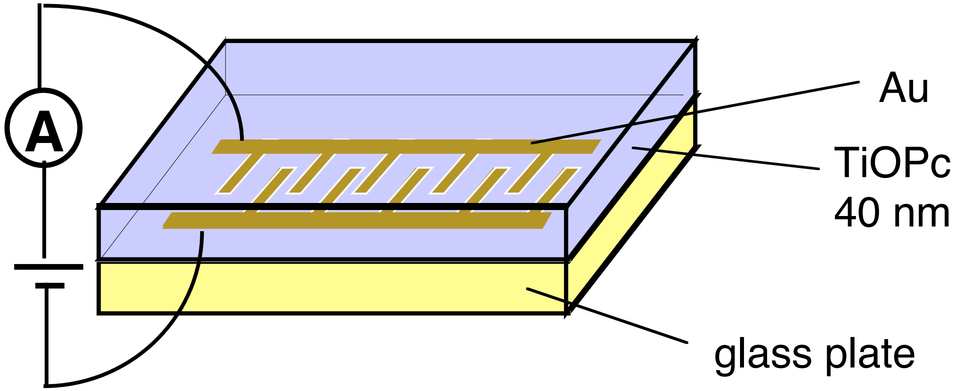

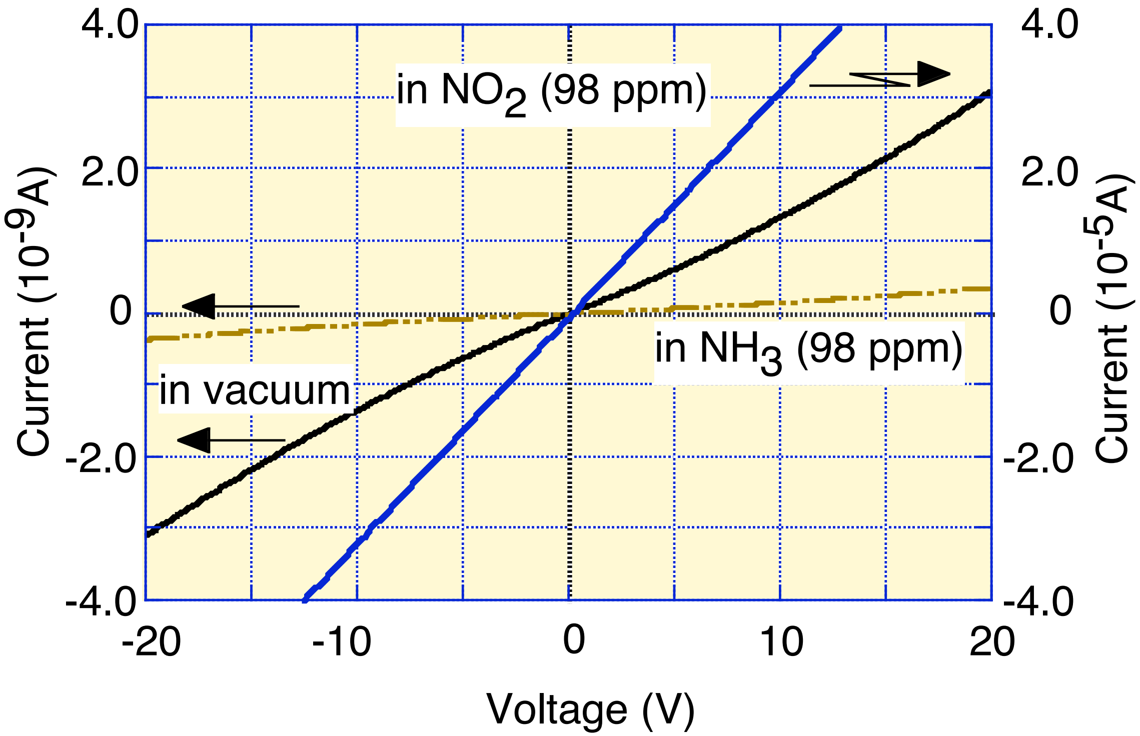

Response curves of VOPc / IDT to NO_2 (100 ppm) and NH_3 (100 ppm)

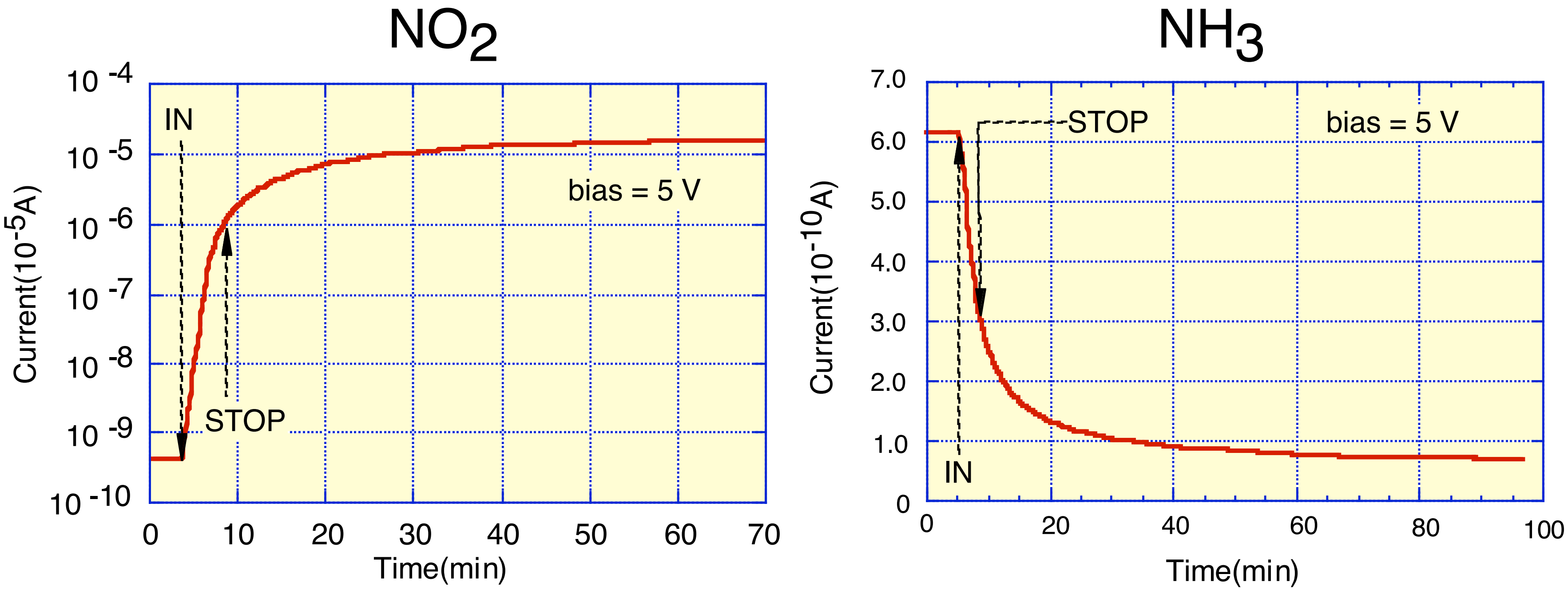

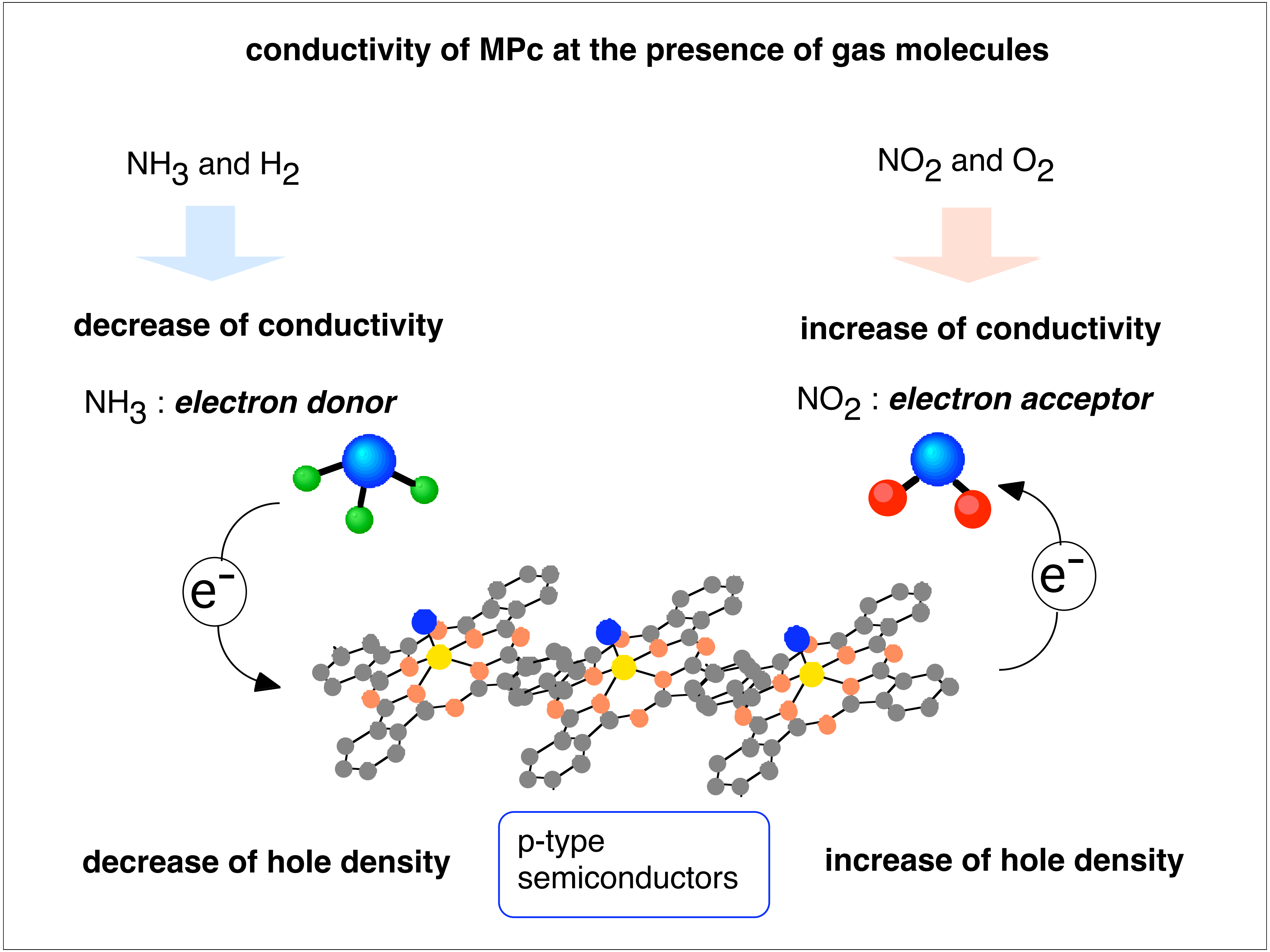
conductivity of MPc at the presence of gas molecules
NH3 and H2
decrease of conductivity
NH3 : electron donor
NO2 and O2
increase of conductivity
NO2 : electron acceptor
e-
e-
decrease of hole density
p-type semiconductors
increase of hole density

Nanotube Molecular Wires as Chemical Sensors
J. Kong, , , & H. Dai @ Stanford
Science 287, 622 (2000).

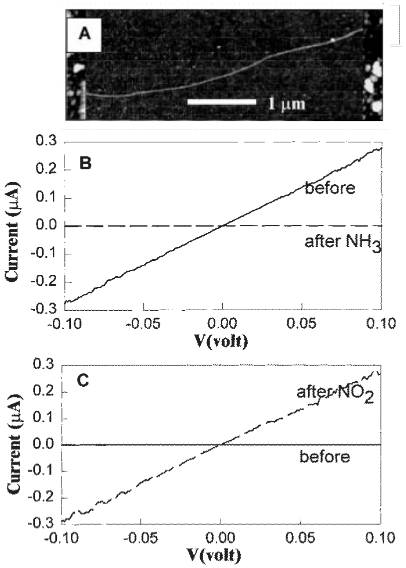

Fig. 1. Changes of electrical characteristics of a semiconducting SWNT in chemical environments. (**A**) Atomic force microscopy image of a metal/S-SWNT/metal sample used for the experiments. Nanotube diameter is ~1.8 nm. The metal electrodes consist of 20-nm-thick Ni, with 60-nm-thick Au on top. (**B**) Current versus voltage curves recorded before and after exposure to NH_3. (**C**) Current versus voltage curves recorded under $V_g = +4$ V, before and after NO_2 exposure.

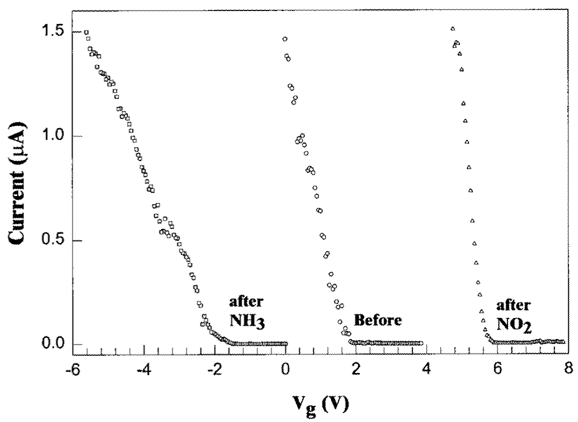

Fig. 2. Chemical gating effects to the semiconducting SWNT. Current versus gate voltage curves before NO_2 (circles), after NO_2 (triangles), and after NH_3 (squares) exposures. The measurements with NH_3 and NO_2 were carried out successively after sample recovery.

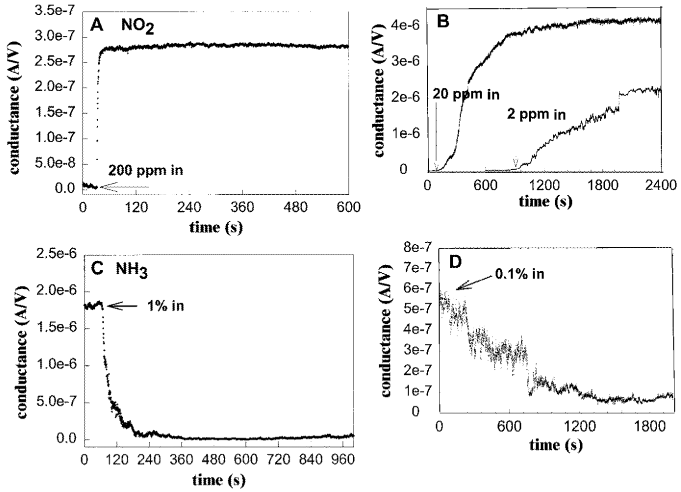

Fig. 3. Electrical response of a semiconducting SWNT to gas molecules. (**A**) Conductance (under $V_g = +4$ V, in an initial insulating state) versus time in a 200-ppm NO_2 flow. (**B**) Data for a different S-SWNT sample in 20- and 2-ppm NO_2 flows. The two curves are shifted along the time axis for clarity. (**C**) Conductance ($V_g = 0$, in an initial conducting state) versus time recorded with the same S-SWNT sample as in (A) in a flow of Ar containing 1% NH_3. (**D**) Data recorded with a different S-SWNT sample in a 0.1% NH_3 flow. Read 3.5e-7, for example, as 3.5×10^{-7}.

Summary 1

1. Electrical properties of organic semiconductors are affected strongly by the gas molecules adsorbed.

Organic Field-effect Transistor

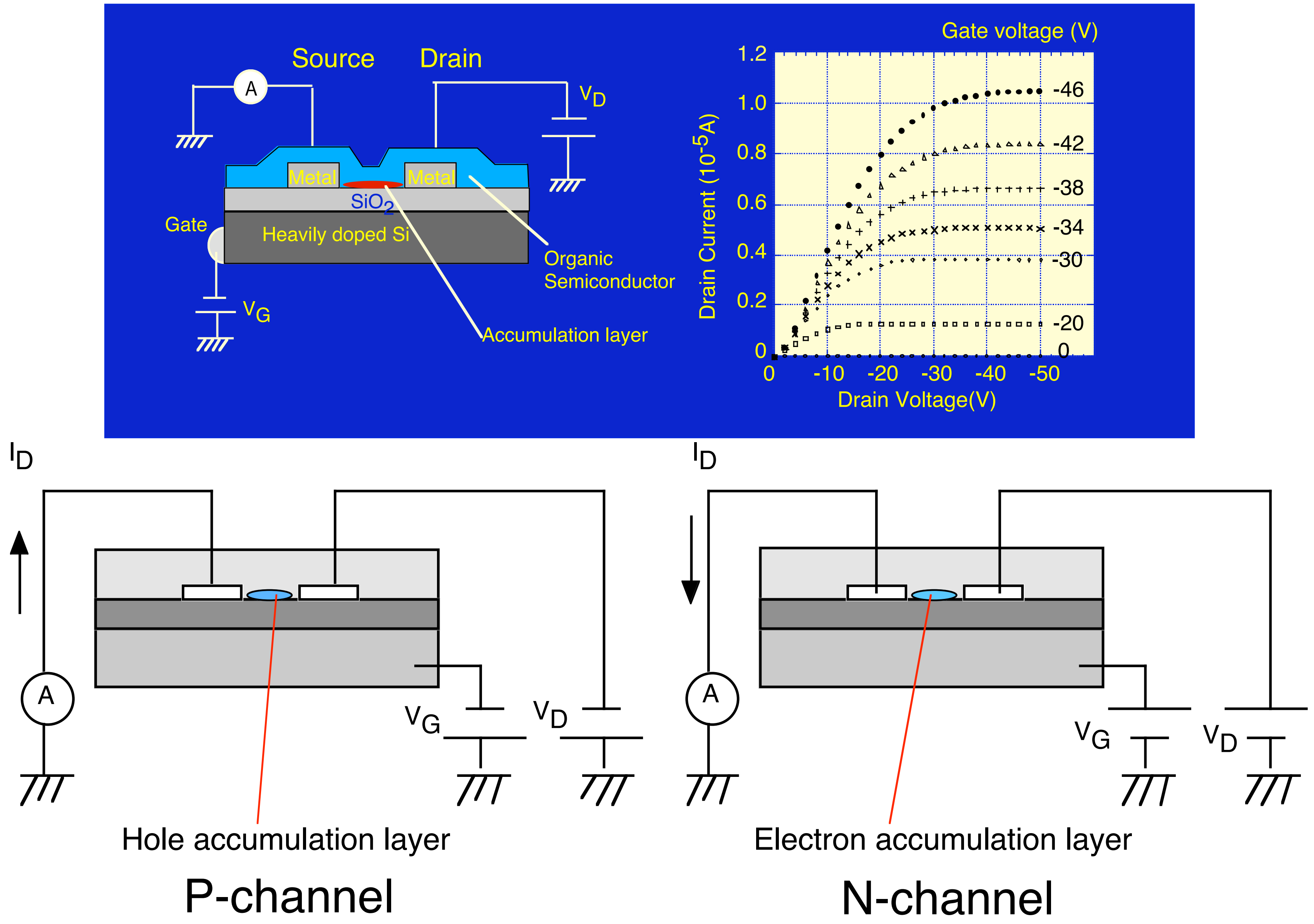

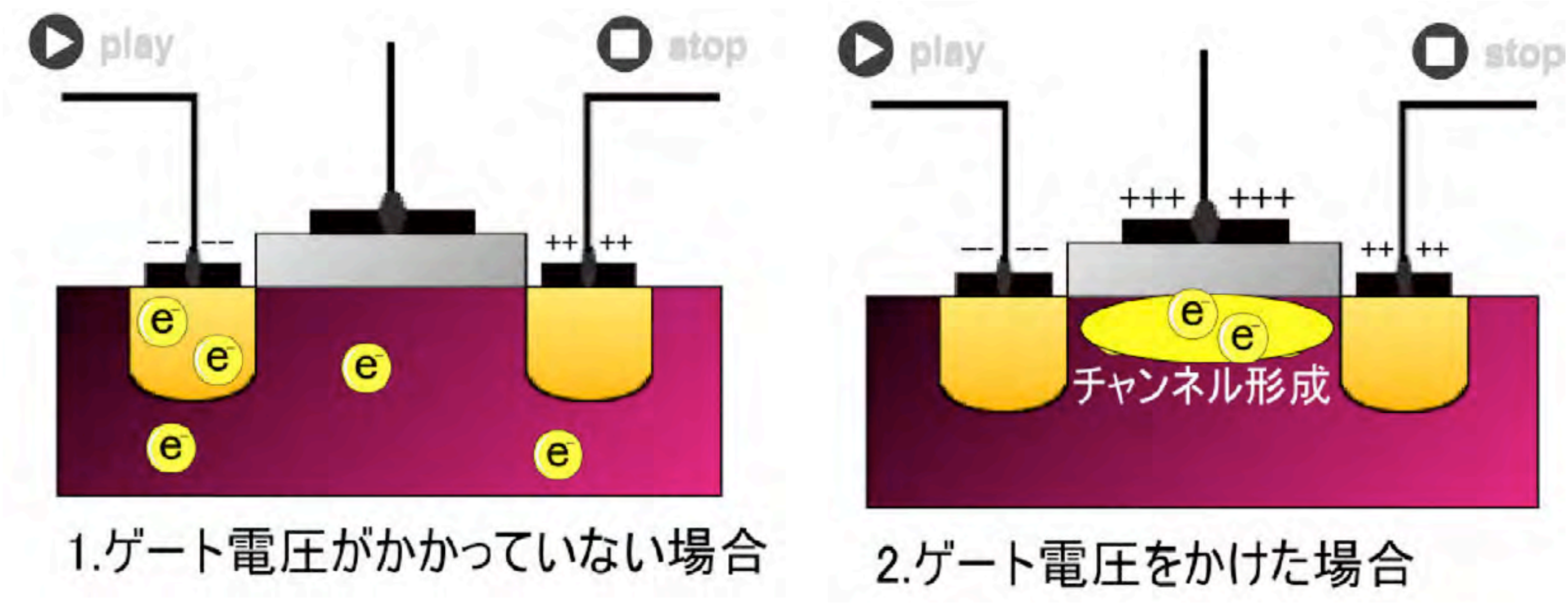

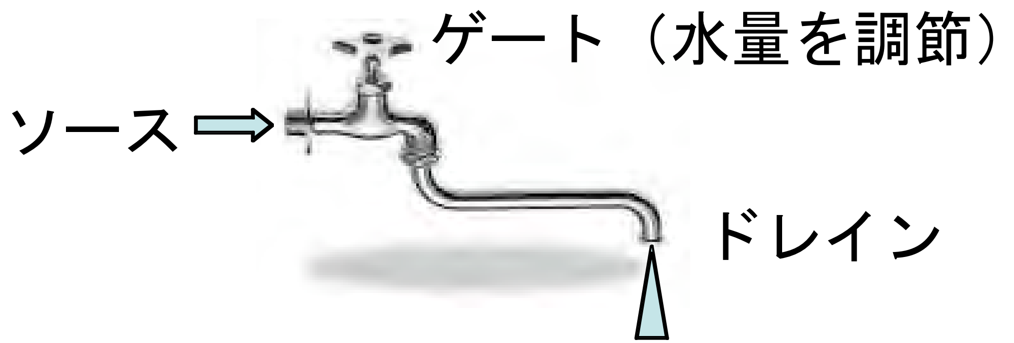

animation

http://www.nanoelectronics.jp/

FET Properties of TiOPc in an O_2 atmosphere

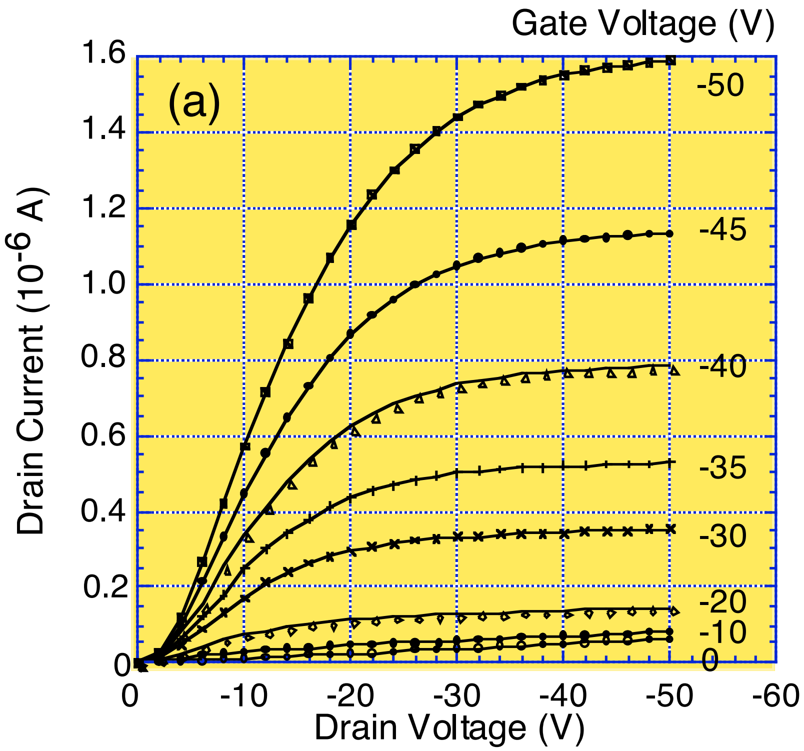

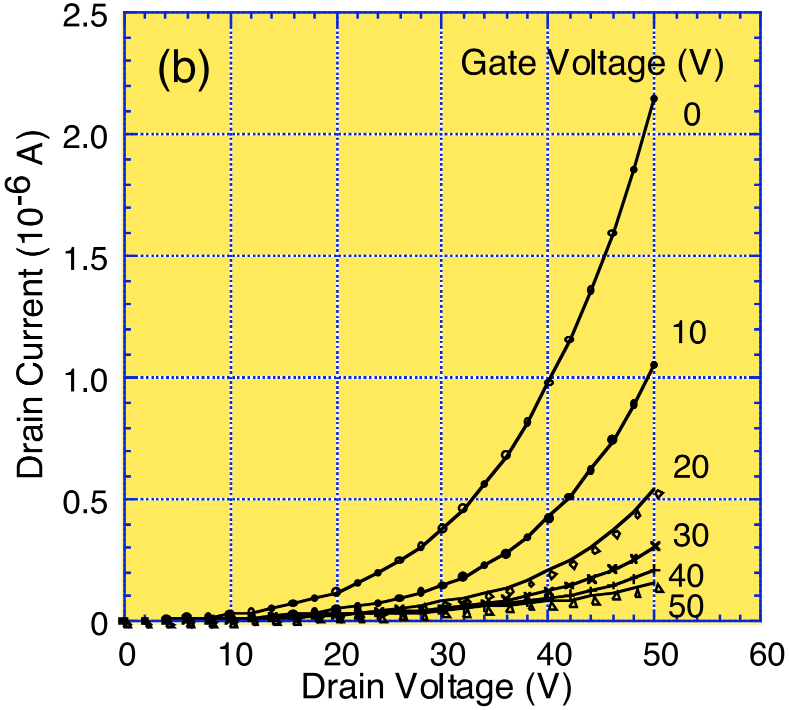

$\mu_p = 1.0 \times 10^{-5}\ cm^2/Vs$

p-type circuit

n-type circuit

FET Properties of TiOPc in Vacuum (1.7×10^{-6} Pa)

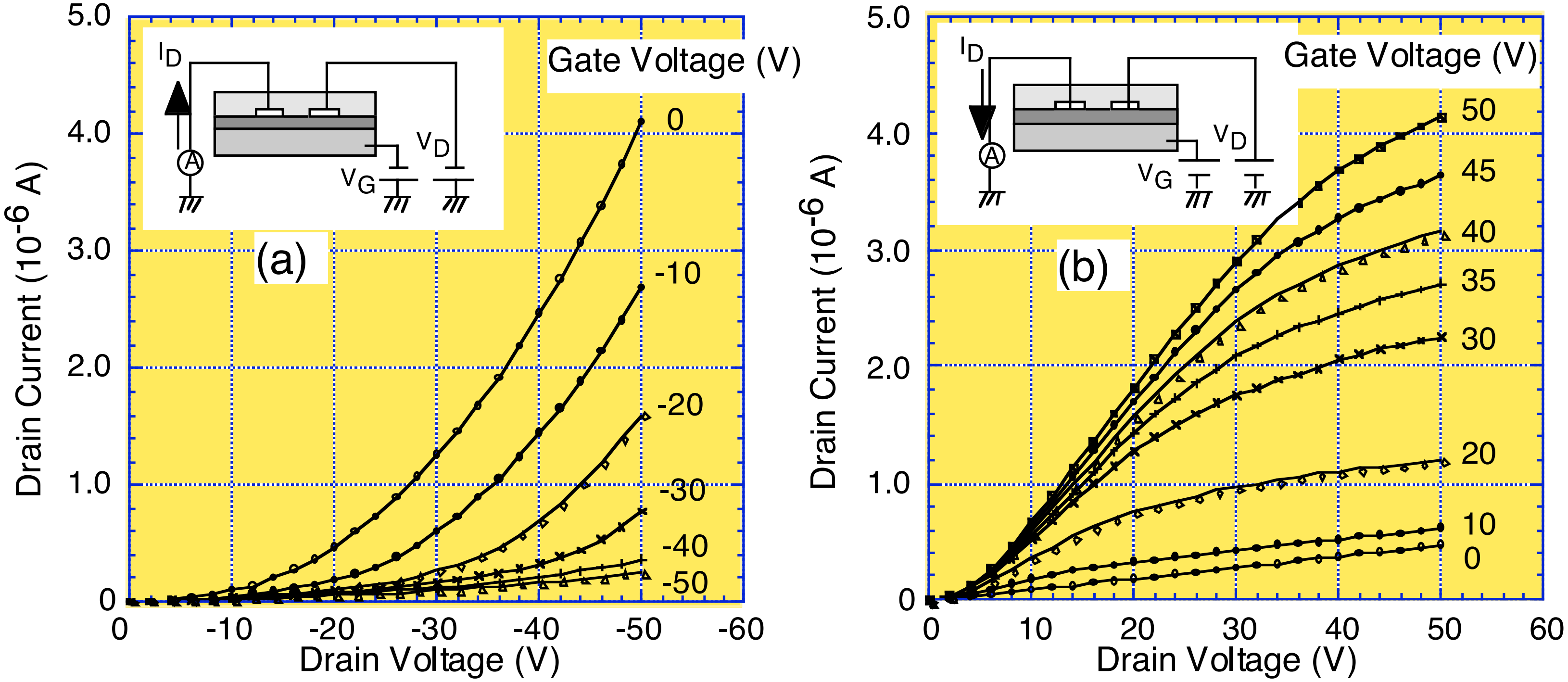

$\mu_n = 9.0 \times 10^{-6}\ cm^2/Vs$

p-type circuit

n-type circuit

oxygen

FET Properties of TiOPc in an O_2 atmosphere

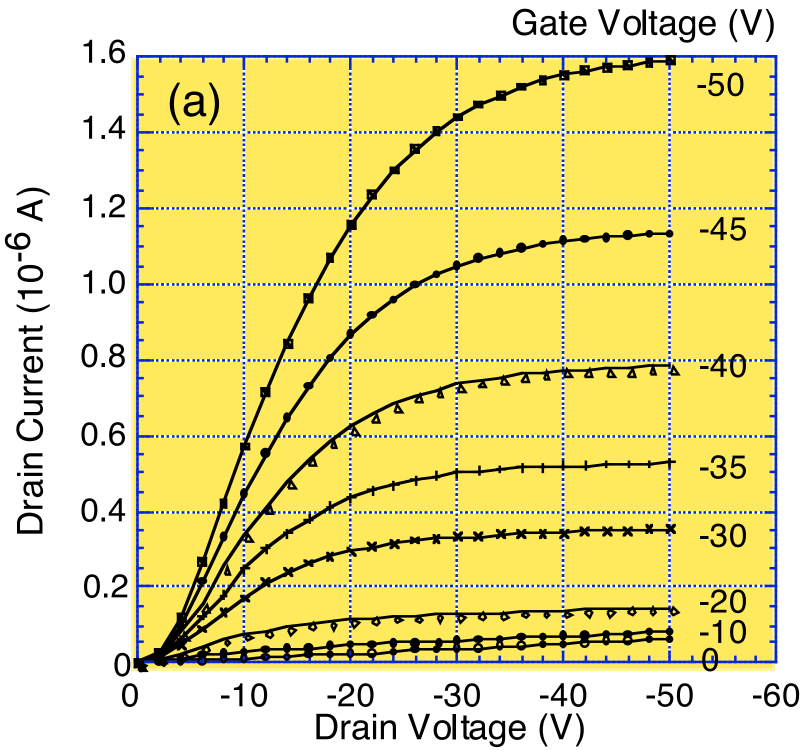

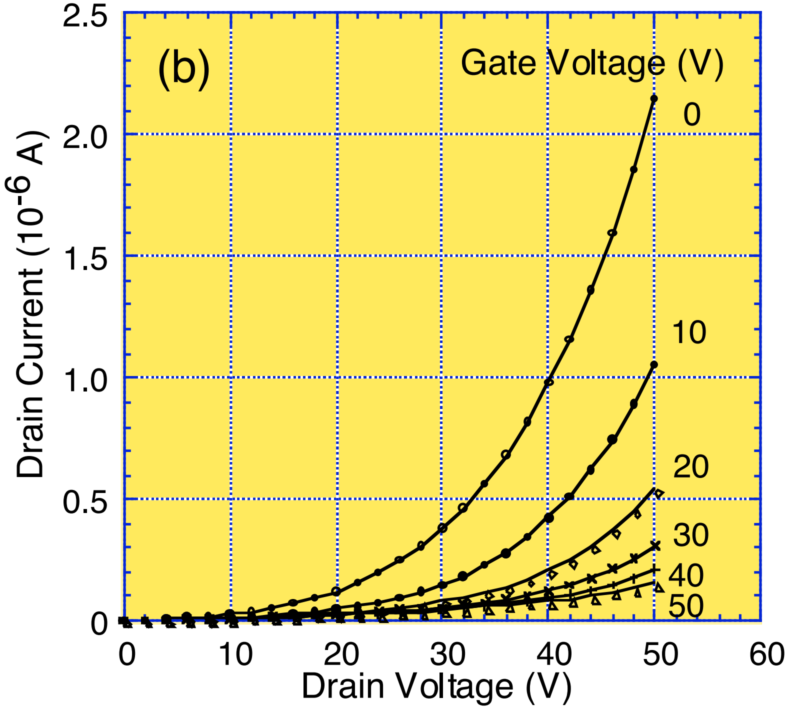

$\mu_p = 1.0 \times 10^{-5}\ cm^2/Vs$

p-type circuit

n-type circuit

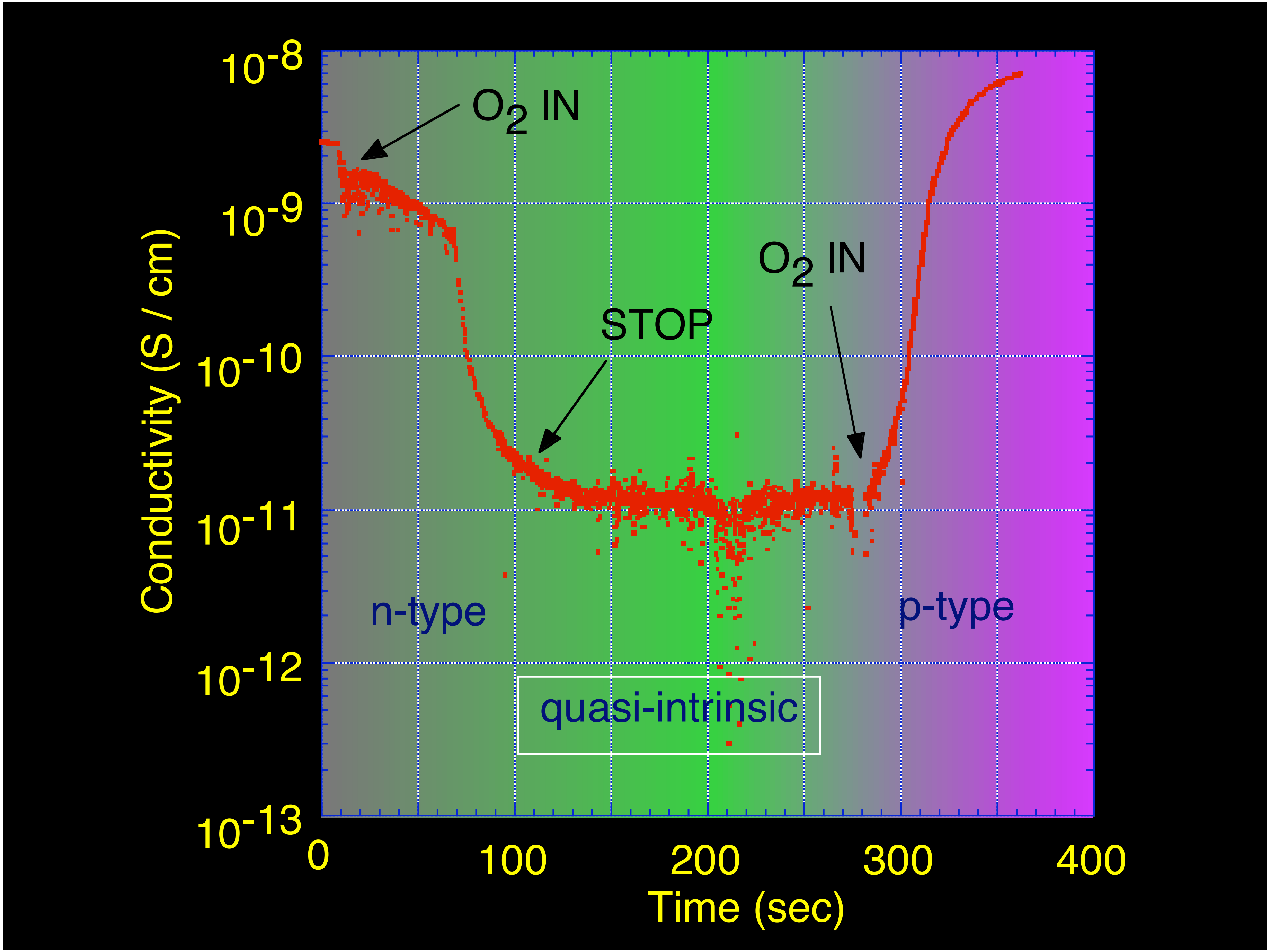

10-8
10-9
10-10
10-11
10-12
10-13
Conductivity (S / cm)
0
100
200
300
400
Time (sec)
O2 IN
STOP
O2 IN
n-type
p-type
quasi-intrinsic

FET Characteristics of TiOPc in UHV

H. Tada, H. Touda, M. Takada, K. Matsushige, APL 76, 873 (2000).

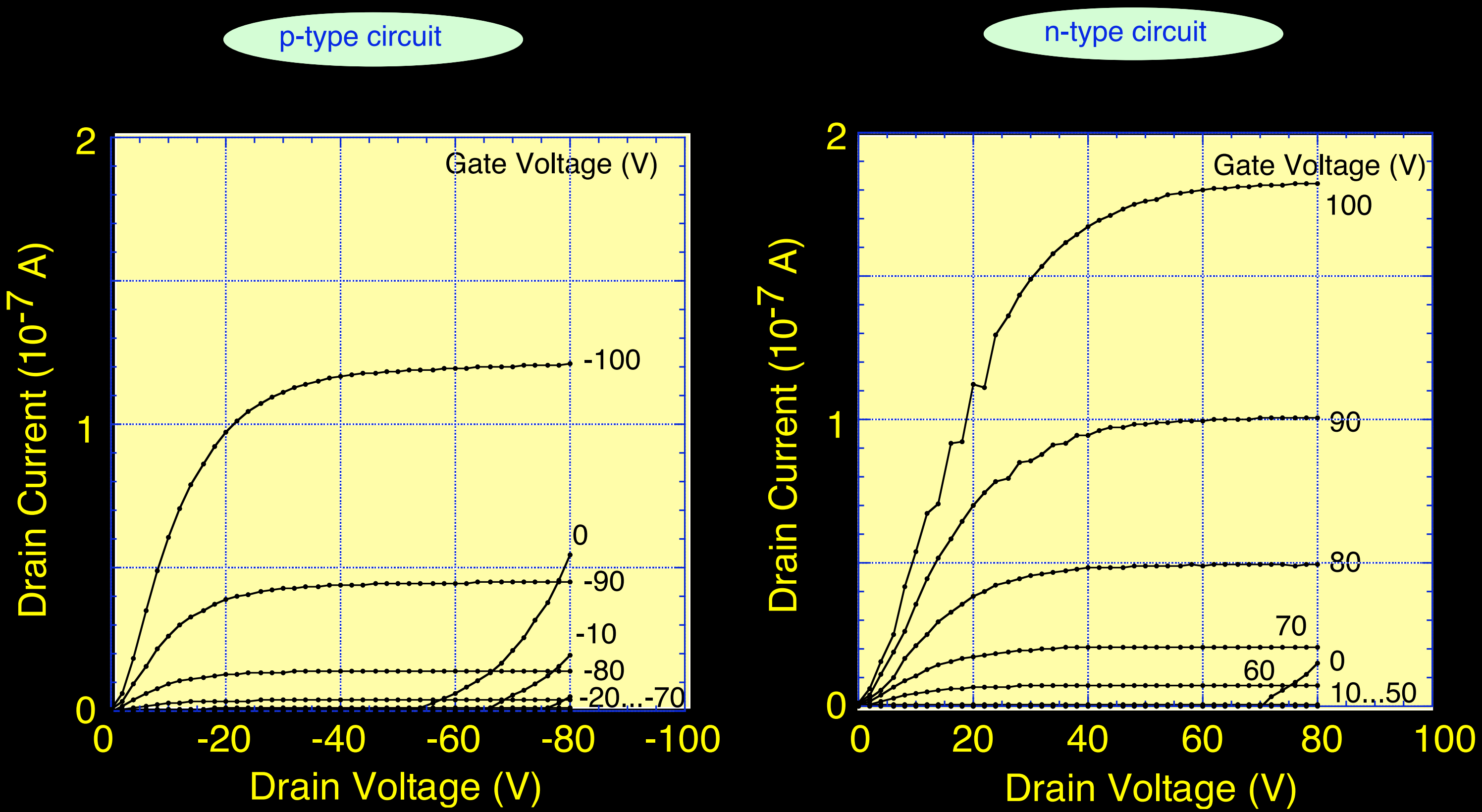

$\mu_p = 2.7 \times 10^{-6}\ cm^2/Vs$

$\mu_n = 2.0 \times 10^{-6}\ cm^2/Vs$

Both p and n type behaviors appeared simultaneously.

Summary 2

1. Electrical properties of organic semiconductors are affected strongly by the gas molecules adsorbed.
2. Organic FET Characteristics are also affected by gas adsorption. Ambipolar operation is observed in OFETs through careful control of impurities.

Ambipolar pentacene field-effect transistors with calcium source-drain electrodes

T. Yasuda, T. Tsutsui et al.,@ Kyushu-U

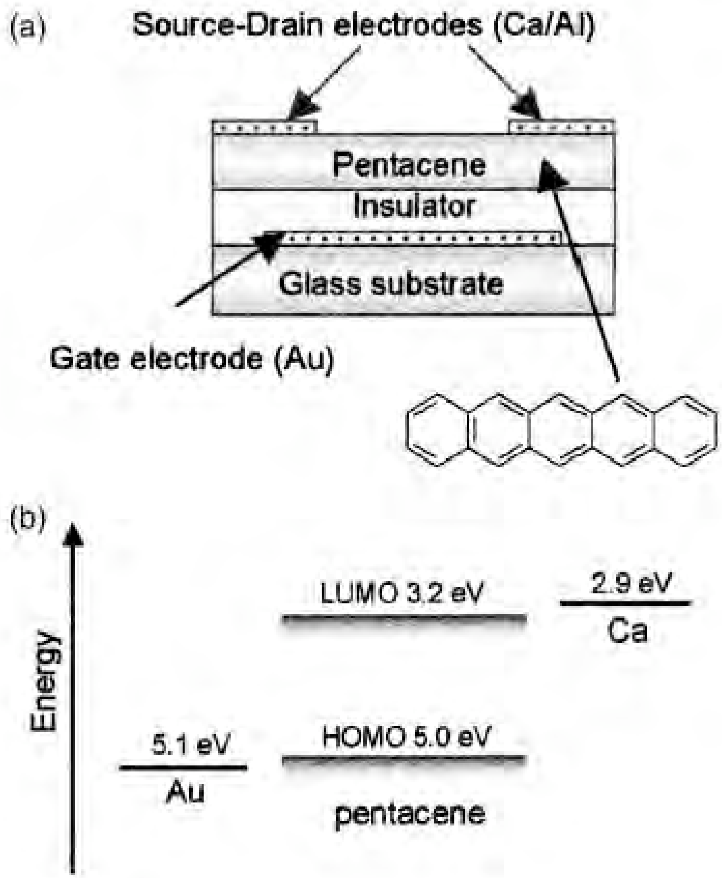

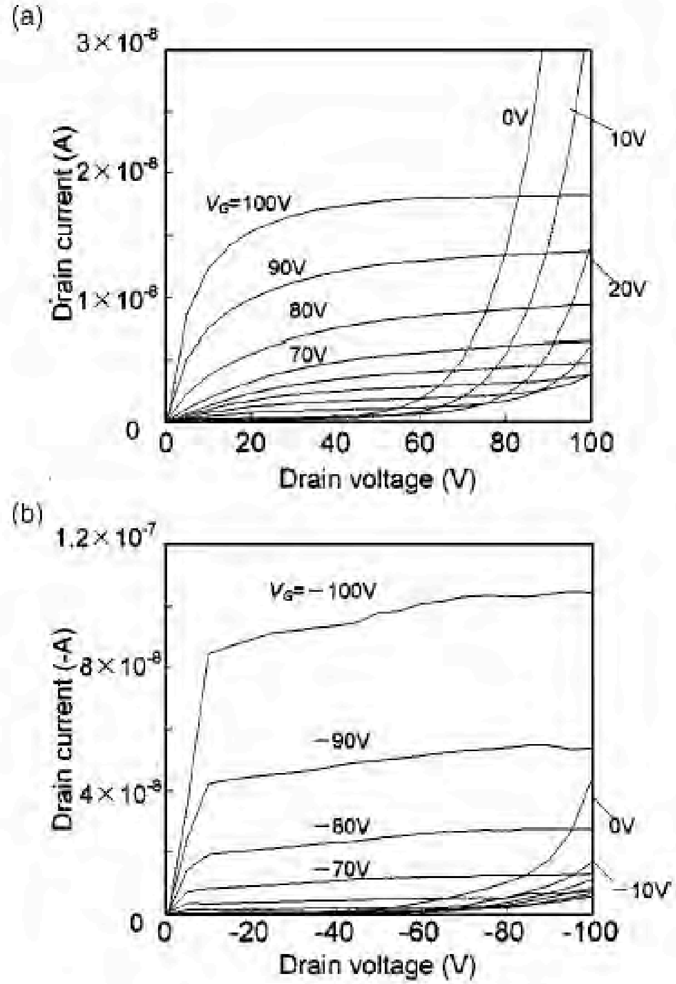

General observation of n-type field-effect behavior in organic semiconductors

L. Chua, R. Friend et al.,@ Cambridge, Nature 434, 194(2005)

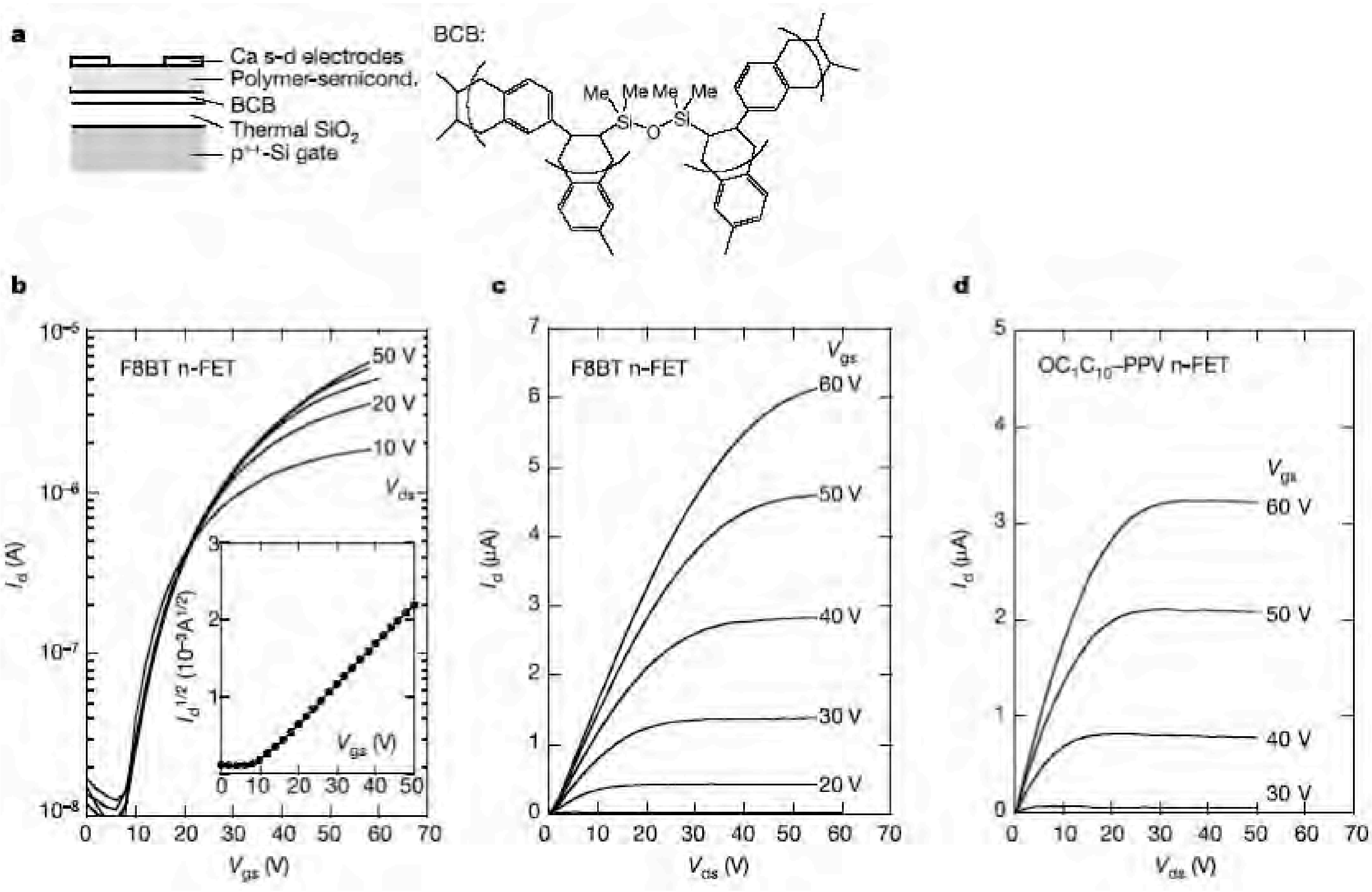

Light-emitting OFETs

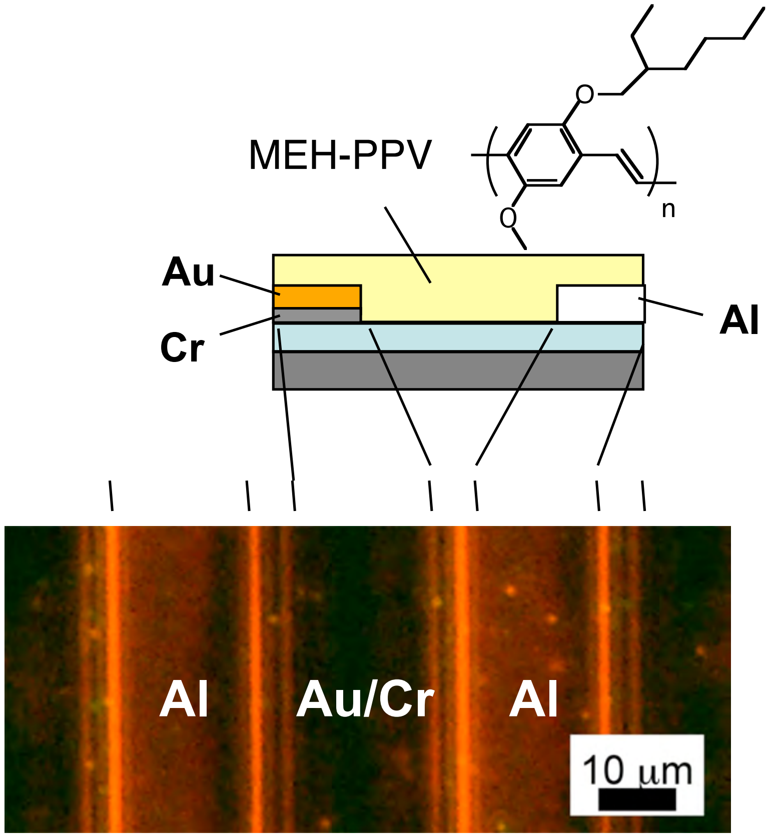

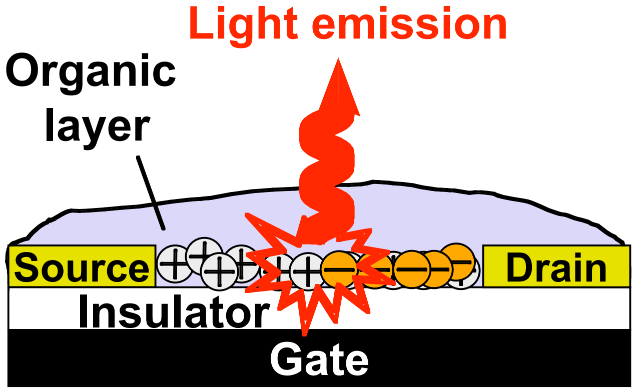

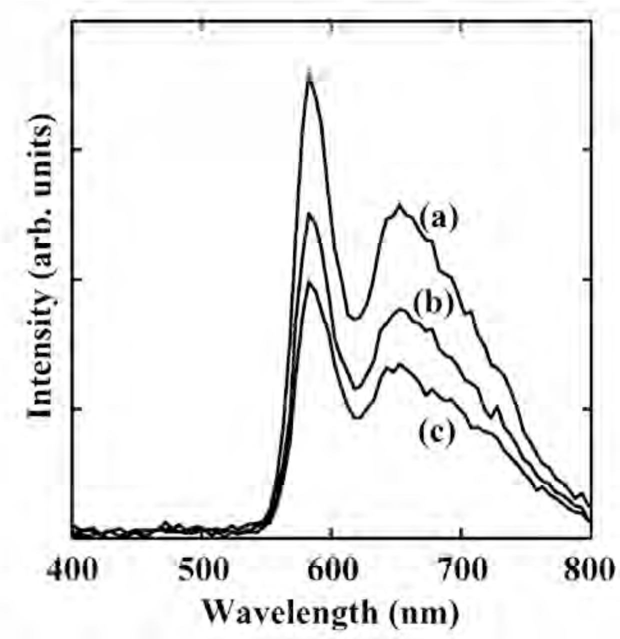

Sakanoue and Tada,
Appl. Phys. Lett. **84**, 3037 (2004).
Chem. Lett. **34**, 494 (2005).

Preparation of Asymmetric Electrodes

1. Electroplating

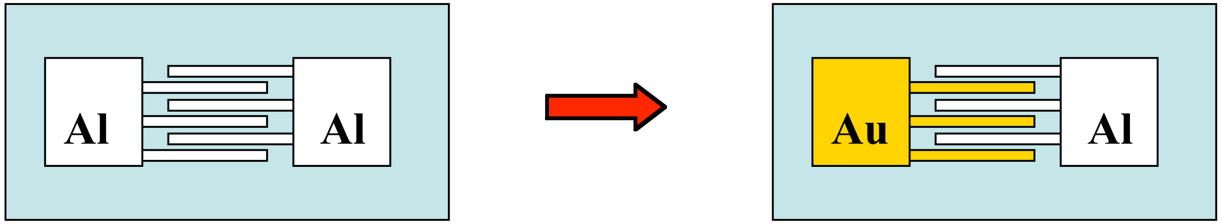

2. Twice of Photolithography & Lift-off

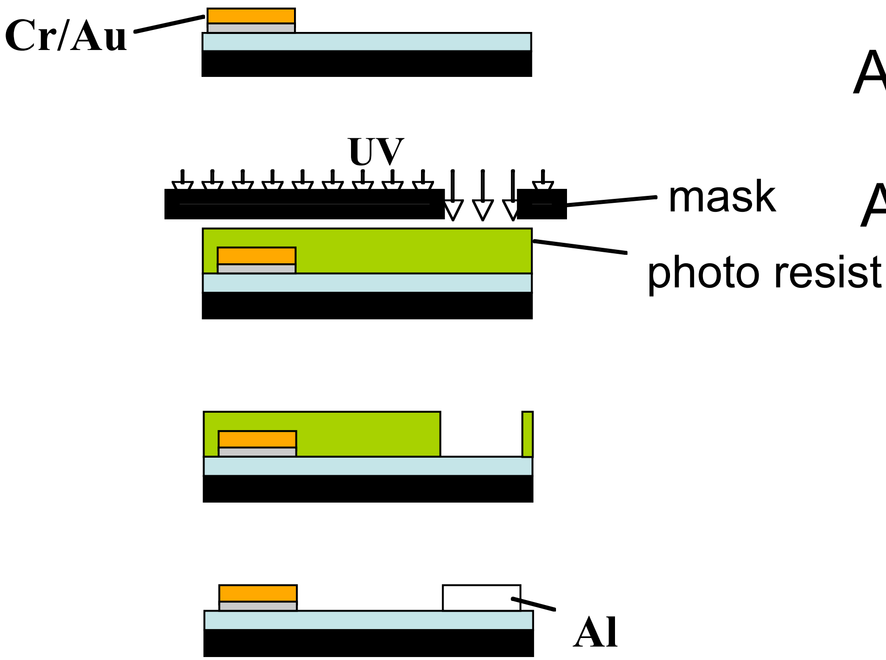

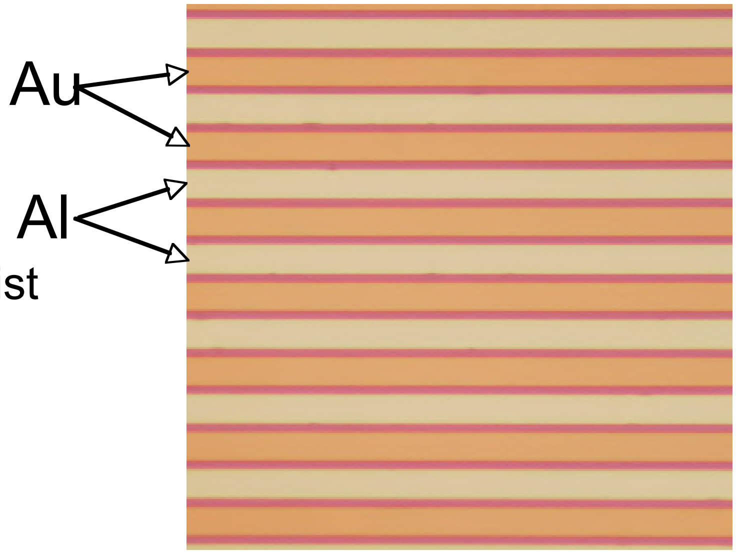

Optical Micrograph

Emission properties

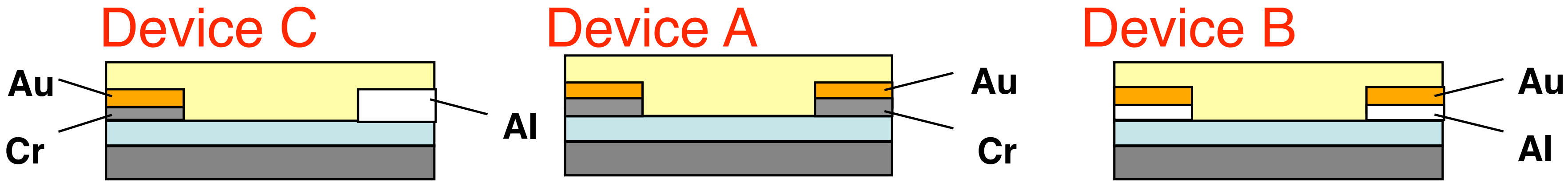

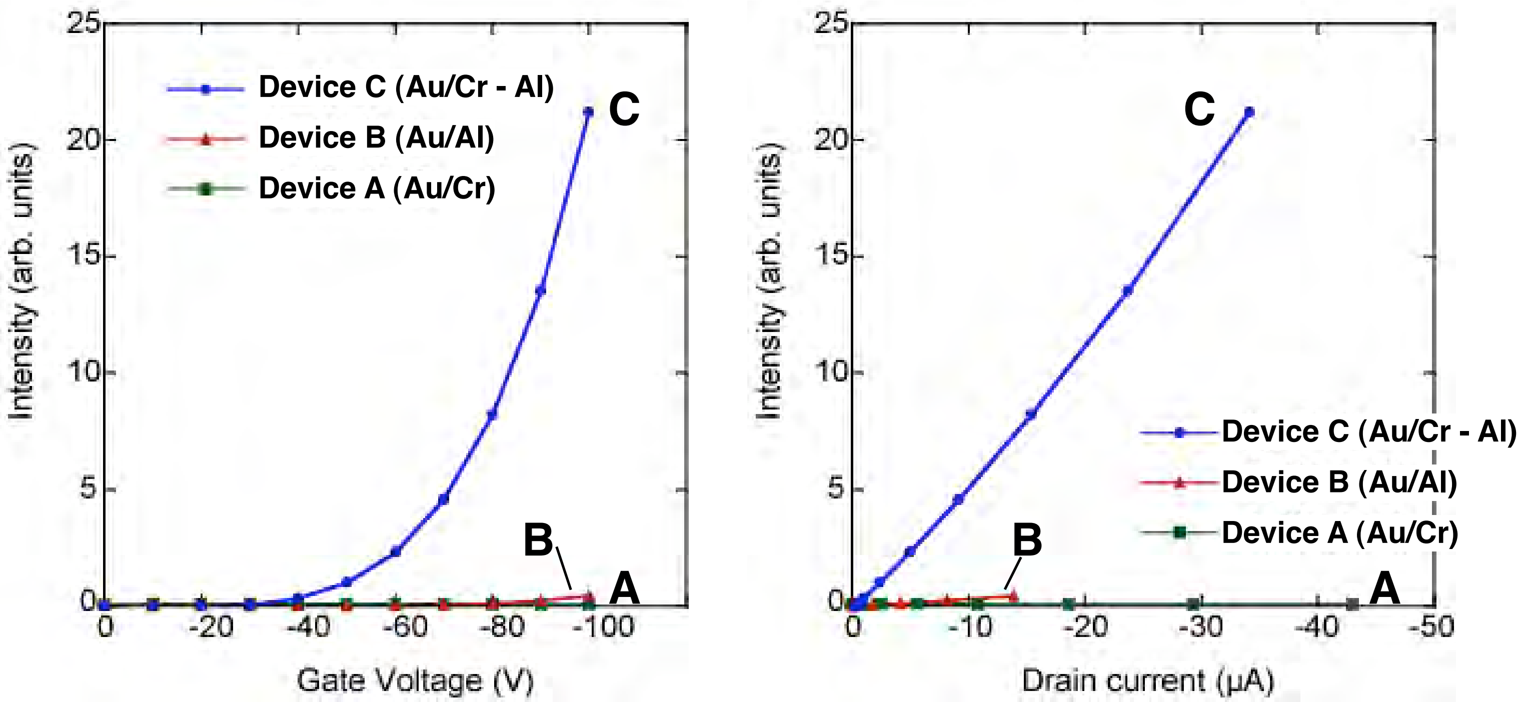

V_d = -100 V

V_d = -100 V

Light-emitting Organic FET

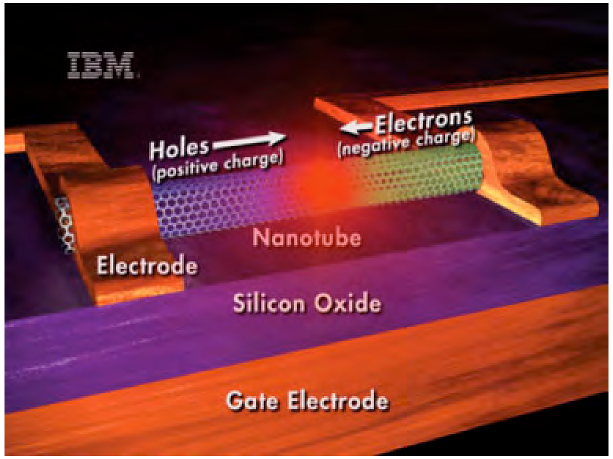

Single-walled carbon nanotube

Misewich *et al.*,
Science, **300**, 783 (2003).

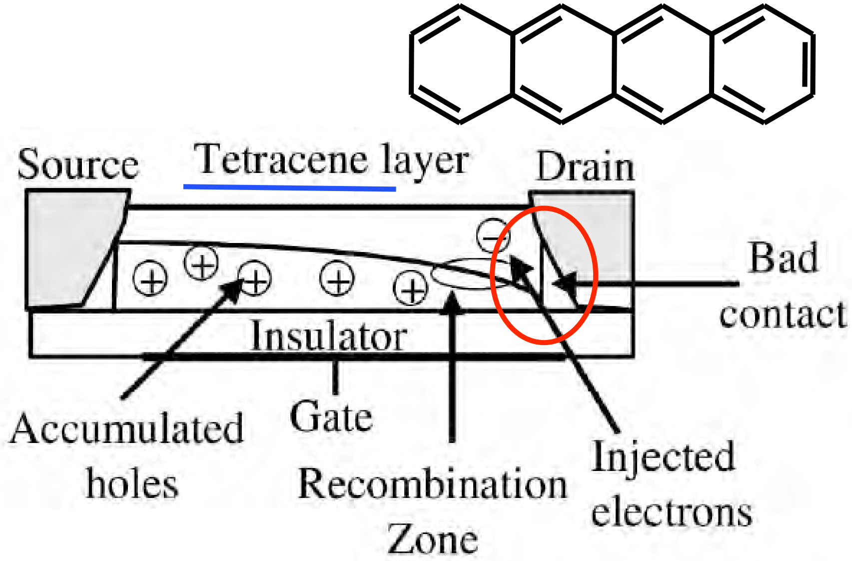

Hepp *et al.*,
Phys. Rev. Lett., **91**, 157406 (2003).

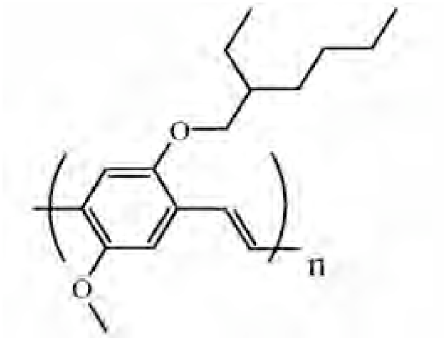

MEH-PPV

Sakanoue *et al.*
Appl. Phys. Lett., **84**, 3037 (2004)

Low-threshold Photopumped Distributed Feedback Plastic Laser Made by Replic Molding
M. Ichikawa @ Shinshu-U, JJAP 42, 5590 (2003).

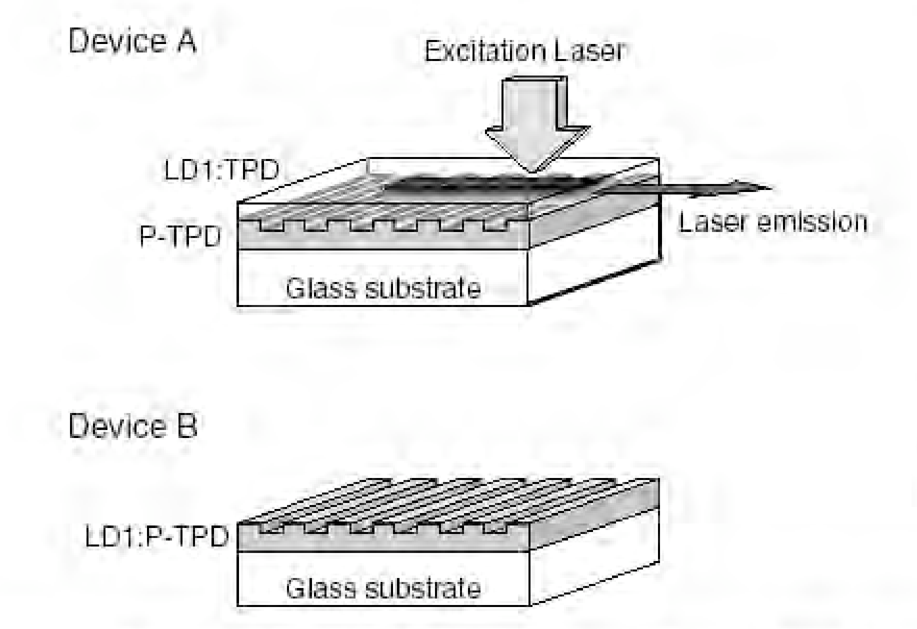

Fig. 1. Schematic diagram of the photopumped organic DFB lasers (Device A and B) used in this study.

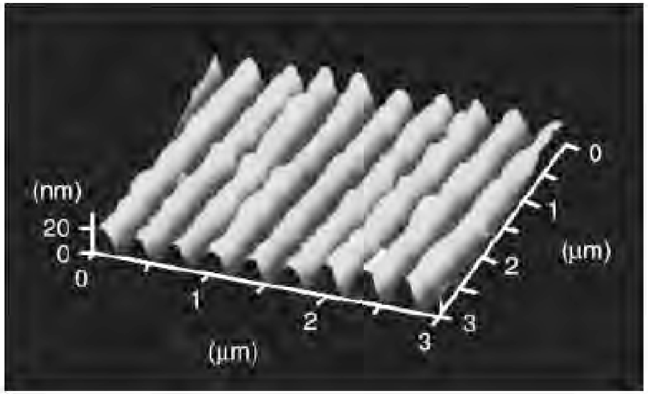

Fig. 3. AFM image of surface relief of P-TPD layer fabricated using replica-molding.

Summary 3

1. Electrical properties of organic semiconductors are affected strongly by the gas molecules adsorbed.
2. Organic FET Characteristics are also affected by gas adsorption. Ambipolar operation is observed in OFETs through careful control of impurities.
3. Work function of the source and drain electrodes is a key factor to determine OFET charatceristics. Ambipolar operation is achieved by choosing appropiate materials for electrodes.
4. Light-emitting OFETs are prepared with asymmetric electrodes in which both electrons and holes are injected into organic films.

Field Effect Carrier Mobility of Organic Films

material	
CuPc	6994
H_2Pc	
$F_{16}CuPc$	
$F_{16}ZnPc$	
pentacen	325 (1997).
a-6T	93).

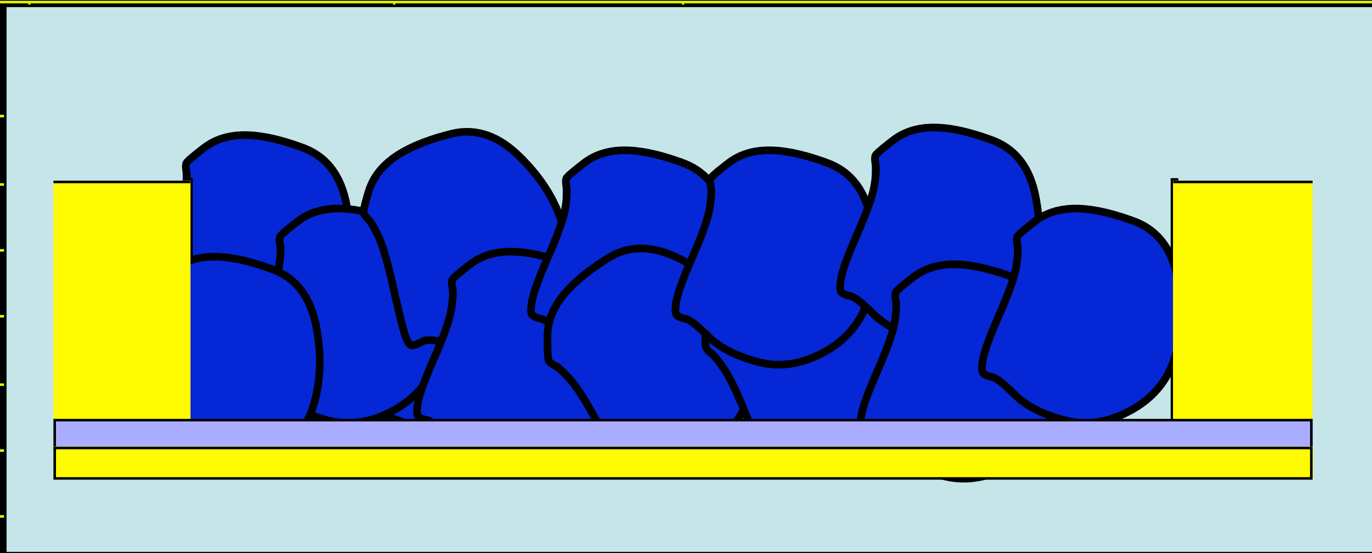

Carrier Mobility of Organic Single Crystals

pentacen	FET at R. T.		3.1 (p), 1.9 (n)	J. H. Schön et al., Synthetic Metals 122, 195 (2001).
C_{60}	FET at R. T.		2.1 (p), 1.8 (n)	
H_2Pc	Time of Flight		1.1 (p) ,1.2 (n)	Cox, J. Phys. C7, 146 (1974).
antracene	Time of Flight	a-axis	1.13 (p), 1.73 (n)	Holstein, Ann. Phys. 8, 325 (1959) .
		b-axis	2.07 (p), 1.05 (n)	
		c’-axis	0.73 (p), 0.39 (n)	

Field-effect transistors on tetracene single crystals

R. W. I. de Boer,[a)] T. M. Klapwijk, and A. F. Morpurgo
Department of Nanoscience, Faculty of Applied Sciences, Delft University of Technology, Lorentzweg 1, 2628 CJ Delft, The Netherlands

μ=0.4 cm^2/Vs APL 83, 4345 (2003)

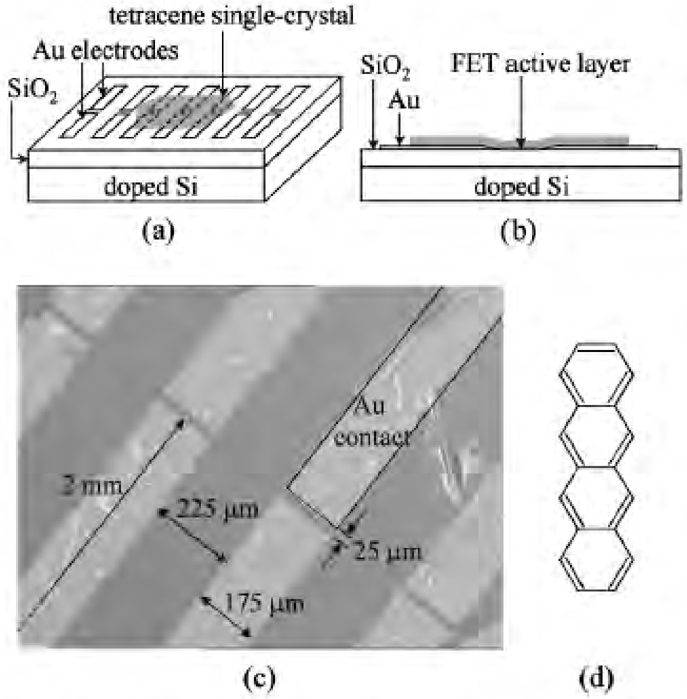

FIG. 1. Schematic representation (a) and side view (b) of a tetracene single-crystal FET. (c) Optical microscope image of a tetracene single-crystal FET. In this device, the semi-transparent tetracene single crystal extends over several pairs of electrodes, which are clearly visible under it. In most cases smaller crystals have been used which extend over only one or two pair of contacts. These different configurations allow us to study transistors with different *W*/*L* ratios on the same crystal. (d) Molecular structure of the tetracene molecule.

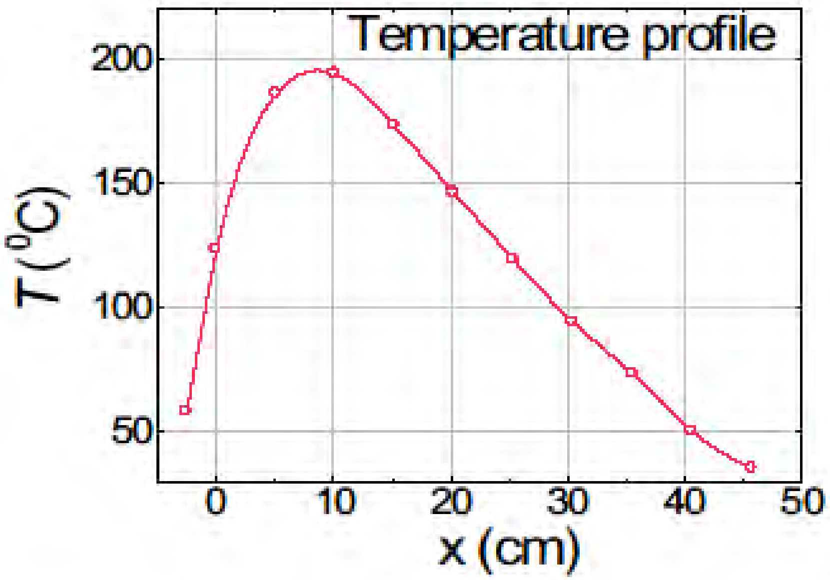

Single-crystal organic field effect transistors with the hole mobility ~8 $cm^2/V\,s$

V. Podzorov,[a] S. E. Sysoev, E. Loginova, V. M. Pudalov,[b] and M. E. Gershenson
Department of Physics and Astronomy, Rutgers University, Piscataway, New Jersey 08854

(Received 10 June 2003; accepted 4 September 2003)

We report on the fabrication and characterization of *single-crystal* organic *p*-type field-effect transistors (OFETs) with the field-effect mobility $\mu \sim 8$ $cm^2/V\,s$, substantially higher than that observed in thin-film OFETs. The single-crystal devices compare favorably with thin-film OFETs not only in this respect: the mobility for the single-crystal devices is nearly independent of the gate voltage and the field effect onset is very sharp. The subthreshold slope as small as $S = 0.85$ V/decade has been observed for a gate insulator capacitance $C_i = 2 \pm 0.2$ nF/cm^2. This corresponds to the *intrinsic* subthreshold slope $S_i \equiv SC_i$ at least one order of magnitude smaller than that for the best thin-film OFETs and amorphous hydrogenated silicon (α-Si:H) devices. [DOI: 10.1063/1.1622799]

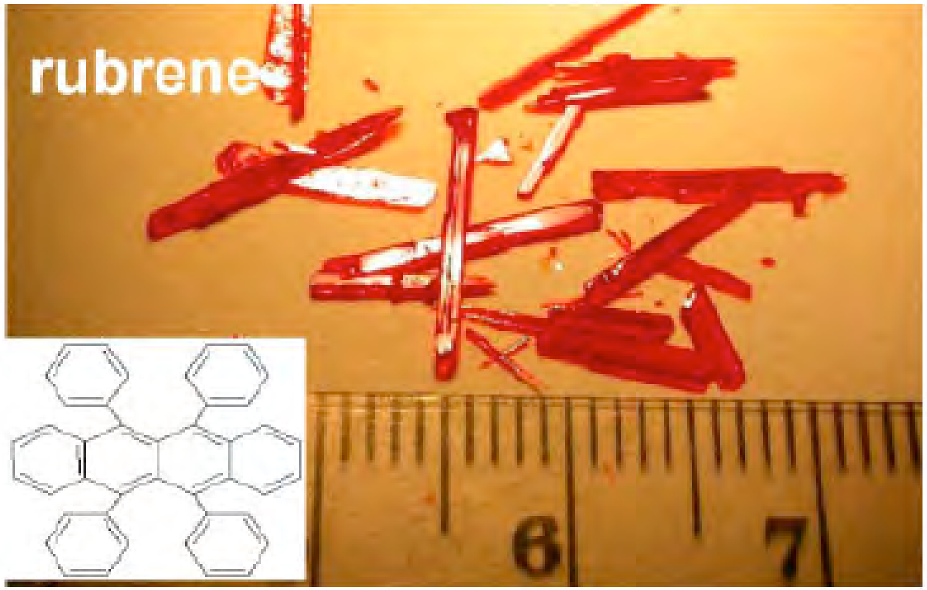

High Mobility of Dithiophene-Tetrathiafulvalene Single-Crystal Organic Field Effect Transistors

Marta Mas-Torrent,*,† Murat Durkut,† Peter Hadley,† Xavi Ribas,‡ and Concepció Rovira‡

Department of NanoScience, Delft University of Technology, Lorentzweg 1, 2628 CJ Delft, The Netherlands, and Institut de Ciència de Materials de Barcelona, Campus de la Universitat Autònoma de Barcelona, 08193 Bellaterra, Spain

JACS 126, 984 (2004)

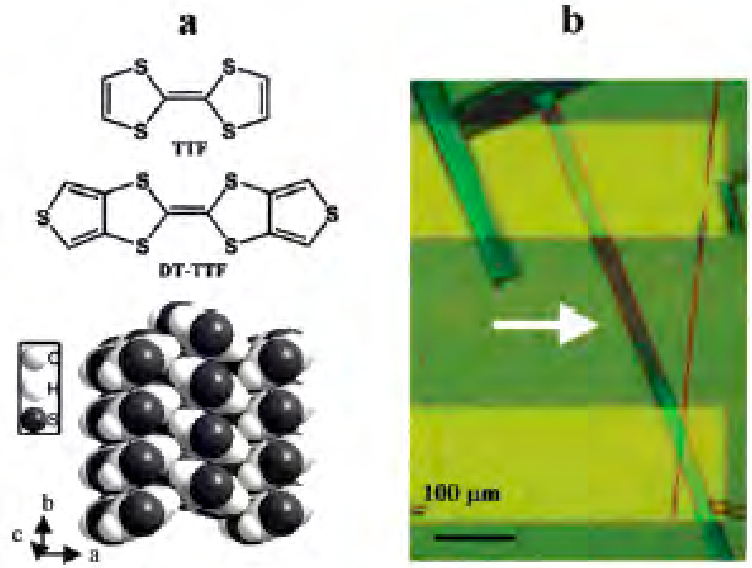

Figure 1. (a) Molecular structure of TTF and DT-TTF and crystal packing of DT-TTF. (b) The arrow points at the studied single crystal of DT-TTF formed on the microfabricated electrodes. The thin crystal to the right of the main bridging crystal was broken to avoid its contribution to the measurements.

$\mu = 1.4\ cm^2/Vs$

BTQBT 単結晶ワイヤーFET の作製

5 μm

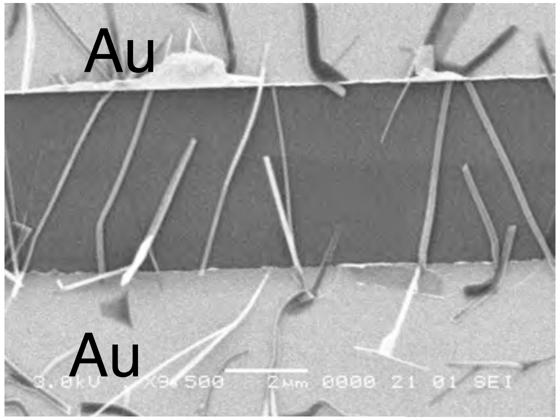

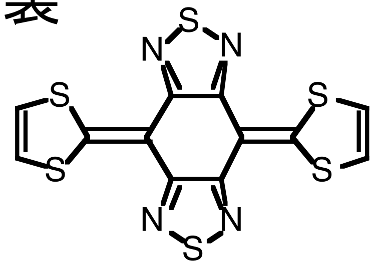

太さ 10-100 nm
長さ 5-30 mmの単結晶が
金電極に選択的にアンカー
(S と Au の親和性）

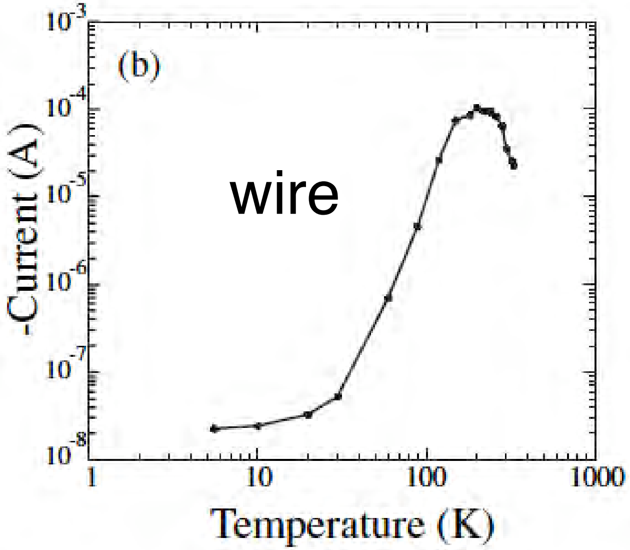

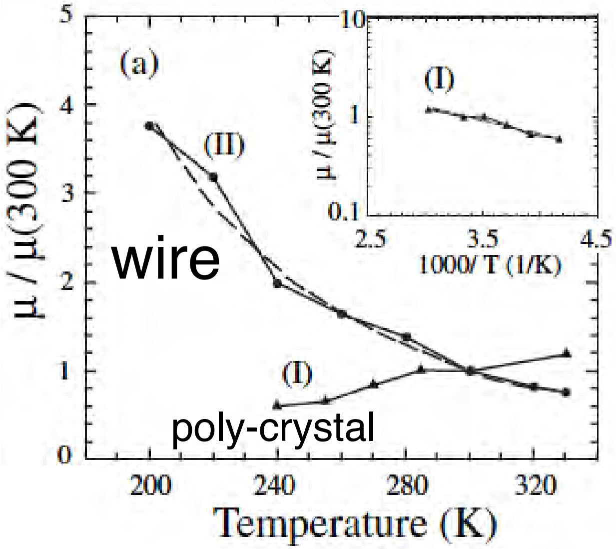

単結晶ワイヤー(II)：移動度が温度とともに減少（格子散乱の影響）
多結晶グレイン(I) ：熱活性化型の伝導

Film Morphology

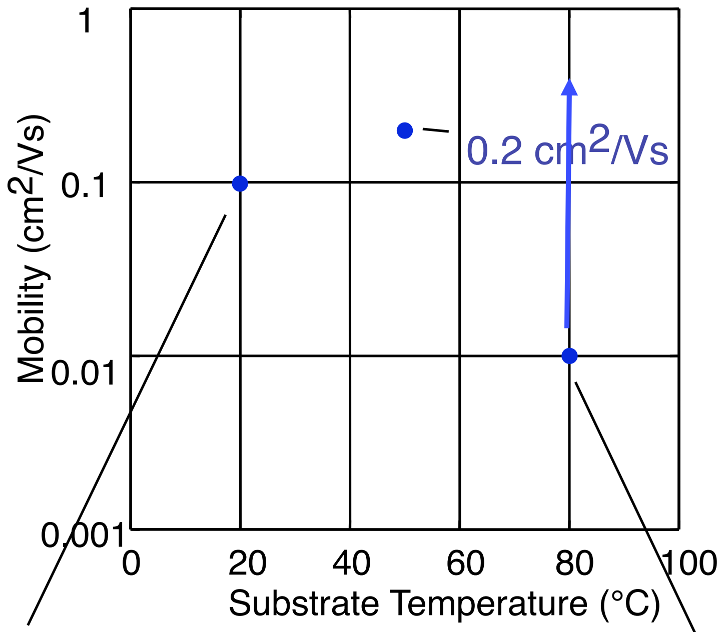

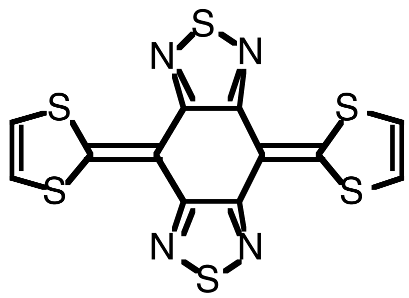

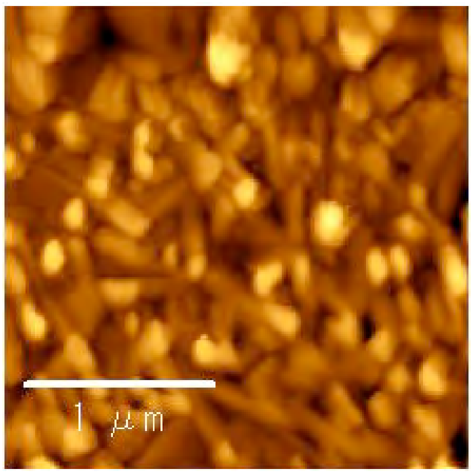

Small grains

AFM

SEM

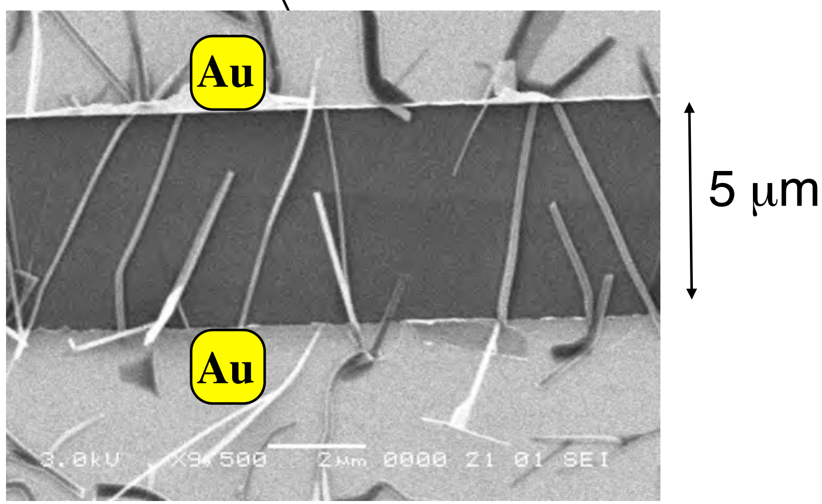

Wire

Summary 4

1. Electrical properties of organic semiconductors are affected strongly by the gas molecules adsorbed.
2. Organic FET Characteristics are also affected by gas adsorption. Ambipolar operation is observed in OFETs through careful control of impurities.
3. Work function of the source and drain electrodes is a key factor to determine OFET charatceristics. Ambipolar operation is achieved by choosing appropiate materials for electrodes.
4. Light-emitting OFETs are prepared with asymmetric electrodes in which both electrons and holes are injected into organic films.
5. Low carrier mobilities in thin film OFETs are caused by the existence of grain boundaries.
6. OFETs based on sigle crystals exhibit high carrier mobilities.

Our Research Targets

1 μm   100 nm   10 nm   1 nm

	Organic Field Effect Transistor	Electrochemical Approach for Molectronics	Molecular Assemblies on Si	Low Temperature STM
Target	Organic Laser Spin Transistor	Molecular-scale Electronic Devices		Spin-polarized STM
	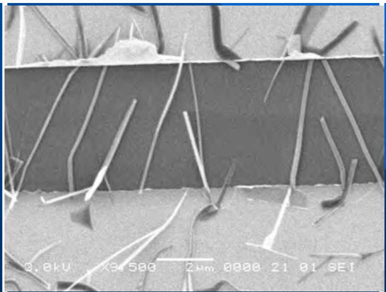 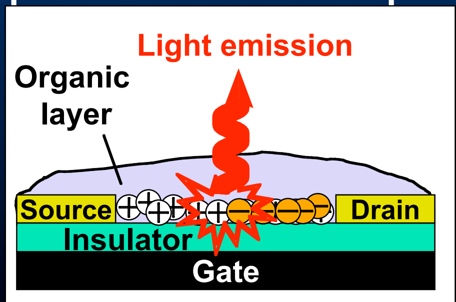	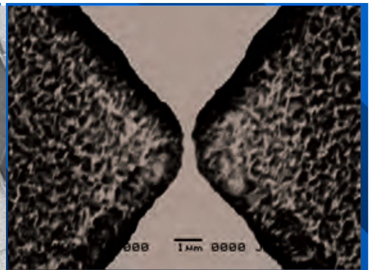	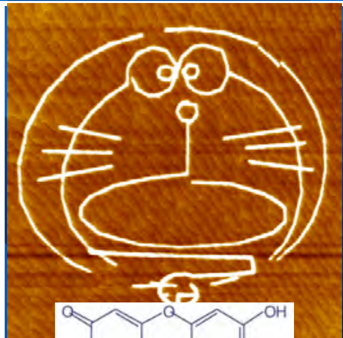 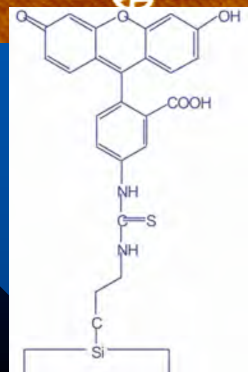	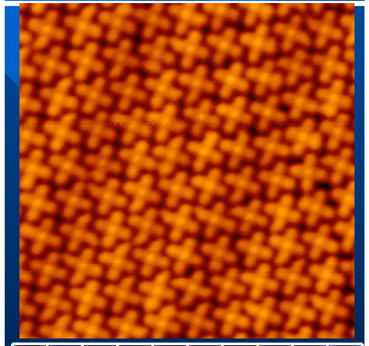 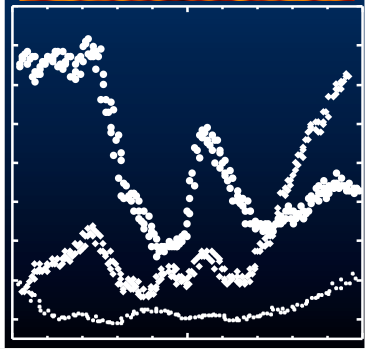

Nanogap Electrodes for Molecular-scale Electronics

Methods

Electron Beam Lithography	: (a few) - 30 - 100 nm
Focused Ion Beam	: 5 nm
Shadow (Mask) Deposition	: 10-20 nm
Electromigration	: 1 - 10 nm
Electroplating	: a few - 10 nm
(SAM) template	: molecular scale - 100 nm

EB lithography

Multi-curve Fitting Analysis of Temperature-Dependent I-V Curves of Poly-hexathienylphenanthroline-Bridged Nanogap Electrodes
K. Araki, H. Endo, H. Tanaka and T. Ogawa, JJAP 43, L634 (2004).

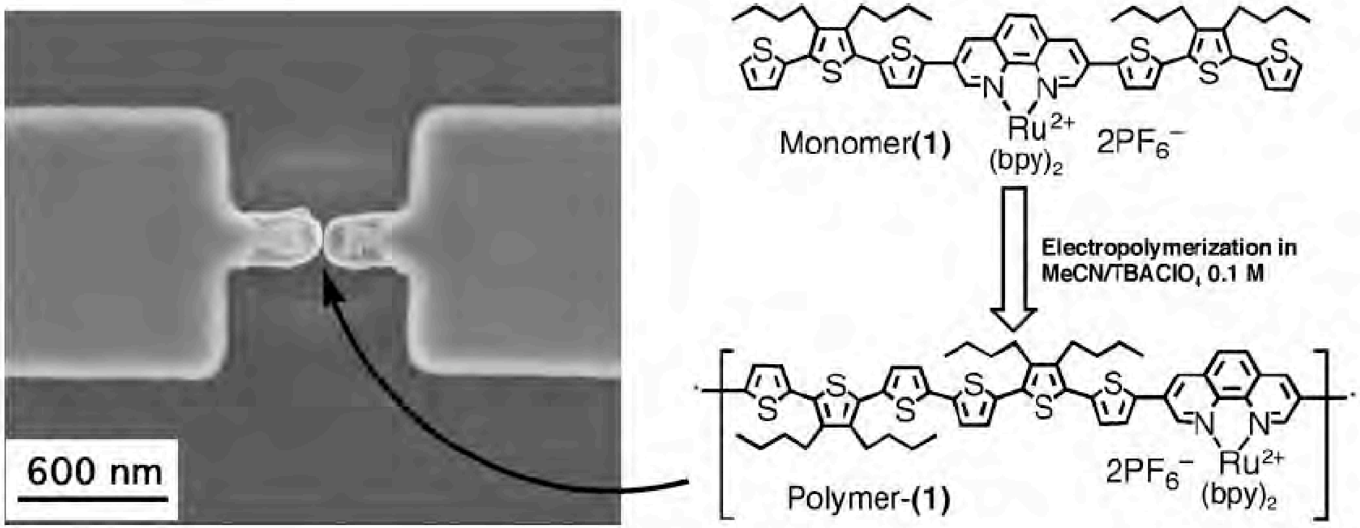

Fig. 1. Left: SEM micrograph showing a typical gold electrode with a gap of ~15 nm. Right: scheme of the electropolymerization reaction starting from monomer (1).

Gap = 15 nm
Thickness = Ti(2.6 nm)+Au(11 nm)

FIB

Fabrication of nano-gap electrodes for measuring electrical properties of organic molecules using focused ion beam
T. Nagase et al., @ KARC-CRL, Thin Solid Films 438/439, 374 (2004).

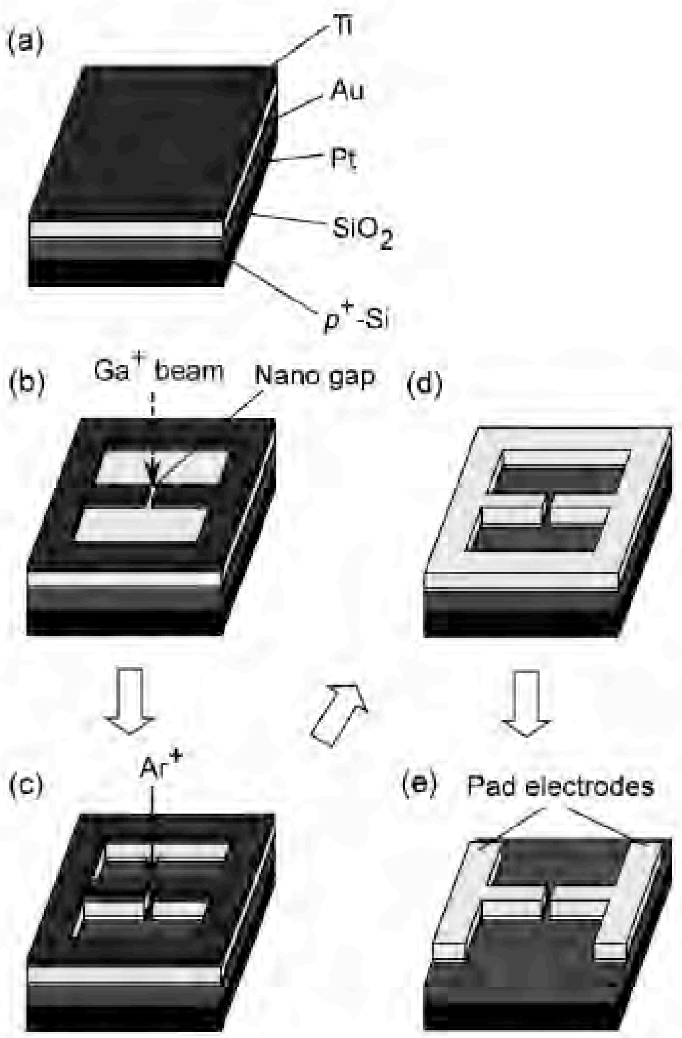

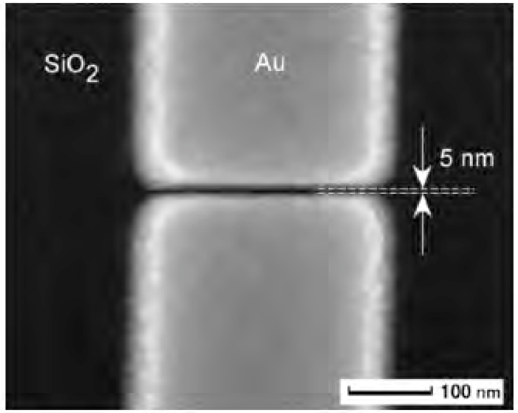

Fig. 3. SEM image of nano-gap electrode on SiO_2 substrate after transferring Ti mask pattern by Ar^+ etching and etching Ti mask with hot acid solution. Width of gap is ~5 nm.

Gap= 5 nm
Thickness = Pt (12nm)+Au(70nm)

Fig. 1. Schematic diagram of the FIB lithographic process for fabricating nano-gap electrodes: (a) Structure of the sample. (b) Mask fabrication by FIB etching. (c) Pattern transfer by Ar^+ etching. (d) Mask removal by wet etching. (e) Pad electrodes fabrication by photolithography.

Shadow deposition

A Reliable Method for fabricating sub-10 nm Gap Junctions Without Using Electron Beam Lithography
Y. Naitoh, K. Tsukagoshi,K. Murata and W. Mizutani @ AIST,
E-Journal of Sur. Sci. & Nanotech. 1, 41 (2003).

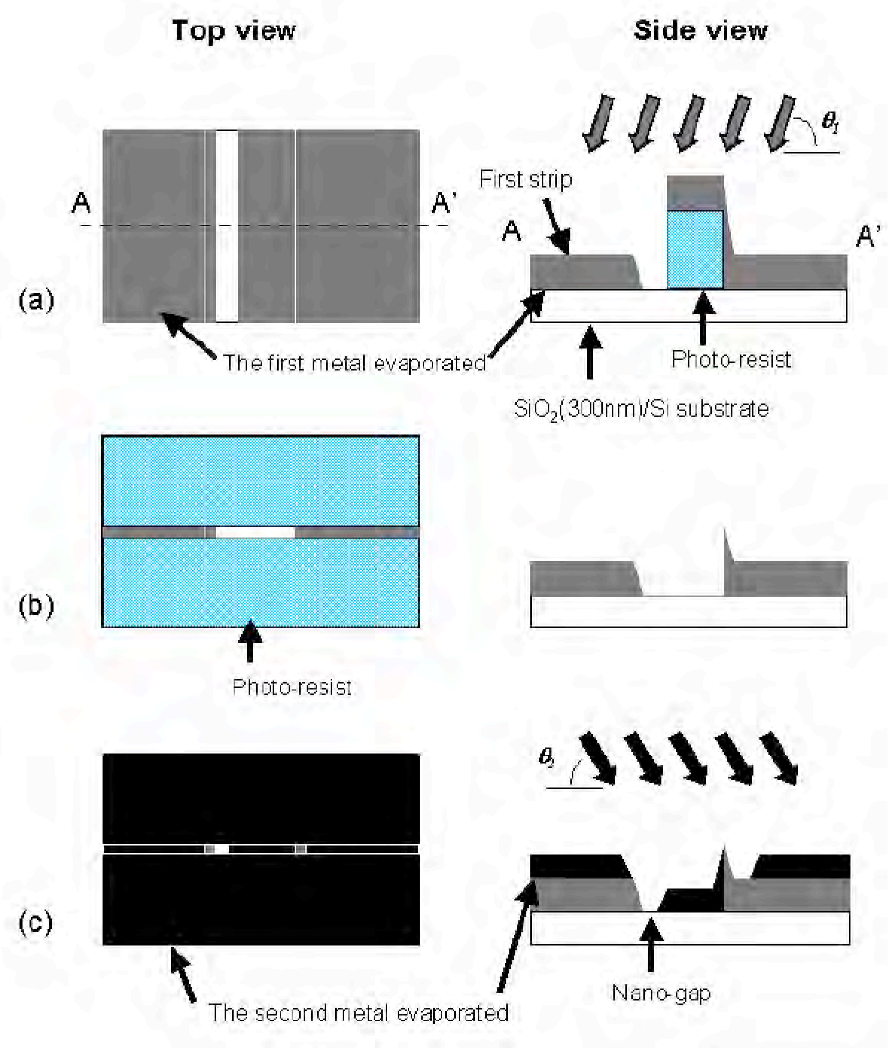

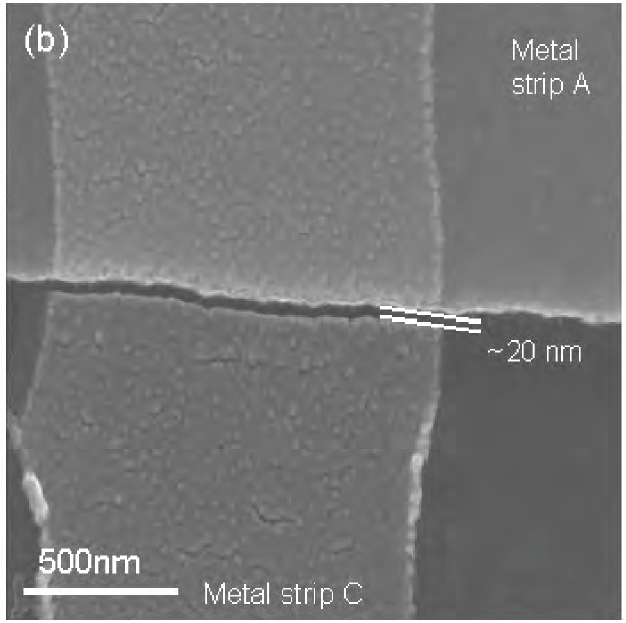

Gap= 10-20 nm

electromigration

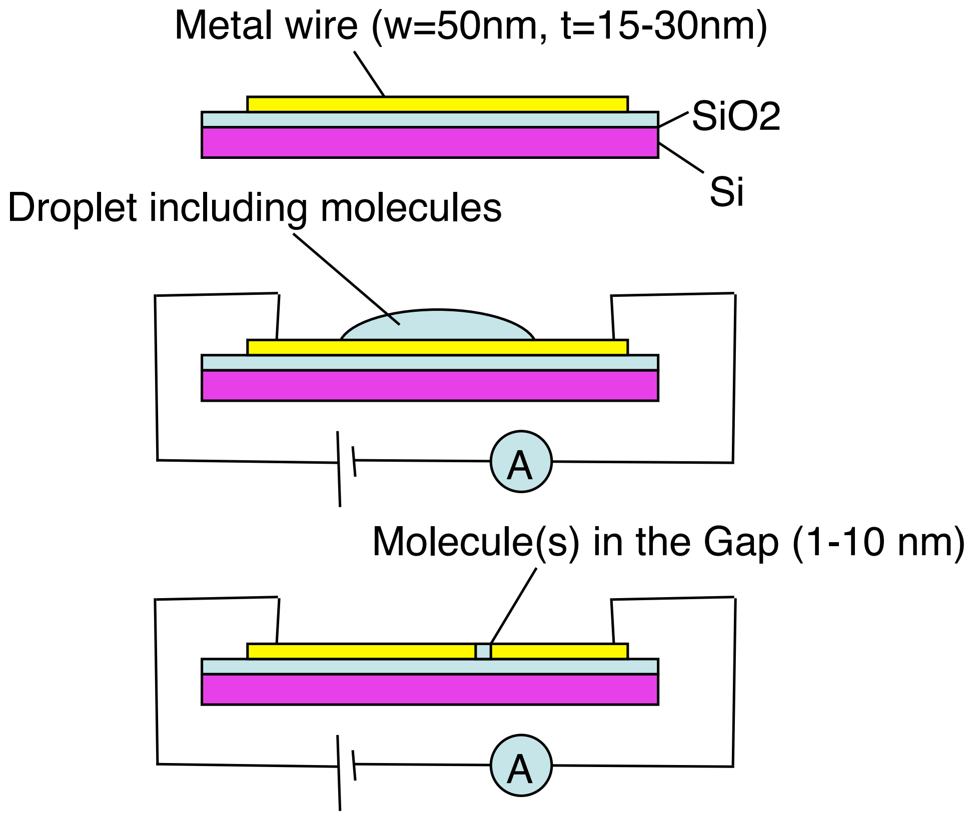

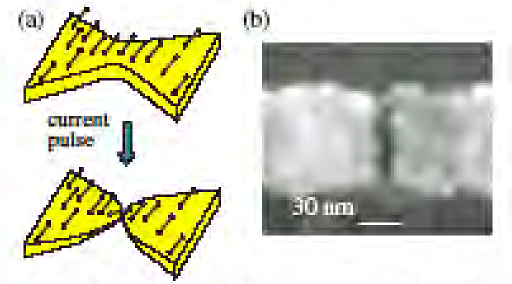

Figure 1. (a) A diagram of the electromigration technique for the fabrication of closely spaced electrodes bridged by individual molecules. (b) A micrograph of a typical result, with electrodes separated by <3 nm.

L. H. Yu and D. Natelson @ Rice Univ.,
Nanotechonology 15, S517 (2004).

Nano-gap electrodes prepared by electroplating

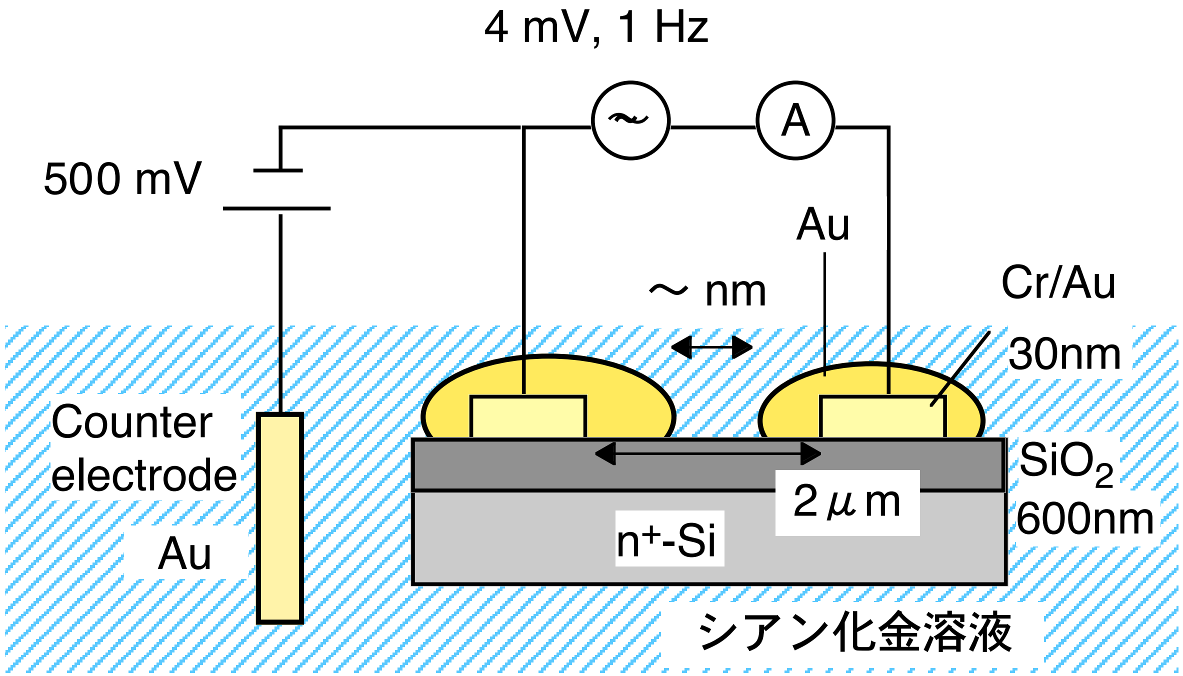

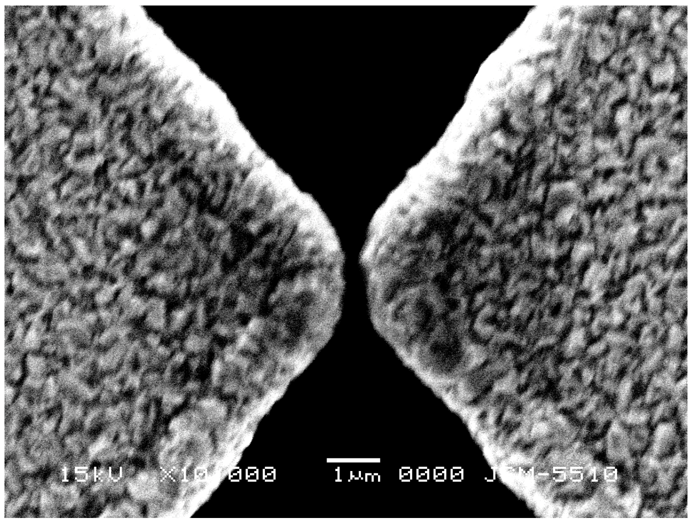

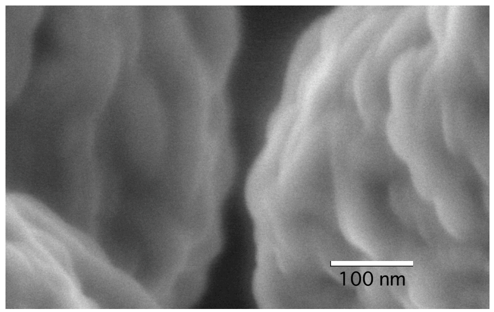

Synthesis of 10nm-length molecular wire

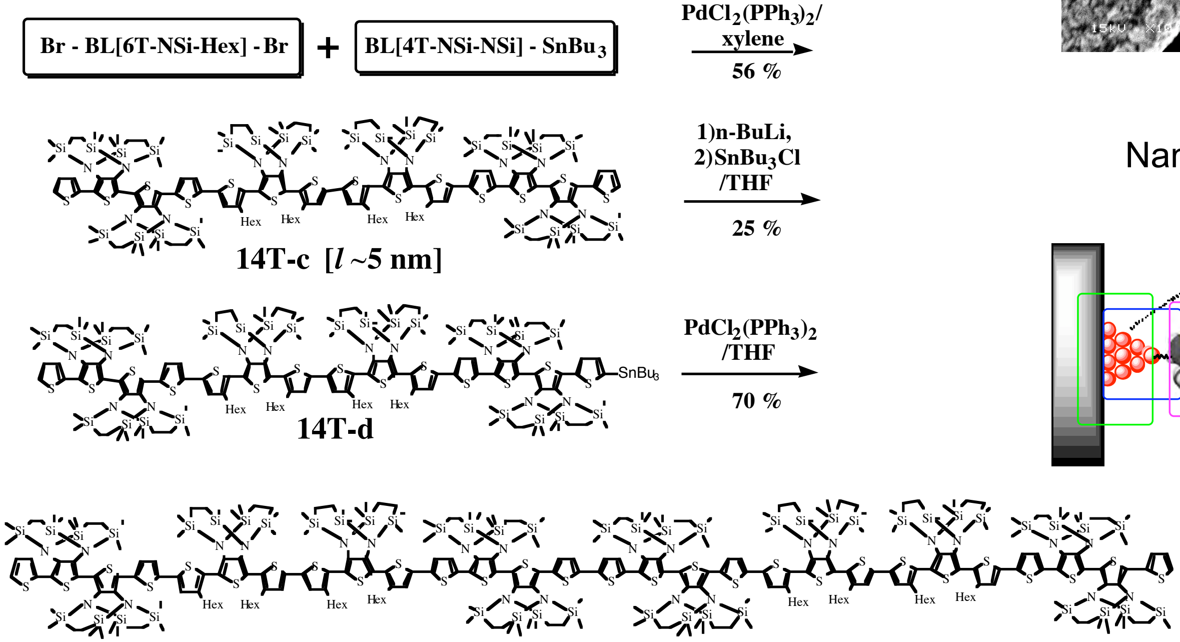

28T-a [l ~10 nm]

合成スキーム－4

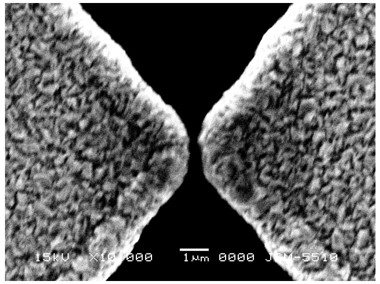

Nano-gap electrodes

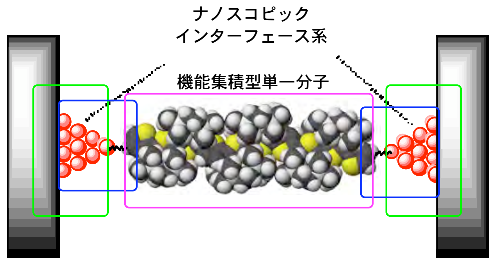

Shoji Tanaka @ IMS

Our Research Targets

1 μ m — 100 nm — 10 nm — 1 nm

	Organic Field Effect Transistor	Electrochemical Approach for Molectronics	Molecular Assemblies on Si	Low Temperature STM
Target	Organic Laser Spin Transistor	Molecular-scale Electronic Devices		Spin-polarized STM

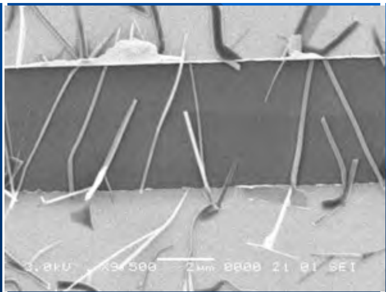

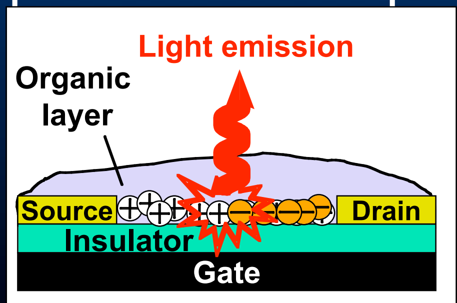

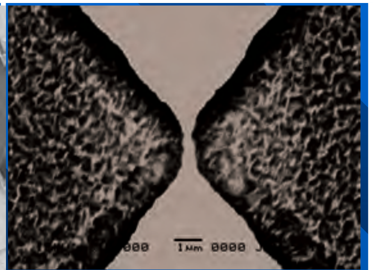

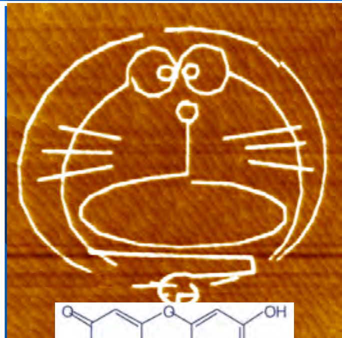

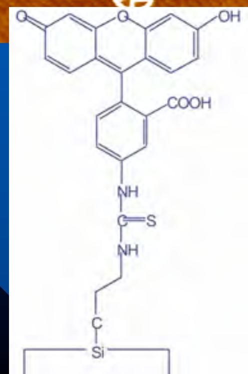

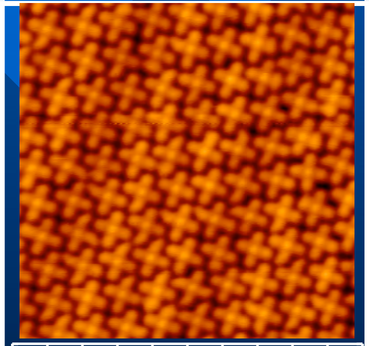

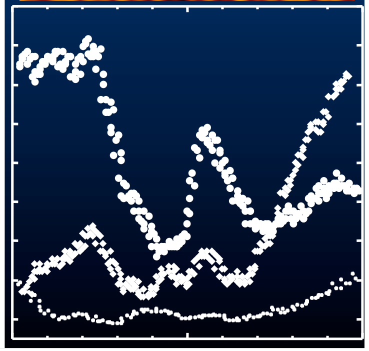

Difficulties in The Au-S System

How can we put the molecule to the specific site ?

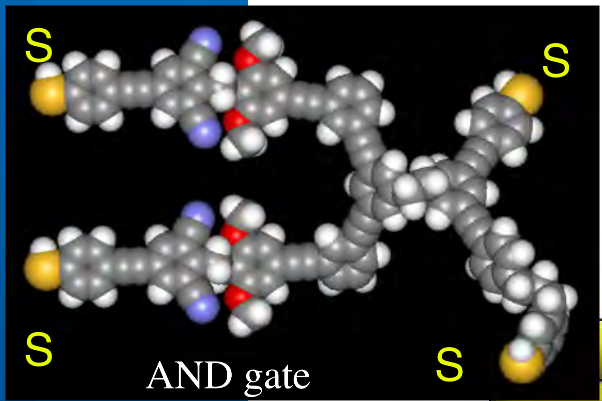

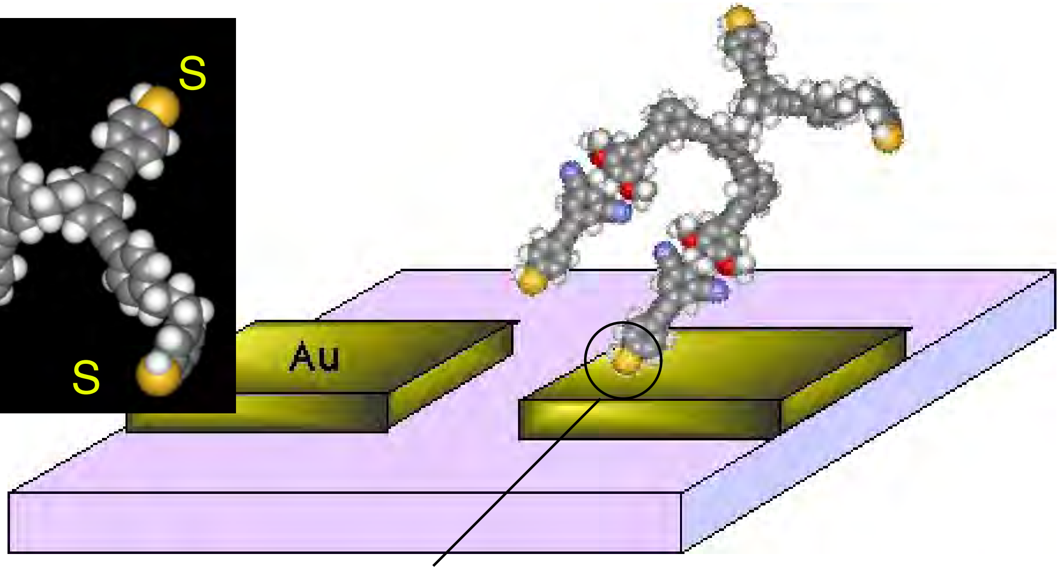

Ambiguous contact gives unreliable results

Visualization and Spectroscopy of a Metal-Molecule-Metal Bridge

G. V. Nazin, X. H. Qiu, W. Ho @ UC Irvine, Science302, 77 (2003).

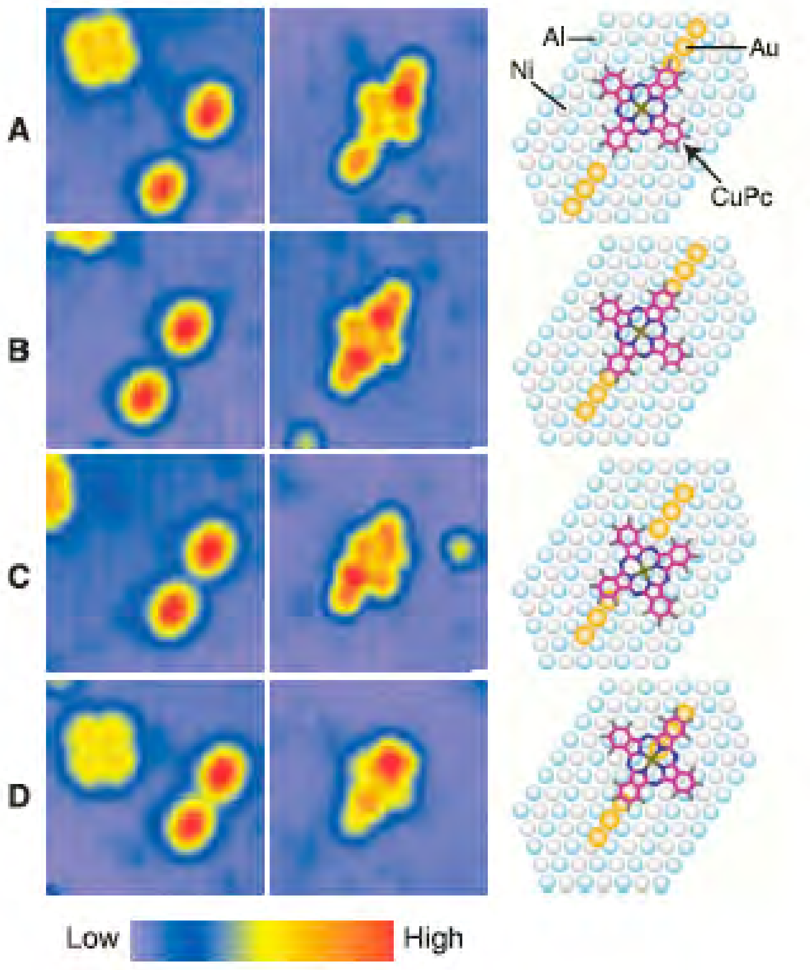

Fig. 2. CuPc@2Au_3 hybrid structures for different spacings between the two Au_3 chains. Left column: Bare 2Au_3 junctions before the molecules were added (imaging conditions: V_{bias} = 1 V, I = 1 nA; image size is 47 Å by 47 Å). Middle column: Assembled hybrid structures (V_{bias} = 0.5 V, I = 1 nA; these imaging conditions emphasize the molecular adsorption configuration). Right column: Schematics attributed to each adsorption configuration. (**A**) Six Ni-Ni lattice constants between the Au_3 chains. (**B**) Five lattice constants. (**C**) Four lattice constants. (**D**) Three lattice constants. All structures were built with the procedure described in Fig. 1.

Difficulties in The Au-S System

How can we put the molecule to the specific site ?

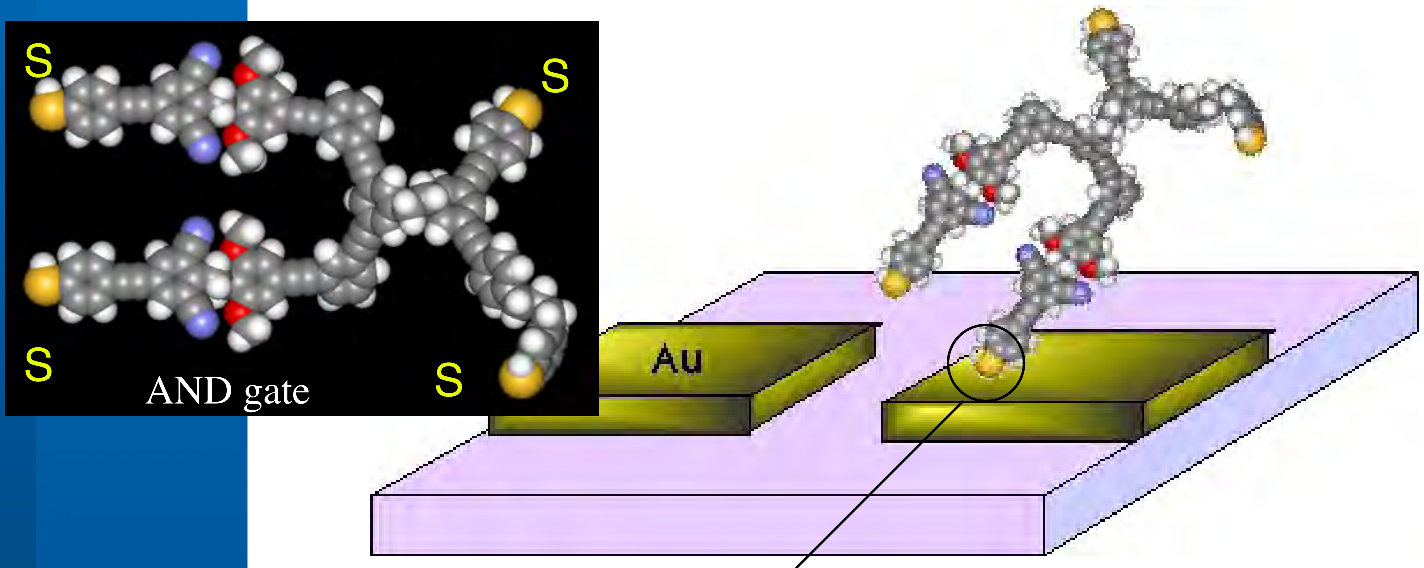

Ambiguous contact gives unreliable results

Reproducible Measurement of Single-Molecule Conductivity

X. D. Cui, S. M. Lindsay et al., @Arizona State U., Science 294, 571 (2001).

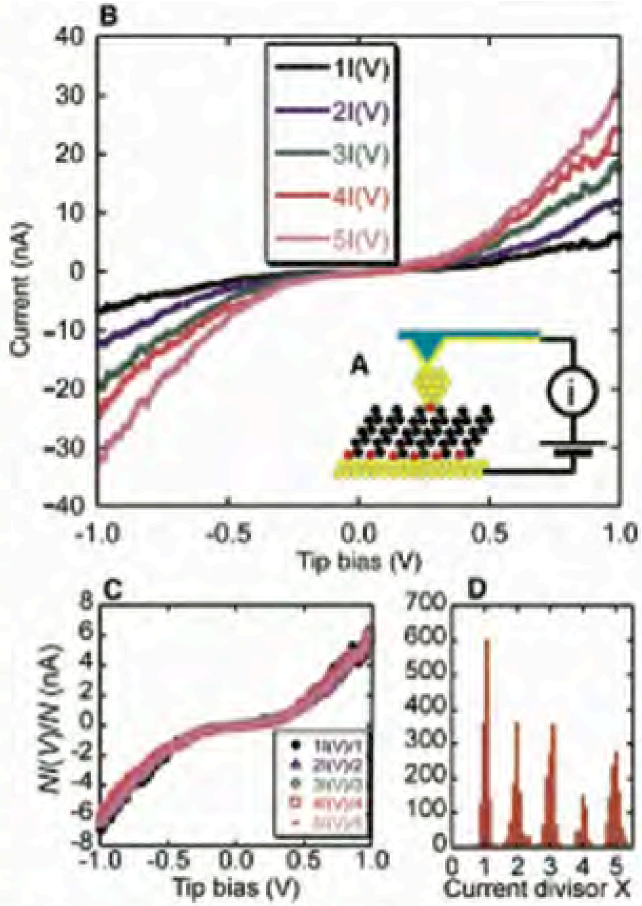

Fig. 1. (A) Schematic representation of the experiment. The sulfur atoms (red dots) of octanethiols bind to a sheet of gold atoms (yellow dots), and the octyl chains (black dots) form a monolayer. The second sulfur atom of a 1,8-octanedithiol molecule inserted into the monolayer binds to a gold nanoparticle, which in turn is contacted by the gold tip of the conducting AFM. (B) $I(V)$ curves measured with the apparatus diagrammed in (A). The five curves shown are representative of distinct families, $NI(V)$, that are integer multiples of a fundamental curve, $I(V)$ ($N = 1, 2, 3, 4$, and 5). (C) Curves from (B) divided by 1, 2, 3, 4, and 5. (D) Histogram of values of a divisor, X (a continuous parameter), chosen to minimize the variance between any one curve and the fundamental curve, $I(V)$. It is sharply peaked at integer values 1.00 ± 0.07 (1256 curves), 2.00 ± 0.14 (932 curves), 3.00 ± 0.10 (1002 curves), 4.00 ± 0.10 (396 curves) and 5.00 ± 0.13 (993 curves). (Spreads are ± 1 SD.) Of 4579 randomly chosen curves, over 25% correspond to the $X = 1$ (single-molecule) peak. No obvious correlation was noted between particle size and number of molecules contacted. Conducting atomic force microscopy data were acquired with a PicoSPM microscope (Molecular Imaging) using silicon cantilevers (spring constant, 0.35 N/m) sputter-coated with 5 nm of chromium followed by 50 nm of gold. Imaging was done under toluene in a nitrogen atmosphere.

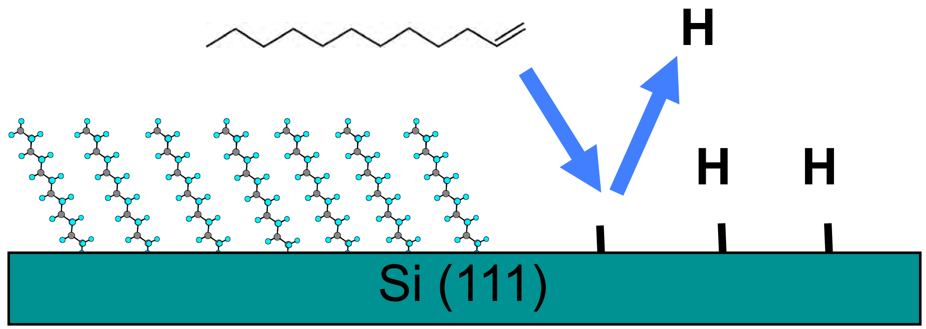

Si-C vs Au-S

	Si-C	Au-S
• Interface	covalent	not clear
• Variation	P-type, N-type low conductive to metallic	△
• Homogeneity	△	○
• Selective Growth	○	△

we can use micro- and nano- fabrication techniques for semiconductor devices

Molecular Assemblies on Silicon Surfaces via Si-C Covalent Bonds

key technology: deactivate of the dangling-bonds

Dry Process

Clean Si(111), Si(100) surfaces in UHV

R. Hamers @ U-Wisconsin
J. Yoshonobu @ U-Tokyo
.
.
.

Wet Process

Termination of dangling -bonds of Si(111) with H and X(halogen) atoms.

J. M. Buriak @ Purdue-U
C. Chidsey @ Stanford
K. Uosaki @ Hokkaido-U
H. Sugimura @ Nagoya-U
T. Osaka @ Waseda-U
.
.
.

Self-directed growth of molecular nanostructures on silicon

G. P. Lopinski et al. @ Steacie Institute for Molecular Science, Canada
Nature 406, 48 (2000).

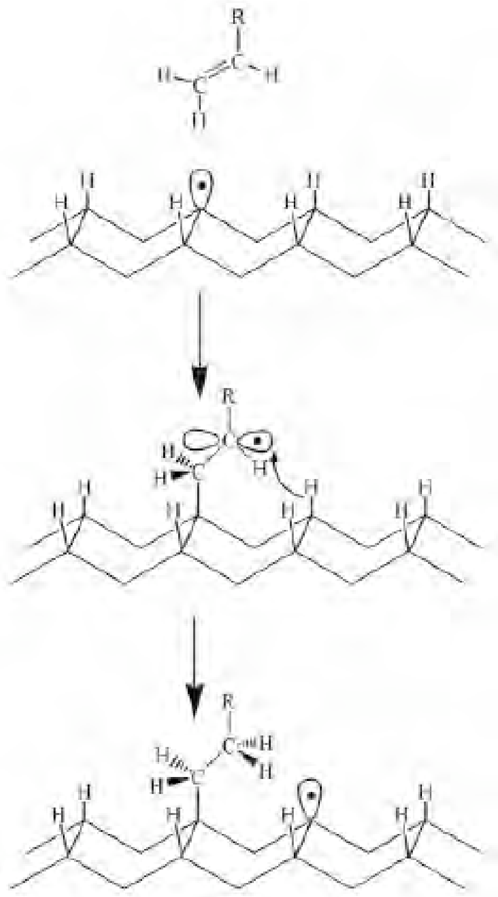

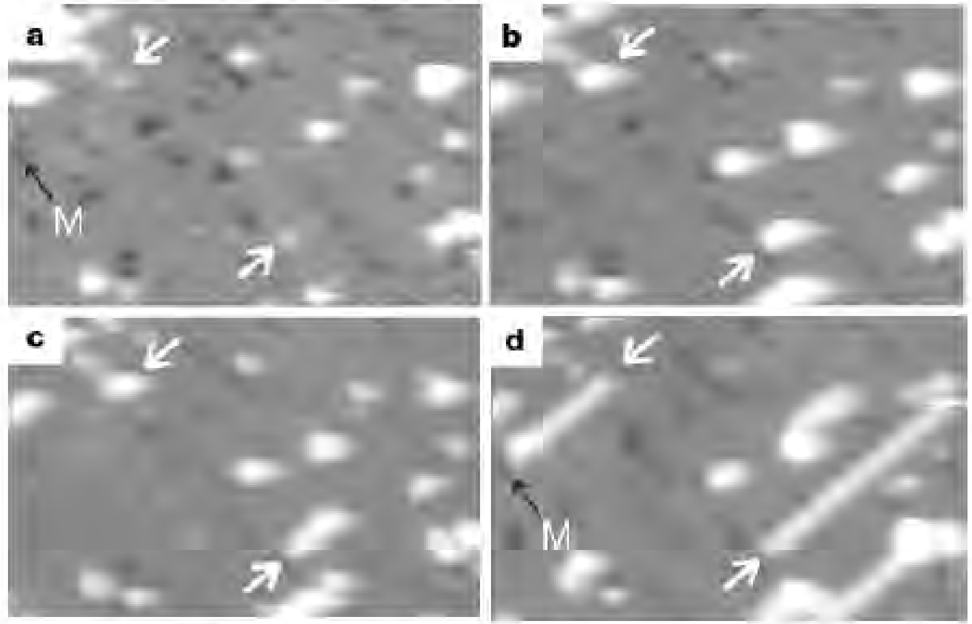

Figure 2 Growth of styrene lines on a H-terminated Si(100) surface with a dilute concentration of single Si dangling bonds. The figure shows a sequence of STM images (250 Å × 140 Å, −2.1 V, 47 pA) corresponding to an increasing exposure to styrene: **a**, 3 L; **b**, 28 L; **c**, 50 L; and **d**, 105 L. The white arrows denote two particular dangling-bond sites that lead to the growth of long styrene lines. The missing dimer defect (M) marked in the figure terminates the growth of the line in the top left-hand corner of the image.

Si-C covalent bond formation on amorphous silicon (wet process)

J. M. Buriak,
Chem. Commun. 1051 (1999).
Adv. Mater. 12, 859 (2000).

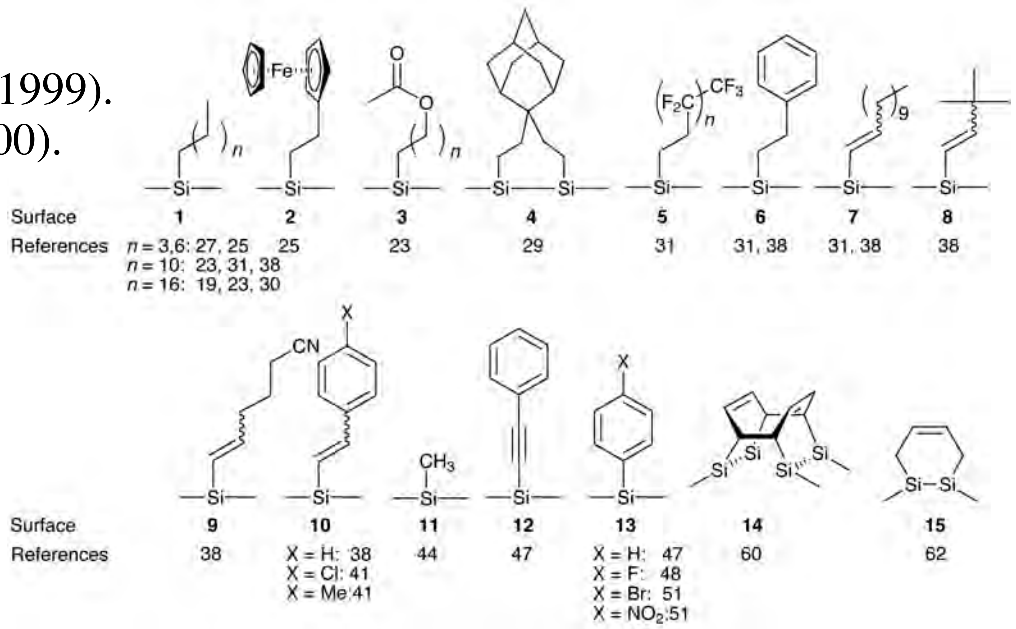

$[RC(O)O]_2$ -> 2 RC(O)O·

RC(O)O· -> R· + CO_2

R· + HSi --> RH + ·Si

R'CH=CH_2 + ·Si -> R'(CH·)CH_2-Si

Experimental

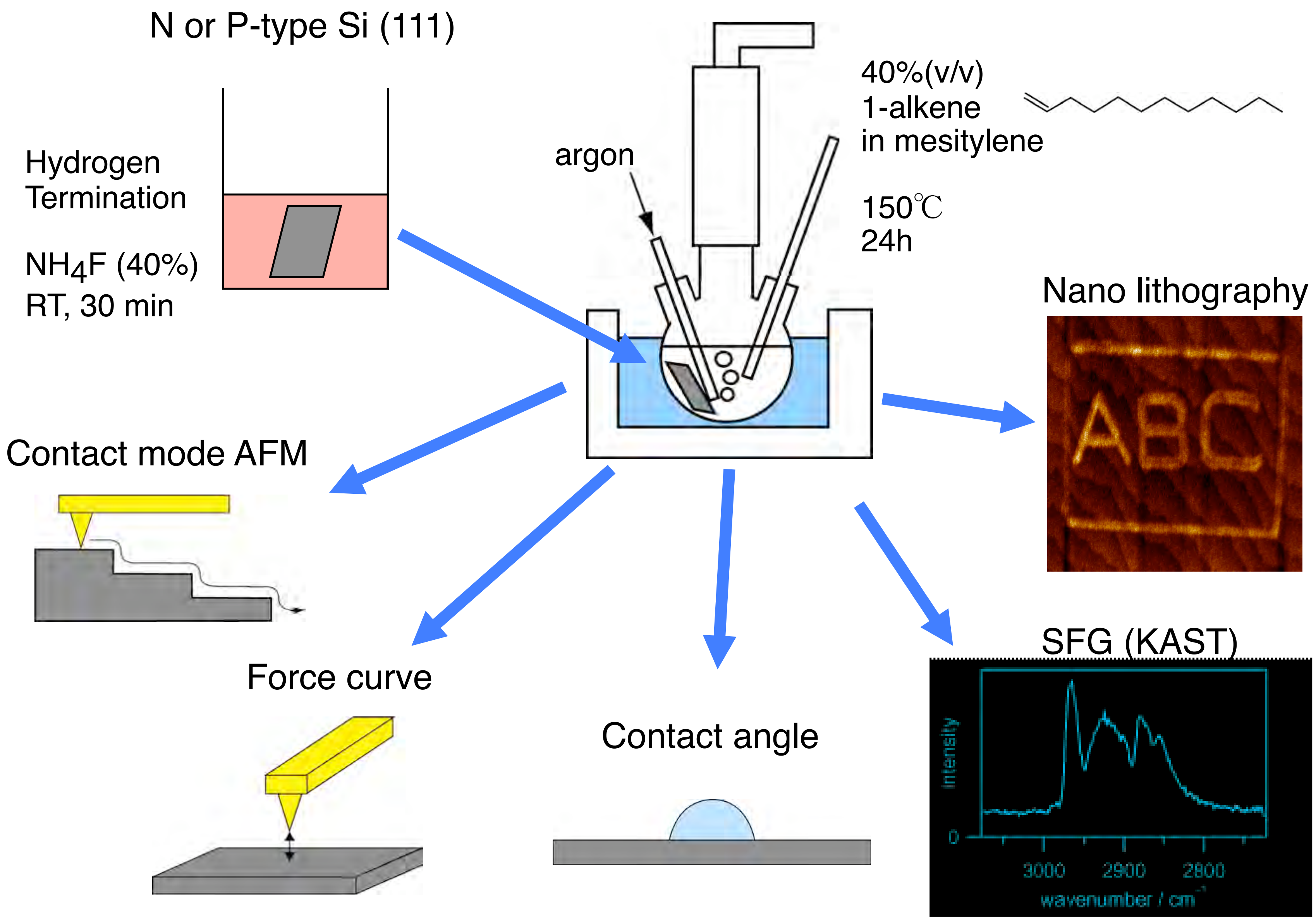

Molecules

C6 ～C18

1-Dodecene
$CH_3(CH_2)_9CH{=}CH_2$ (C12)

1-Octadecene
$CH_3(CH_2)_{15}CH{=}CH_2$ (C18)

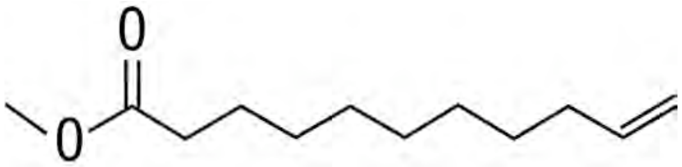

Methyl 10-Undecenoate
$CH_2{=}CH(CH_2)_8\ COOCH_3$

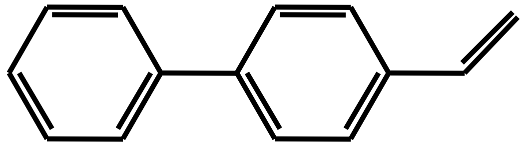

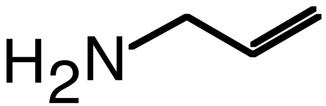

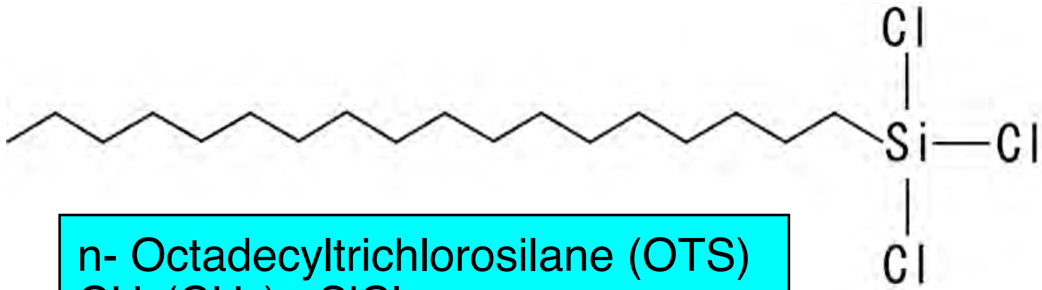

n- Octadecyltrichlorosilane (OTS)
$CH_3(CH_2)_{17}SiCl_3$

Water contact angle measurements

H-terminated Si (111)

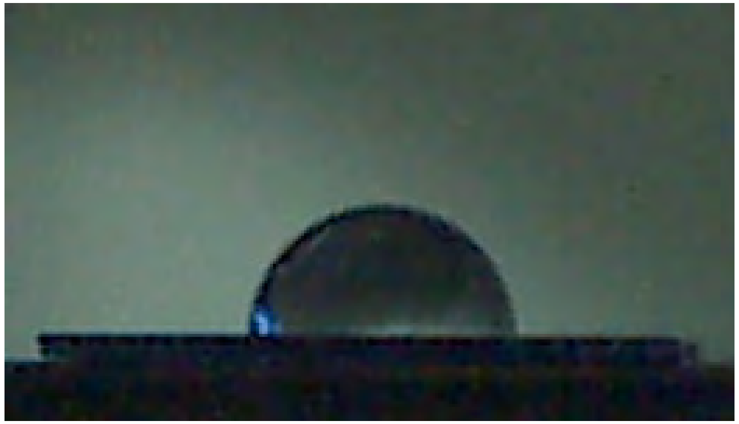

1-Dodecene

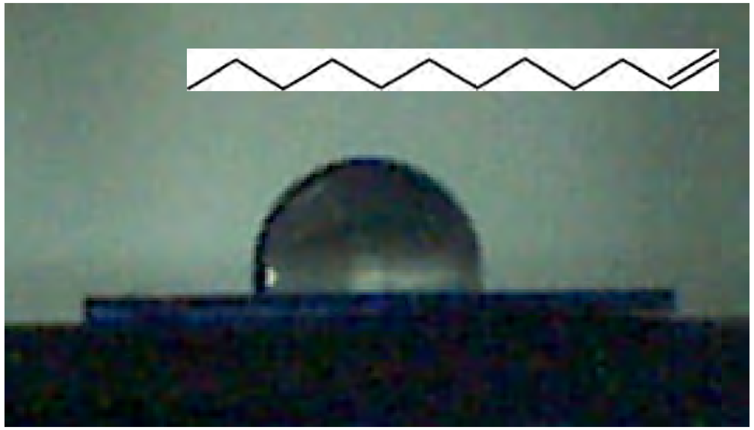

Methyl 10 - Undecenoate

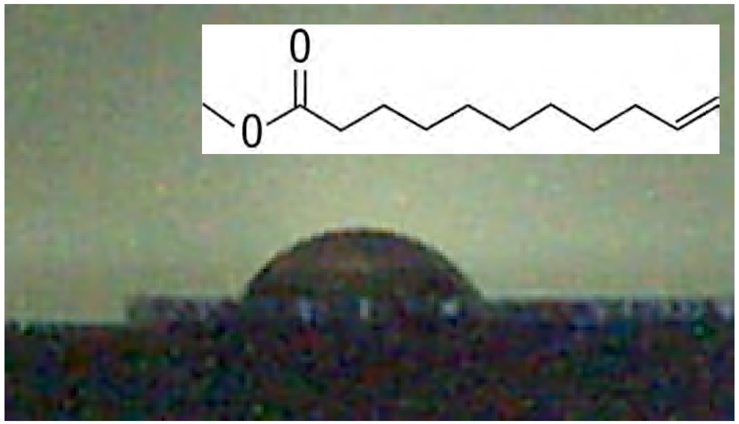

AFM nano lithography

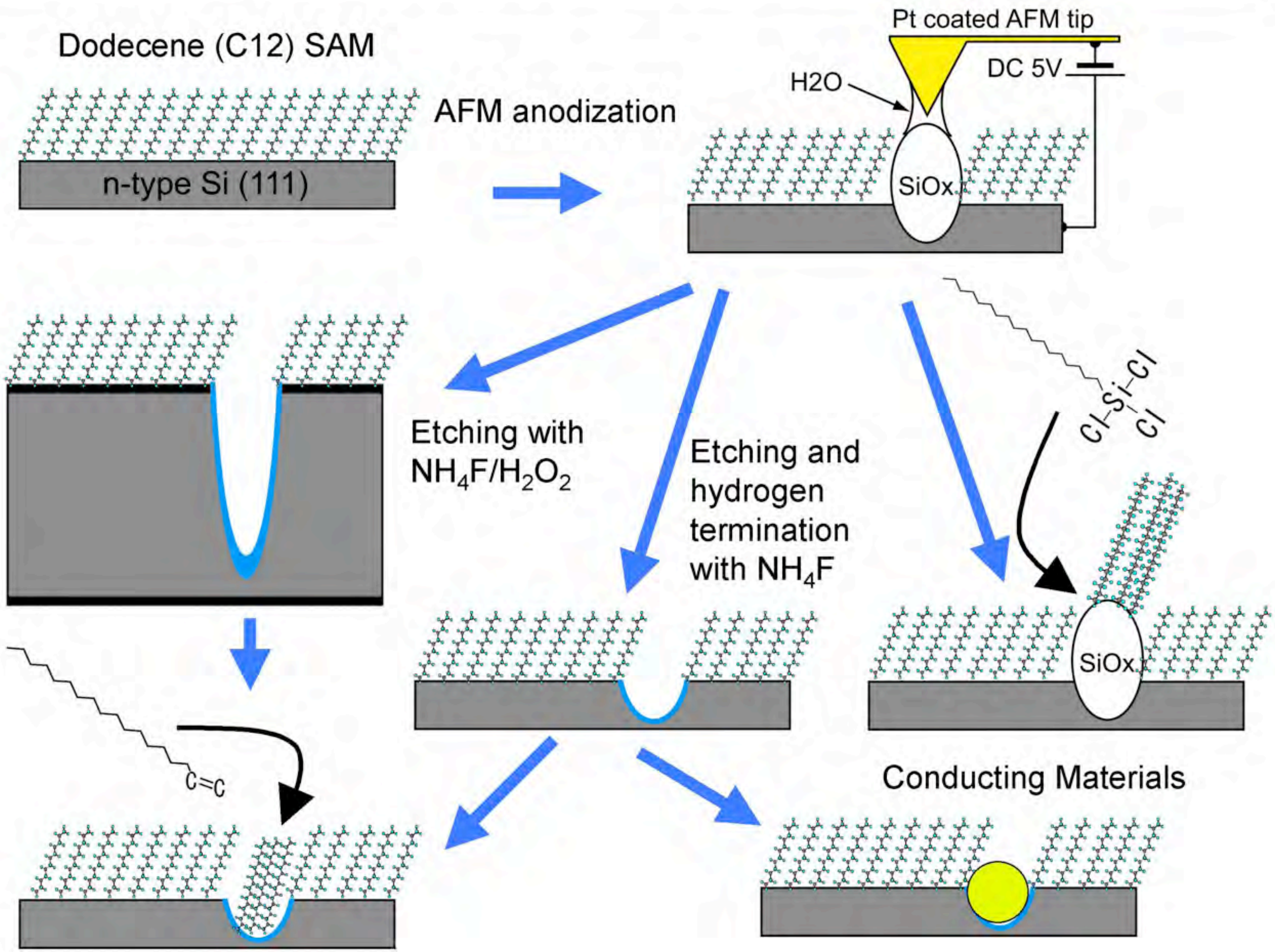

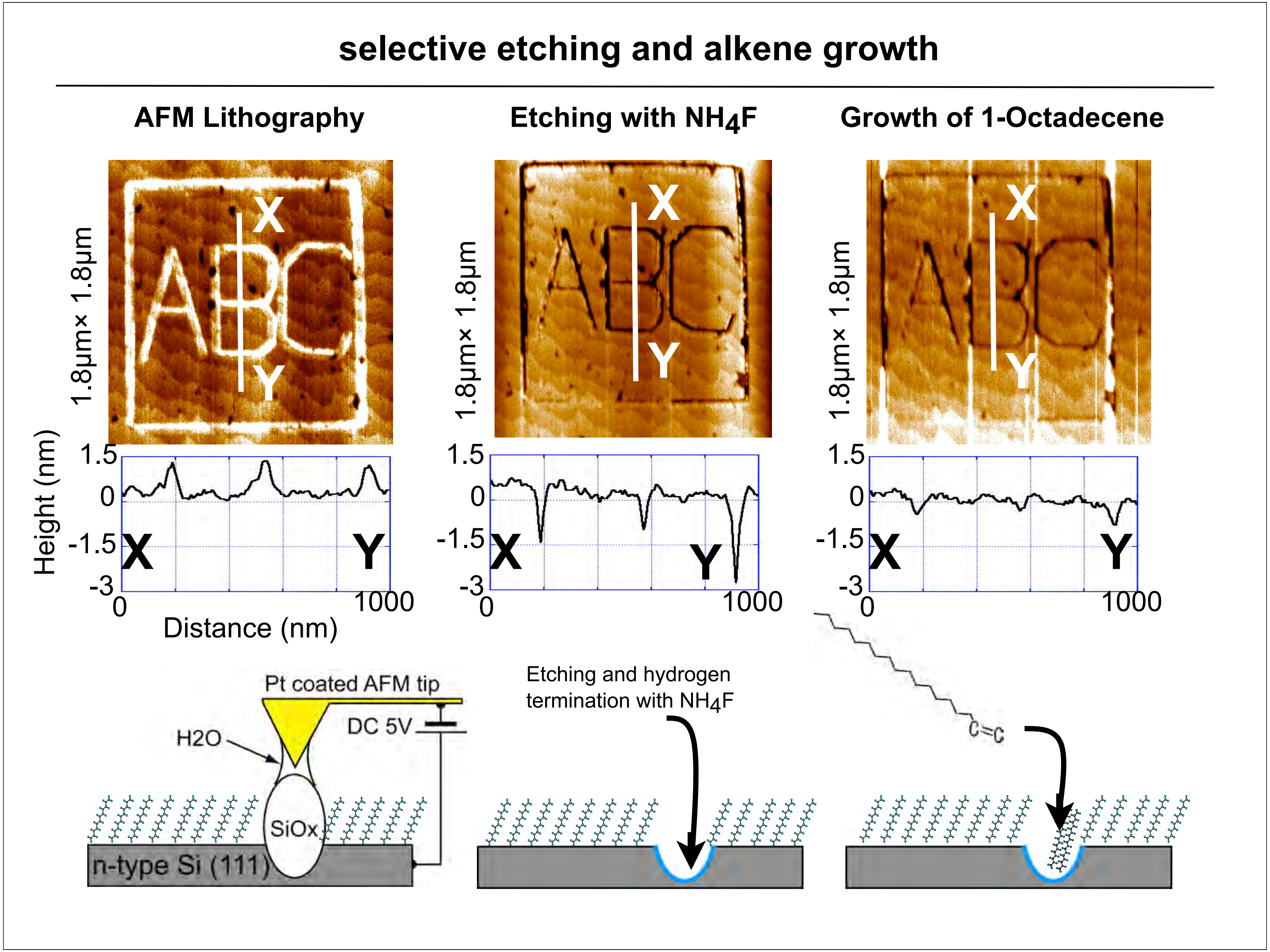
selective etching and alkene growth
AFM Lithography
Etching with NH4F
Growth of 1-Octadecene
X
Y
1.8μm× 1.8μm
Height (nm)
1.5
0
-1.5
-3
0
1000
Distance (nm)
Pt coated AFM tip
DC 5V
H2O
SiOx
n-type Si (111)
Etching and hydrogen termination with NH4F
C=C

色素の選択植え付け

Fluorescein-4-isothiocyanate (l=520 nm)

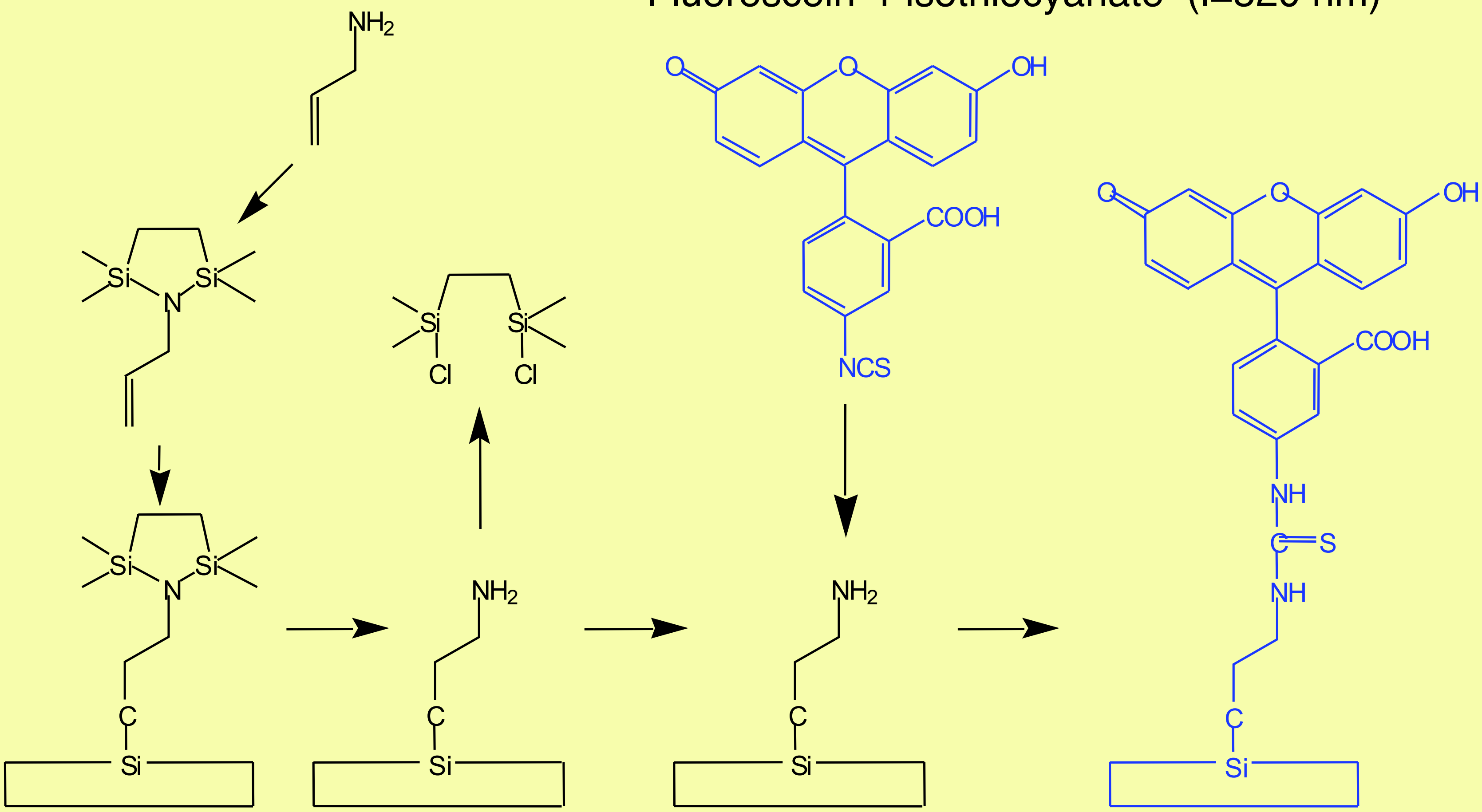

Photoluminescence Spectra of Organic dye on Si

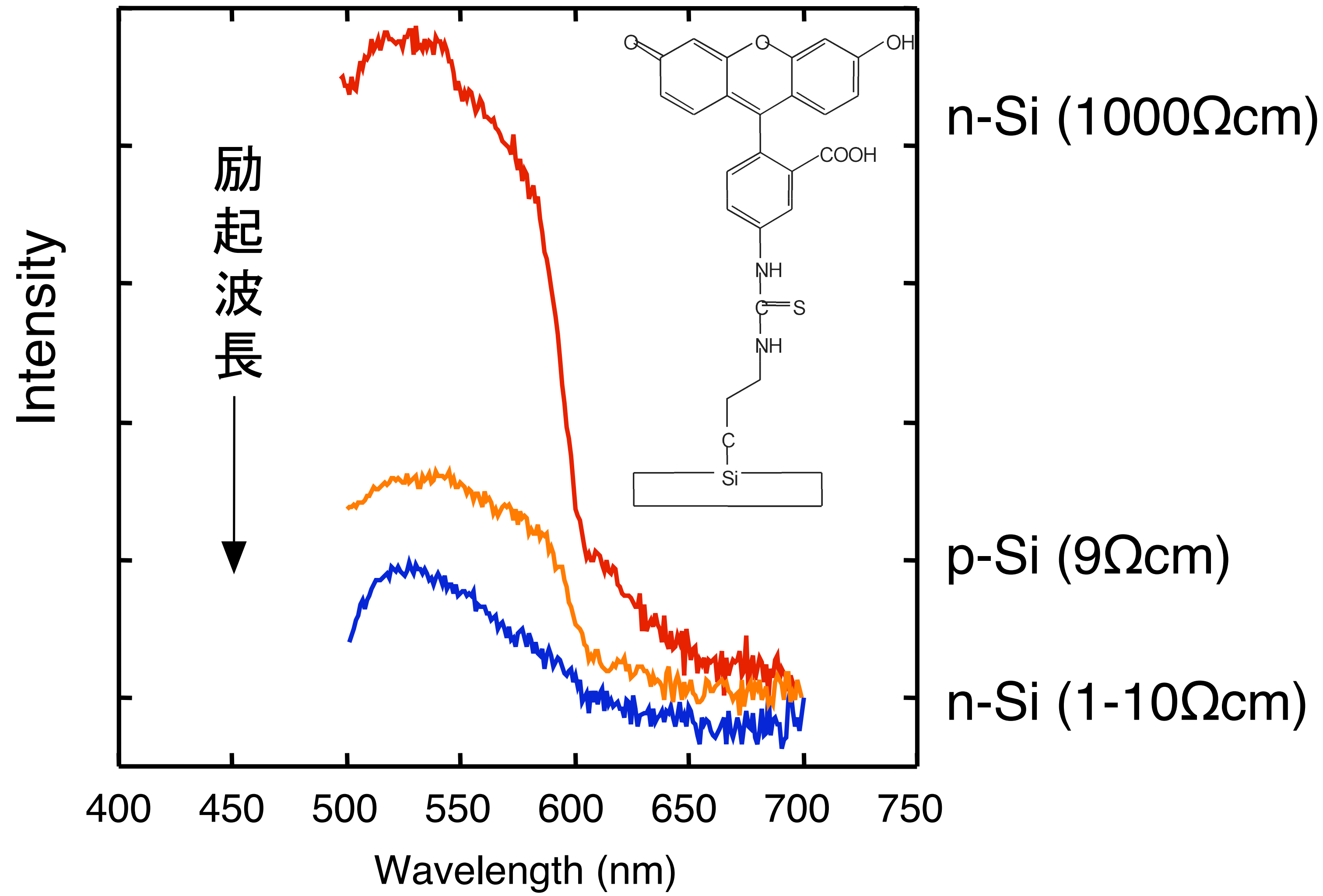

Our Research Targets

1 μ m   100 nm   10 nm   1 nm

	Organic Field Effect Transistor	Electrochemical Approach for Molectronics	Molecular Assemblies on Si	Low Temperature STM
Target	Organic Laser Spin Transistor	Molecular-scale Electronic Devices		Spin-polarized STM

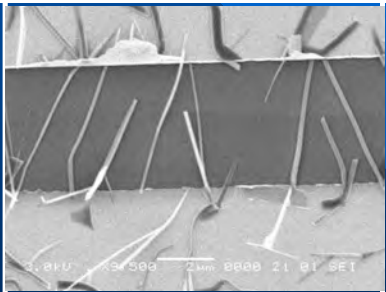

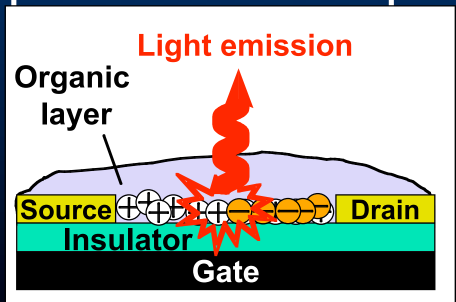

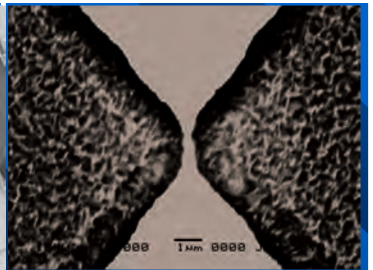

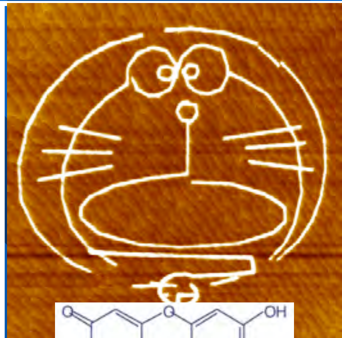

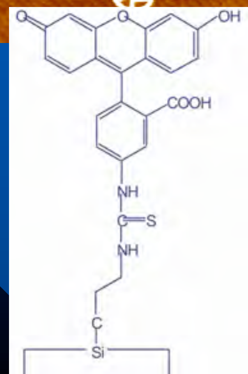

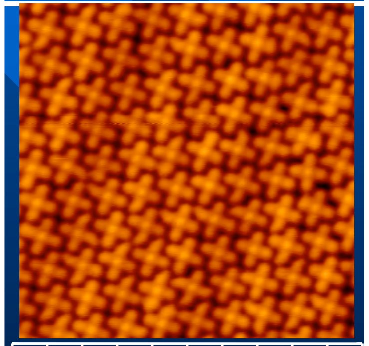

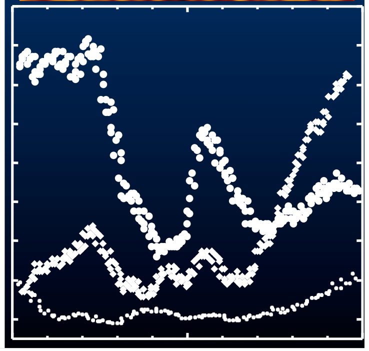

Molecular-based Electronics

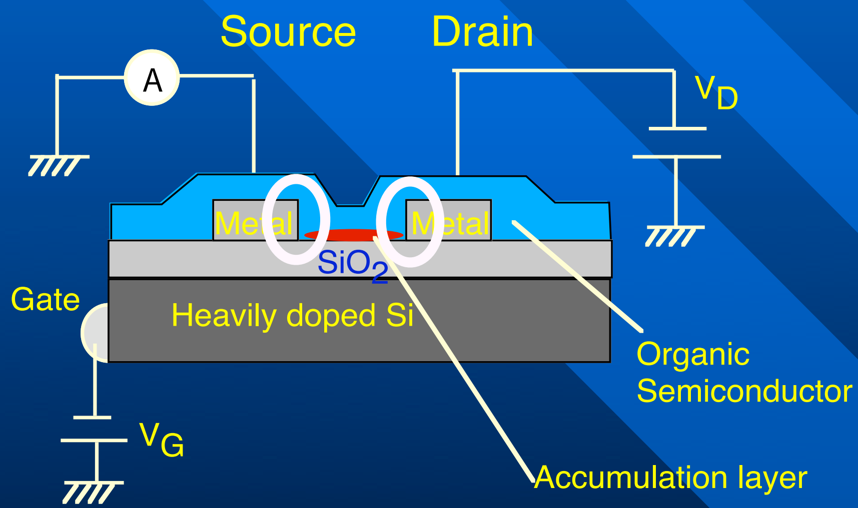

Molecular-scale Electronics

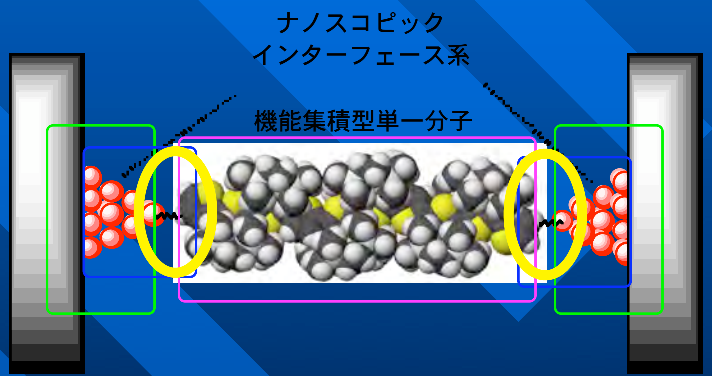

New electronic states induced by adsorption of molecules

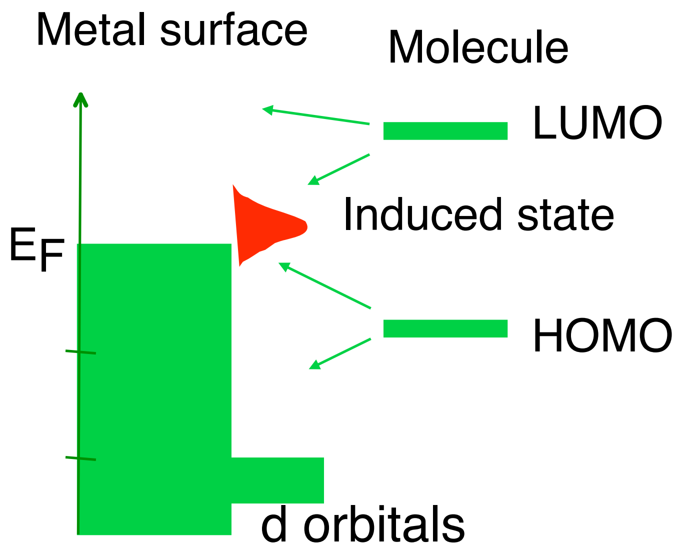

New States around the Fermi Level (E_F); Adsorption-induced states

XPS: N_2, CO, Benzene on Cu(110), Ni(110)

A. Nilsson et al., Phys. Rev. Lett. 78, 2847(1997).

Two-photon photoemission spectroscopy: Benzene on Cu(111)

T. Munakata & K. Shudo, Surf. Sci. 433, 184(1999).

STM, MAES: Benzene on Pd(110)

J. Yoshinobu, et at. Phys. Rev. Lett. 79, 3942(1997).

STM/STS: C60 on Ag(100)

X. Lu et al.@UC Berkeley, Phys. Rev. Lett. 90, 096082 (2003).

Low temperature STM / JEOL 4500LT

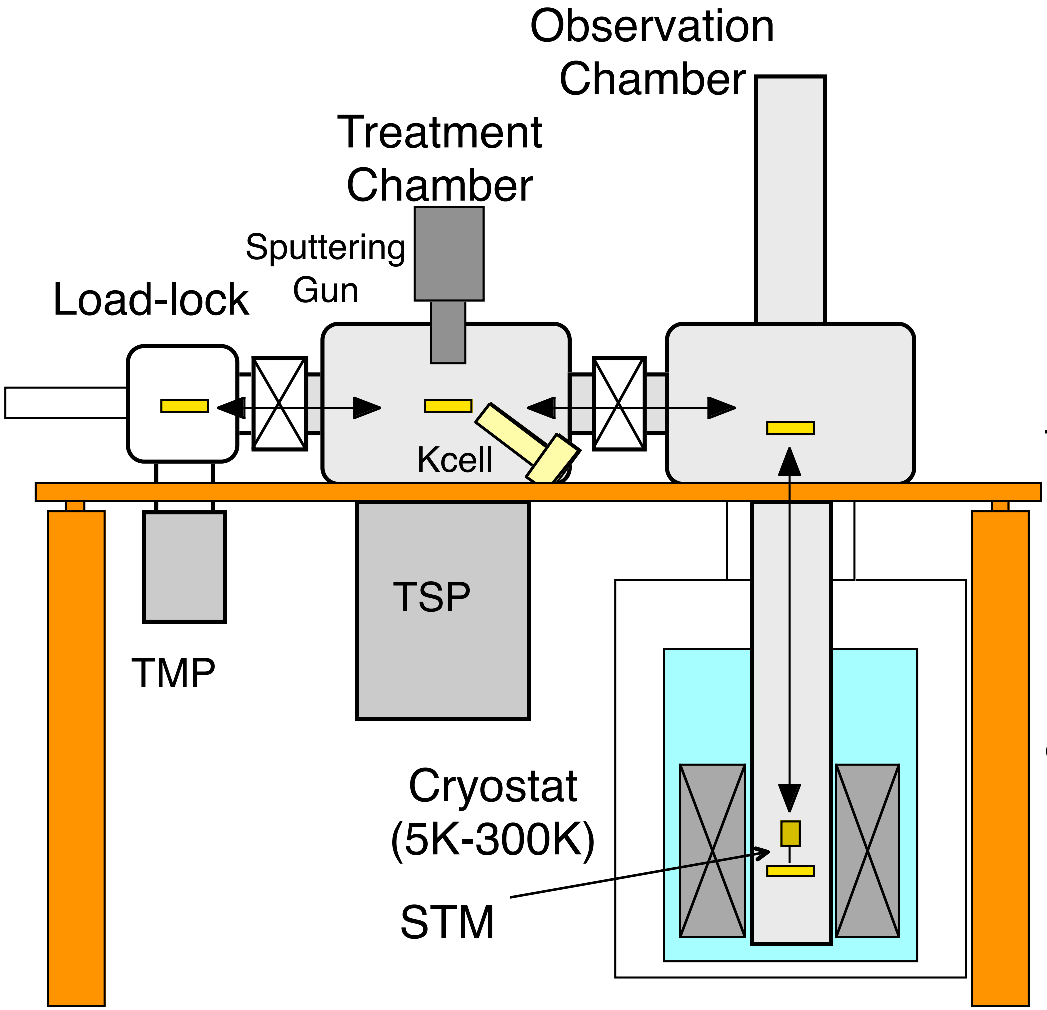

STM at 5K ~ 300K

Base pressure;

Load-lock; < 1.0 x 10^{-6} Pa
Treatment chamber
< 2.0 x 10^{-8} Pa
Observation chamber
< 1.0 x 10^{-8} Pa

dI/dV spectrum ;
Lock-in technique
ac signal(3mV, 320 Hz)
open-loop

Principle of STS

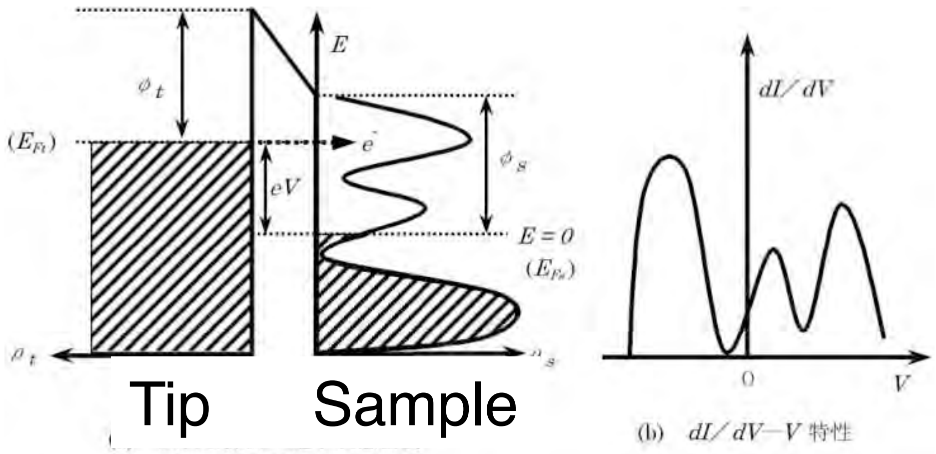

図 2 走査トンネル分光 (STS) の概念図

$$I \fallingdotseq A \int_0^{eV} \rho_t(E)\rho_s(R,E)\,dE \qquad (1)$$

$dI/dV \propto \rho_t(eV)\rho_s(R, eV)$

LDOS of tip LDOS of sample

http://opt-1.matsc.kyutech.ac.jp/afm-2.html

STM images of CoPc multilayers grown epitaxially on Au(111)

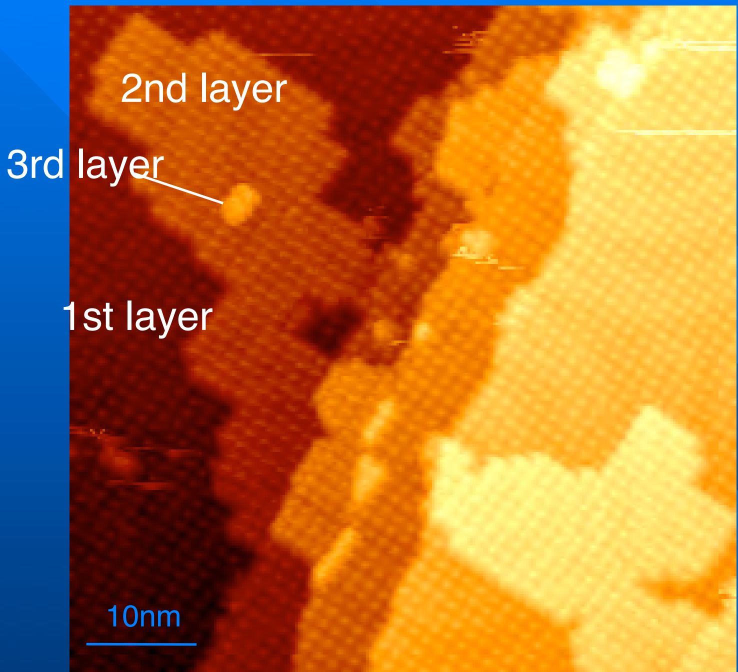

V = -1.2V, It =35pA, 43x43nm

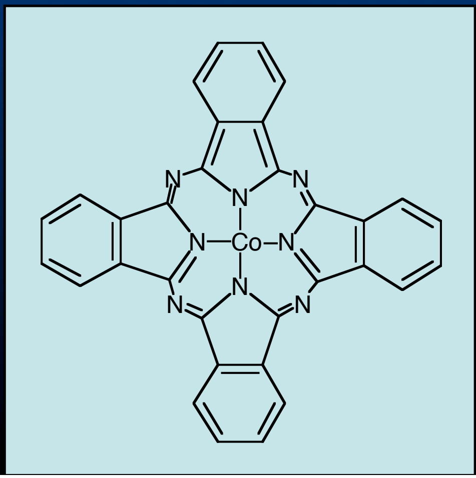

CoPc/Au(111)
@78 K

1 st layer

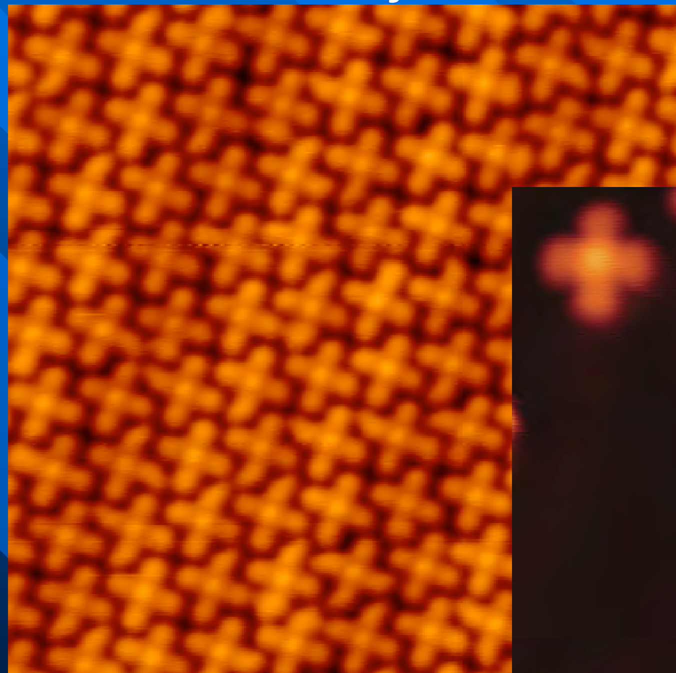

V = 0.9 V, It =265 pA, 15.0

initial statge

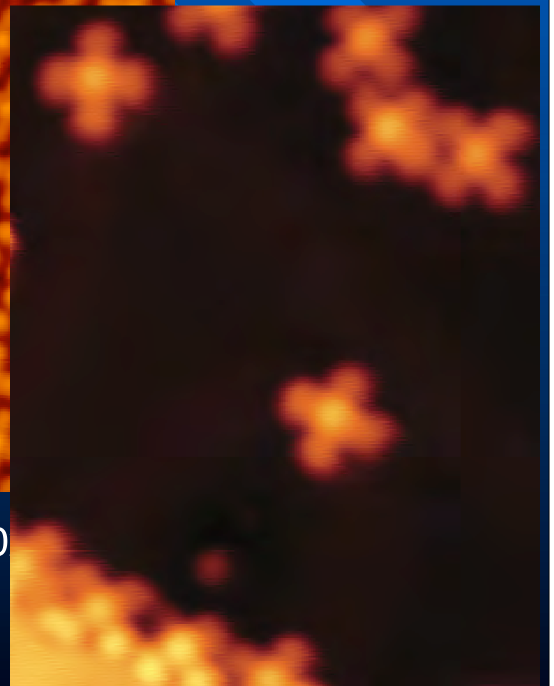

V = -0.5 V, I = 100 pA

Peak Assignment

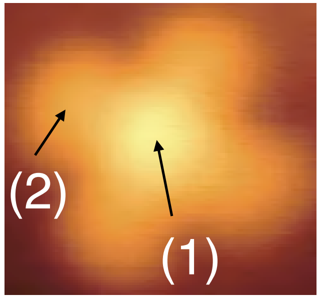

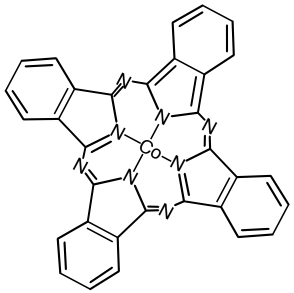

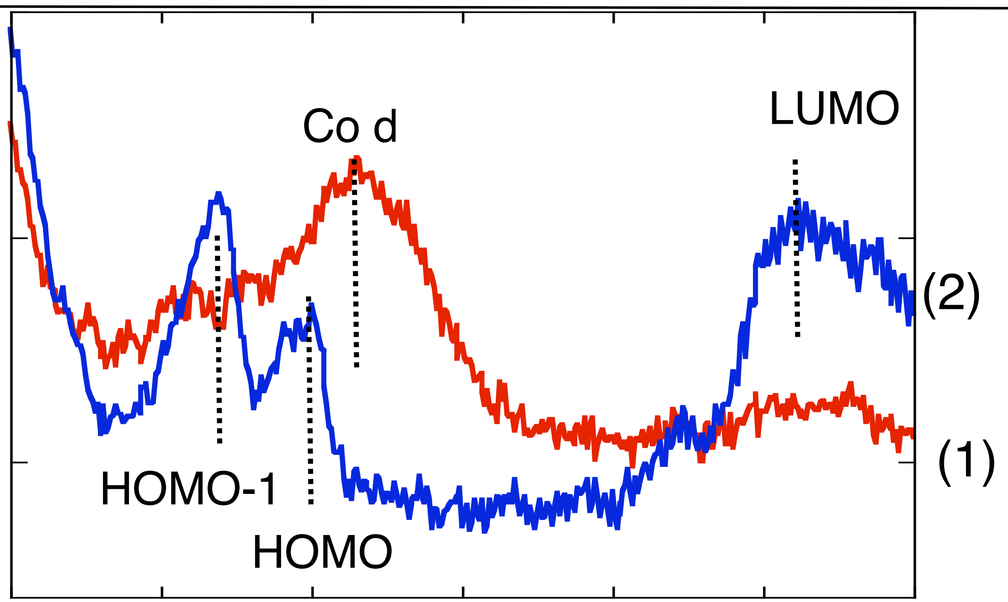

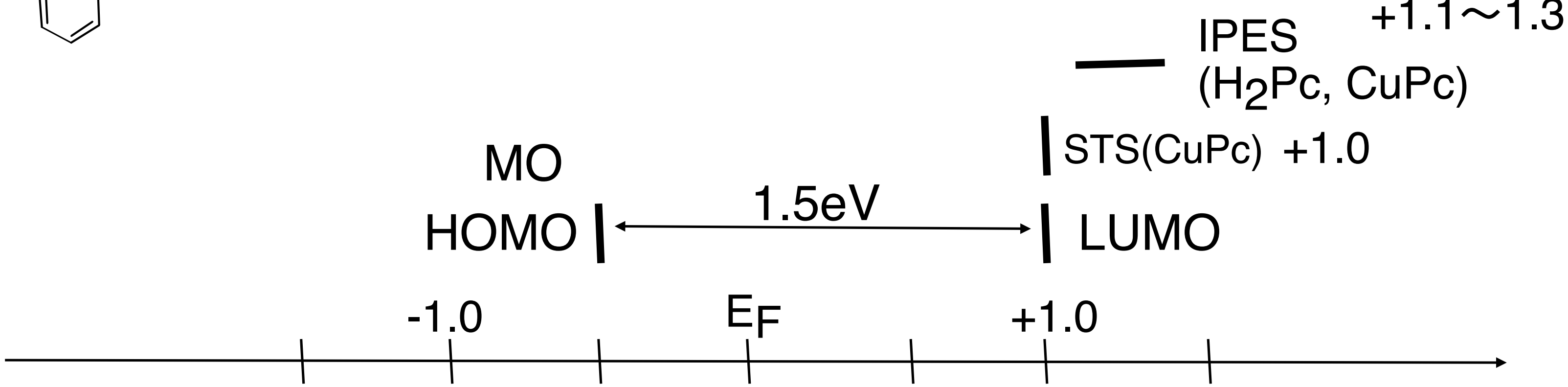

STS(CuPc on NiAl); Science302,77 (2004), IPES(CuPc,NiPc on Cu); J. Chem. Phys. 93, 6859(1990)

STM image of CoPc on Cu(100) at 5K

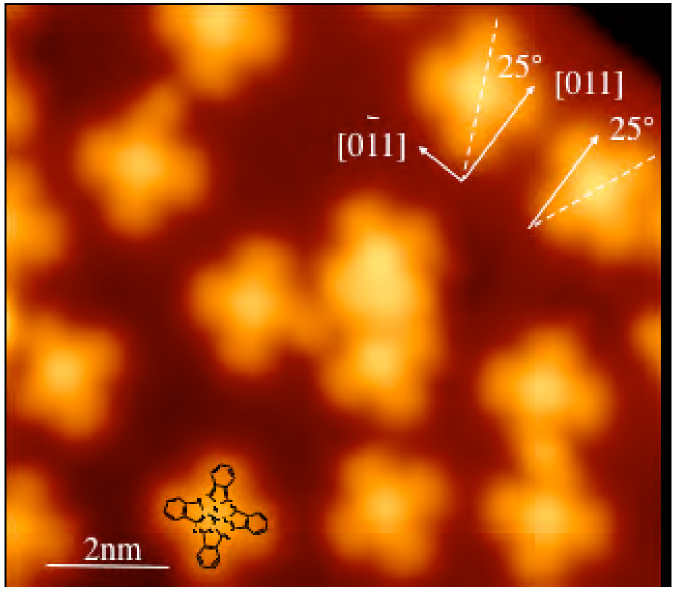

11 nm x 9 nm

dI/dV spectra of CoPc/Cu(100) at 5K

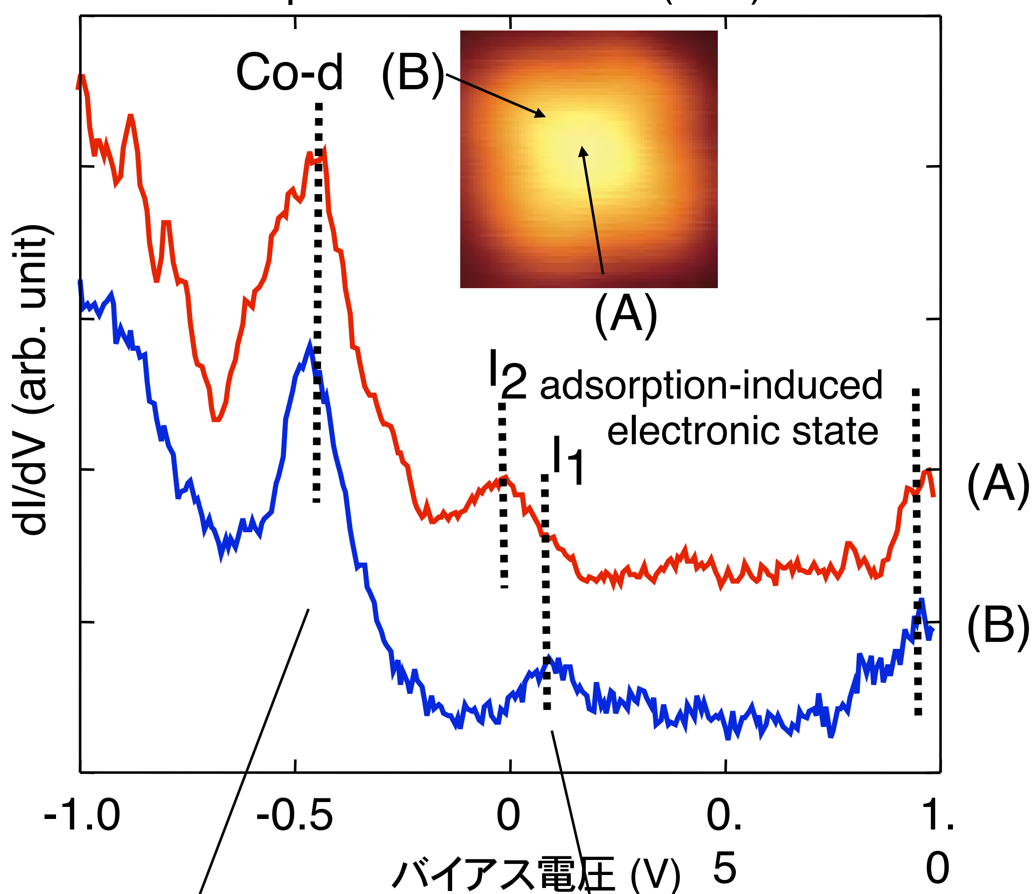

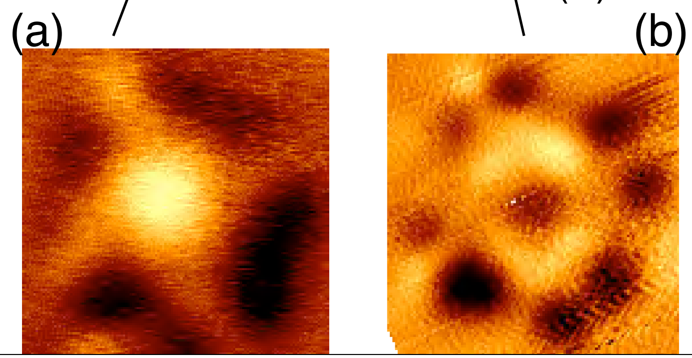

dI/dV images of CoPc/Cu(100)
At -0.3 V(a) and +0.05 V(b)

dI/dV images of a single CoPc molecule

CoPc

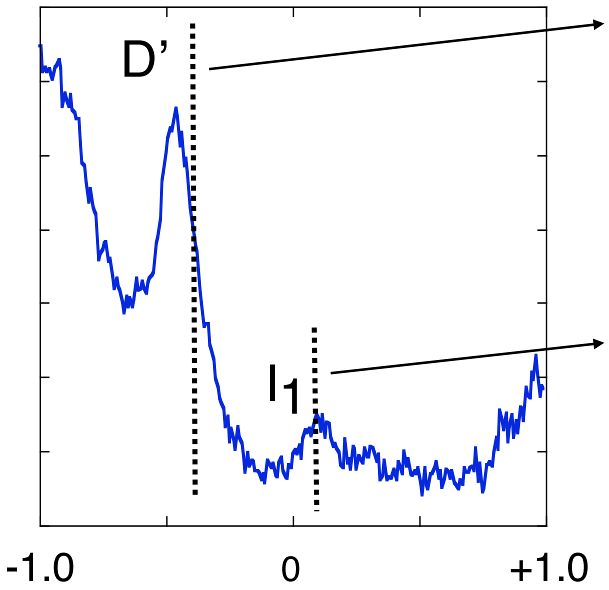

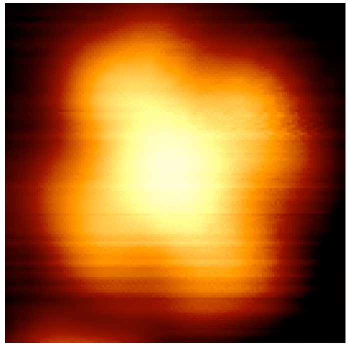

STM image

V = -0.3 V, I_t =0.3 nA

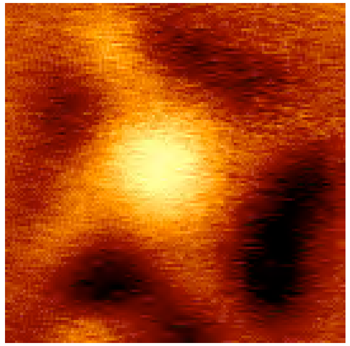

dI/dV image (-0.3 eV)

Co atom

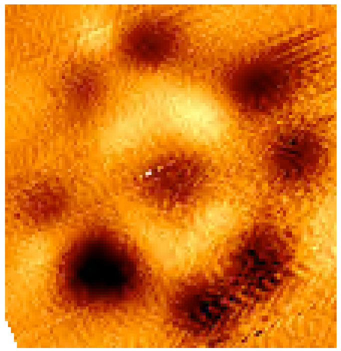

dI/dV image (+50 meV)

porphyrine ring

Summary

dI/dV spectroscopy of CoPc on Au(111)、Cu(100)

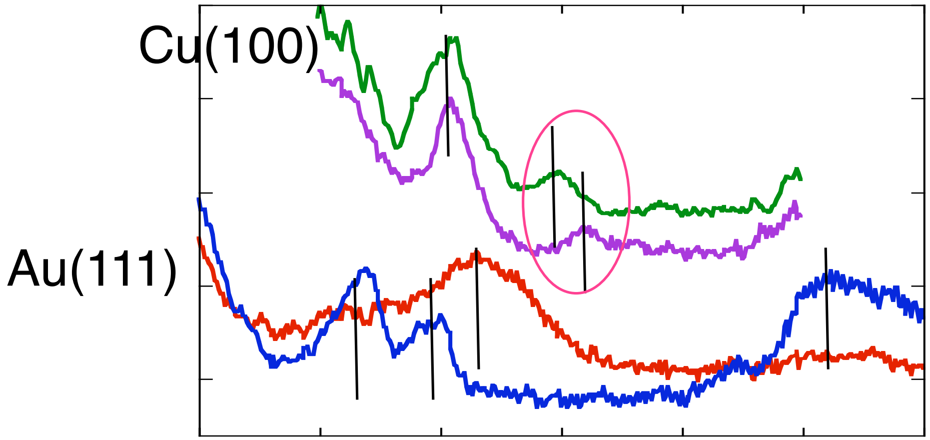

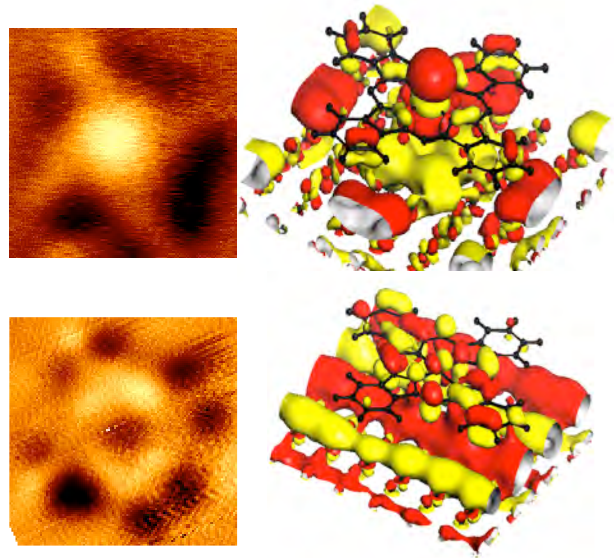

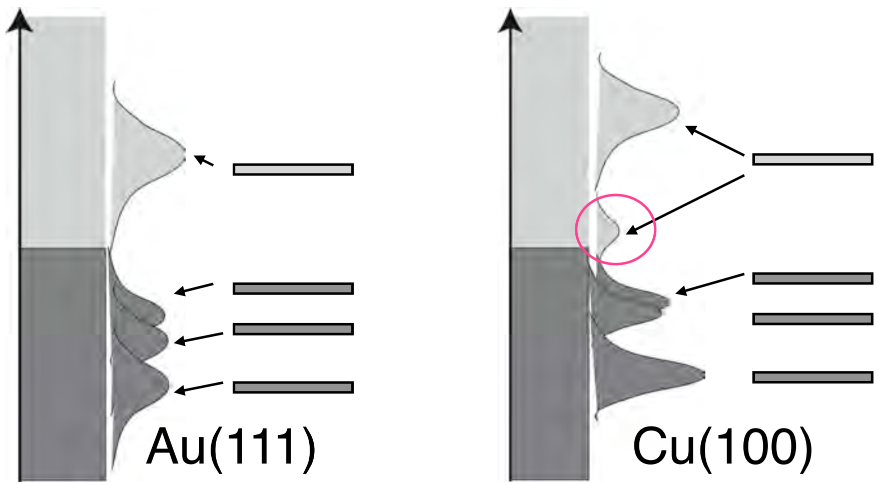

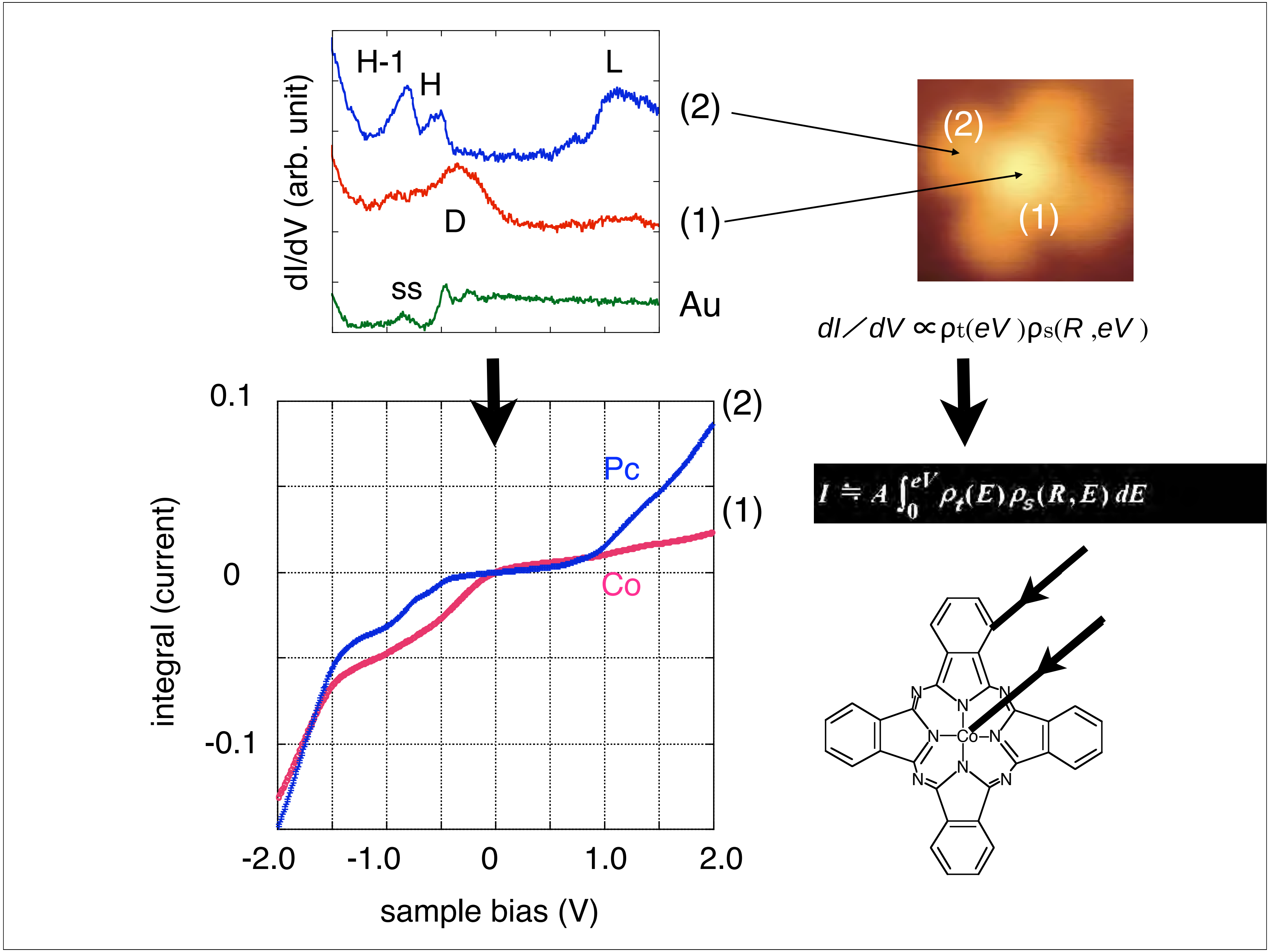
H-1
H
L
D
ss
dI/dV (arb. unit)
(2)
(1)
Au
dI／dV ∝ ρt(eV)ρs(R ,eV)
I ≒ A ∫0^eV ρt(E) ρs(R, E) dE
0.1
0
-0.1
integral (current)
Pc
Co
-2.0
-1.0
0
1.0
2.0
sample bias (V)
N
Co

STM image of CoPc multilayers grown epitaxially on Au(111) at 78 K

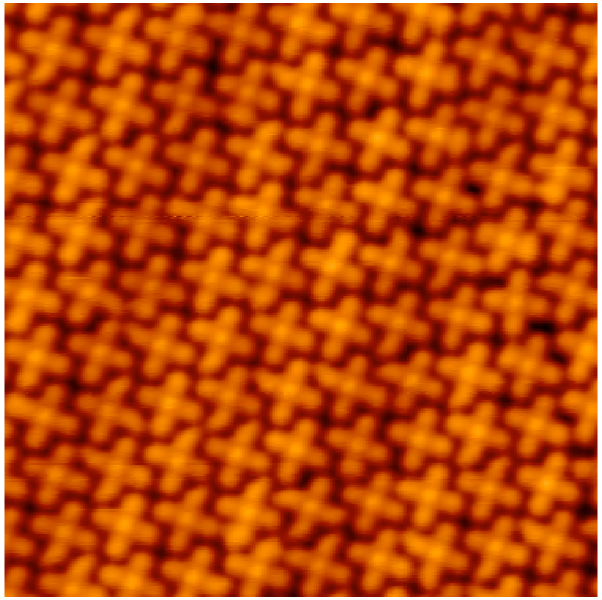

15nm x 15 nm

dI/dV spectra of CoPc/Au(111) at 5K

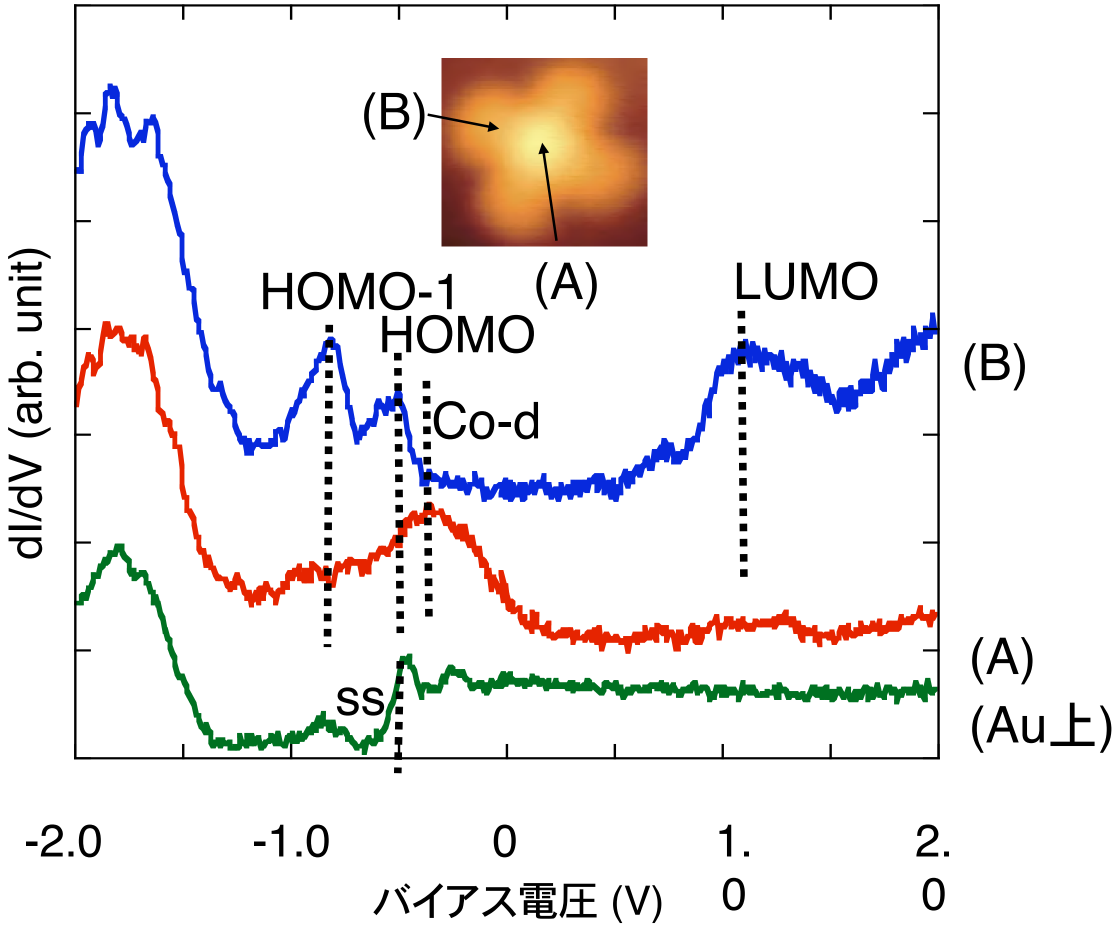

dI/dV images of a single CoPc molecule

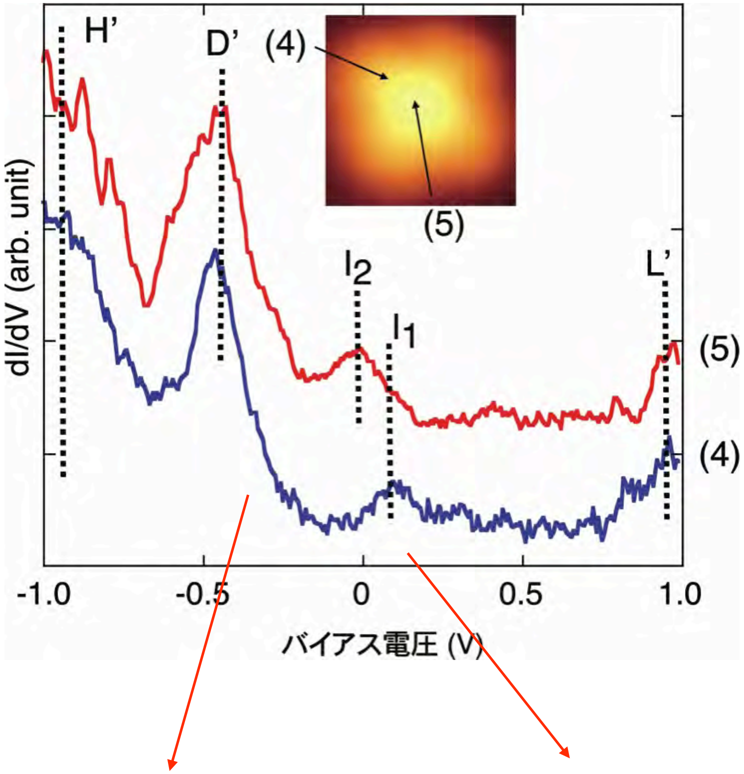

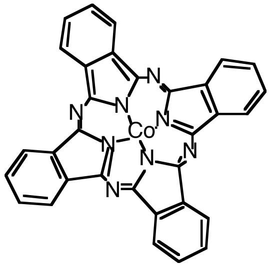

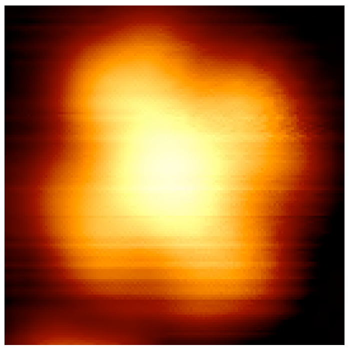

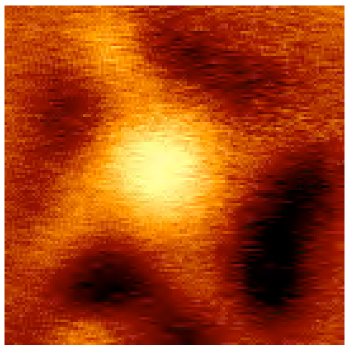

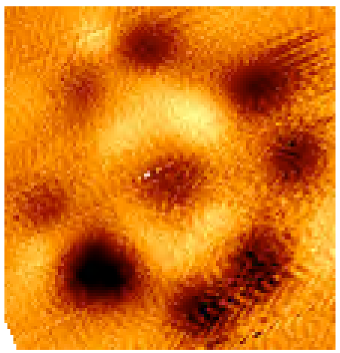

Summary

on Au(111)

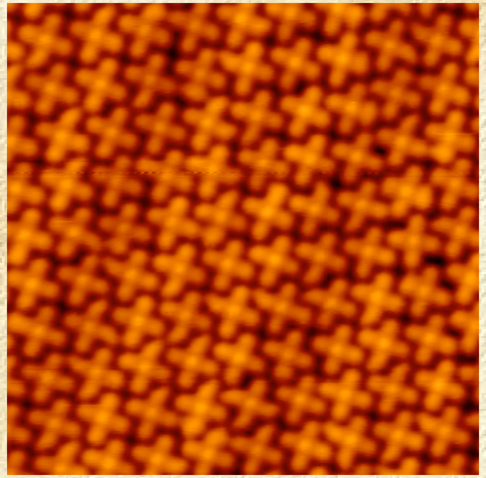

on Cu(100)

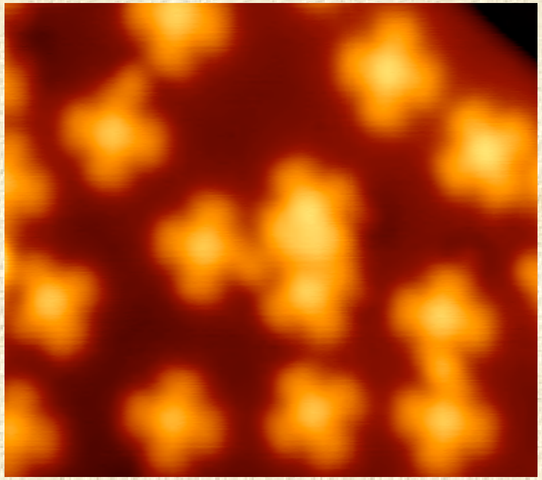

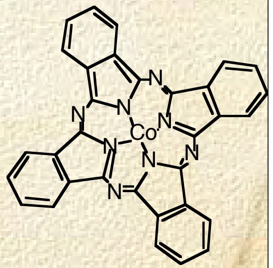

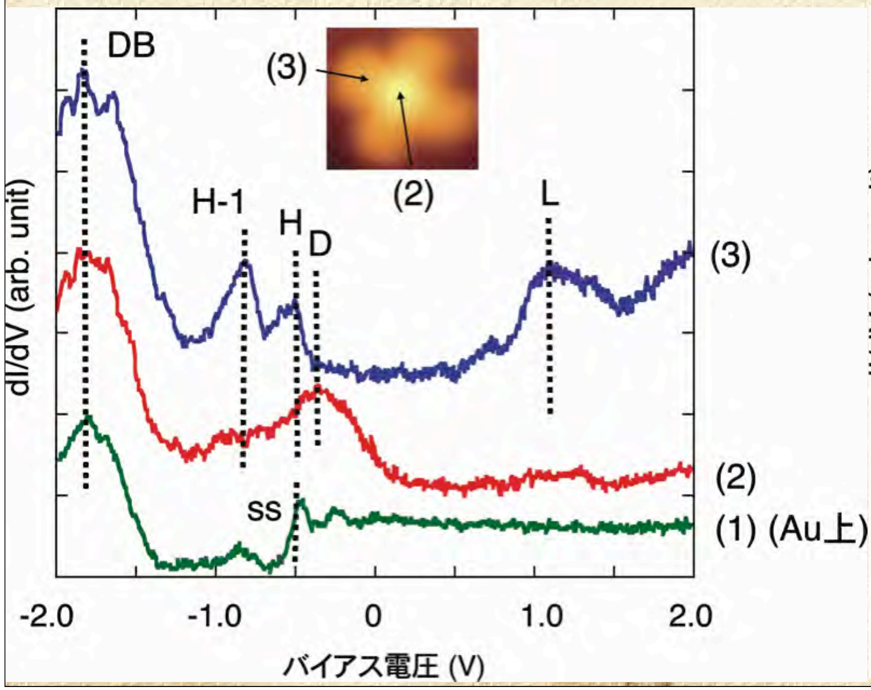

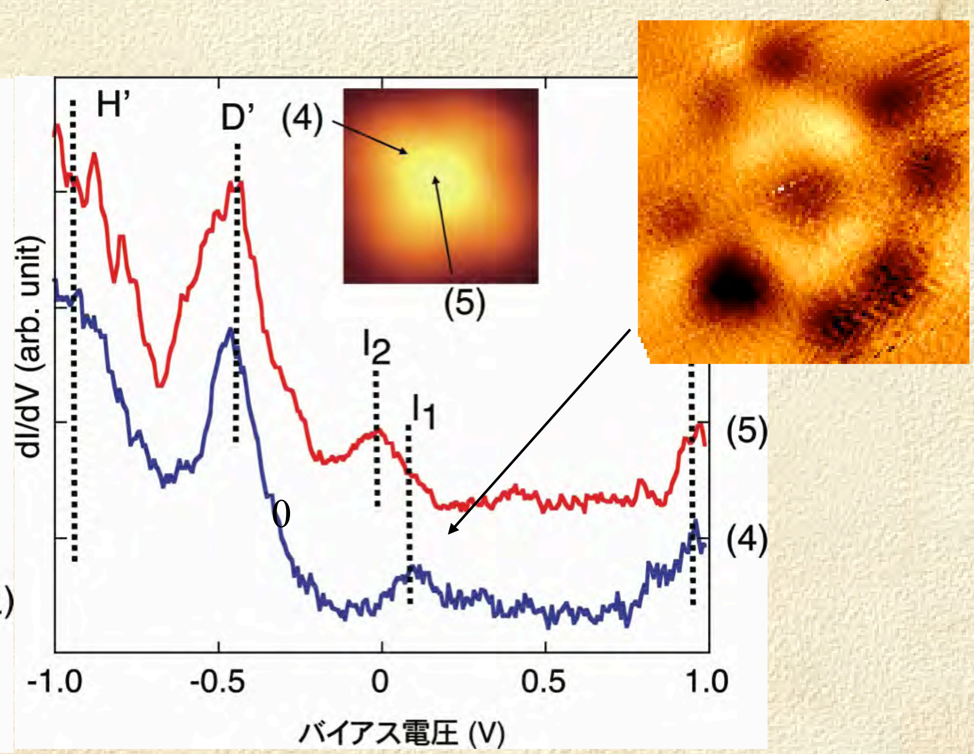

Summary

1 μm　100 nm　10 nm　1 nm

	Organic Field Effect Transistor	Electrochemical Approach for Molectronics	Molecular Assemblies on Si	Low Temperature STM
Target	Organic Laser Spin Transistor	Molecular-scale Electronic Devices		Spin-polarized STM